

10  
20356  
N 91 - 25324

NEW SECONDARY BATTERIES UTILIZING ELECTRONICALLY  
CONDUCTIVE POLYPYRROLE CATHODE

A Dissertation

by

TAEWHAN YEU

Submitted to the Graduate College of  
Texas A&M University  
in partial fulfillment of the requirement for the degree of

DOCTOR OF PHILOSOPHY

December 1990

Major Subject: Chemical Engineering

NEW SECONDARY BATTERIES UTILIZING ELECTRONICALLY  
CONDUCTIVE POLYPYRROLE CATHODE

A Dissertation

by

TAEWHAN YEU

Approved as to style and content by:

---

Ralph E. White  
(Chairman of Committee)

---

Rayford G. Anthony  
(Member)

---

Richard B. Griffin  
(Member)

---

James C. Holste  
(Member)

---

Raymond W. Flumerfelt  
(Head of Department)

December 1990

## ABSTRACT

New Secondary Batteries Utilizing Electronically  
Conductive Polypyrrole Cathode. (December 1990)

Taewhan Yeu, B.S., Chung-Ang University

M.S., University of Detroit

Chairman of Advisory Committee: Dr. Ralph E. White

To gain a better understanding of the dynamic behavior in electronically conducting polypyrroles and to provide guidance toward designs of new secondary batteries based on these polymers, two mathematical models are developed; one for the potentiostatically controlled switching behavior of polypyrrole film, and one for the galvanostatically controlled charge/discharge behavior of lithium/polypyrrole secondary battery cell.

The first model is used to predict the profiles of electrolyte concentrations, charge states, and electrochemical potentials within the thin polypyrrole film during switching process as functions of applied potential and position. Thus, the detailed mechanisms of charge transport and electrochemical reaction can be understood. Sensitivity analysis is performed for independent parameters, describing the physical and electrochemical characteristic of polypyrrole film, to verify their influences on the model performance. The values of independent parameters are estimated by comparing model predictions with experimental data obtained from identical conditions.

The second model is used to predict the profiles of electrolyte concentrations, charge state, and electrochemical potentials within the battery system during

charge and discharge processes as functions of time and position. Energy and power densities are estimated from model predictions and compared with existing battery systems. The independent design criteria on the charge and discharge performance of the cell are provided by studying the effects of design parameters.

To My Parents, Dalyoung and Hwoaja

## ACKNOWLEDGMENTS

The author would like to give special thanks to his parents who gave unfailing encouragement and instilled in him a belief that hard work and dedication can overcome obstacles even in the most trying of circumstances. This work is in no small part due to their guidance and willingness to express their belief in his abilities. The author also would like to give thanks to his wife, Kyung Mi, and his son, Christopher Edward, for their love, patience, humor, advice, and constant support.

The author wishes to express his sincere gratitude to Professor Ralph E. White for his guidance and support throughout the period of this work. Special thanks also go to Professor James C. Holste and Rayford G. Anthony of the Chemical Engineering Department and Professor Richard B. Griffin of the Mechanical Engineering Department for serving as advisory Committee members, and Dr. Mary K. Wicksten from the Department of Biology for serving as a representative of the Graduate Council to the Advisory Committee.

In addition, the author thanks to Professor Charles R. Martin and his research group of the Chemistry Department for their valuable contribution to this work. The author also wishes to express deep appreciation to all members, past and present, of the Electrochemical Engineering Center for upholding and advocating his ability to reach his goal. The author gratefully acknowledges all of unselfish contributions made toward this work.

## TABLE OF CONTENTS

	Page
I. INTRODUCTION . . . . .	1
II. LITERATURE SURVEY . . . . .	5
A. Historical Background . . . . .	5
B. Polymerization . . . . .	7
1. Chemical Synthesis . . . . .	8
2. Electrochemical Synthesis . . . . .	9
C. Structure and Polymerization Mechanisms . . . . .	10
1. Structure . . . . .	10
2. Polymerization Mechanisms . . . . .	13
D. Electrochemical Properties . . . . .	15
E. Transport Properties . . . . .	21
1. Electronic Transport . . . . .	21
2. Mass Transport . . . . .	27
F. Dependency of Properties on Polymerization Conditions . . . . .	30
1. Electrodes . . . . .	30
2. Solvents . . . . .	31
3. Electrolytes . . . . .	33
4. Driving Forces . . . . .	38
5. Others . . . . .	39
G. Modifications of Properties . . . . .	40
H. Applications . . . . .	42
1. Energy Storage Devices . . . . .	43
2. Solar Energy Devices . . . . .	44
3. Electrochromic Display Devices . . . . .	44
4. Others . . . . .	45
III. MATHEMATICAL TREATMENT OF MATERIALS . . . . .	47
A. Electrochemistry . . . . .	47
B. Properties of 1M LiClO <sub>4</sub> -PC Electrolyte . . . . .	48

## TABLE OF CONTENTS (Continued)

	Page
C. Properties of Polypyrrole . . . . .	50
D. Electrochemical Reaction Rate of Polypyrrole . . . . .	52
E. Electrochemical Reaction Rate of Lithium . . . . .	55
 IV. CYCLIC VOLTAMMETRY . . . . .	57
A. Experimental Descriptions . . . . .	58
B. Model Descriptions . . . . .	60
1. Governing Equations – Polypyrrole Electrode Region . . . . .	60
2. Governing Equations – Solution Diffusion Layer . . . . .	67
3. Boundary and Interface Conditions . . . . .	68
4. Initial Conditions . . . . .	71
5. Solution Method . . . . .	71
C. Results and Discussion . . . . .	73
1. Experimental Results . . . . .	74
2. Simulated Results . . . . .	77
3. Sensitivity Analysis . . . . .	87
4. Effects of Parameters . . . . .	90
D. Conclusions and Recommendations . . . . .	96
 V. SECONDARY BATTERY . . . . .	99
A. System Descriptions . . . . .	100
B. Model Descriptions . . . . .	102
1. Governing Equations – Polypyrrole Positive Electrode . . . . .	104
2. Governing Equations – Reservoir . . . . .	106
3. Governing Equations – Separator . . . . .	107
4. Boundary and Interface Conditions . . . . .	108
5. Initial Conditions . . . . .	112
6. Solution Method . . . . .	112
C. Results and Discussion . . . . .	114
1. Charge and Discharge Behavior . . . . .	115
2. Dependent Variables profiles . . . . .	119

**TABLE OF CONTENTS (Continued)**

	Page
3. Effects of Operating Conditions . . . . .	123
4. Effects of Design Parameters . . . . .	124
D. Conclusions and Recommendations . . . . .	128
 LIST OF SYMBOLS . . . . .	 132
REFERENCES . . . . .	136
APPENDIX A . . . . .	146
VITA . . . . .	147

## LIST OF TABLES

Table	Page
I. Electronically conducting polyheterocycles. . . . .	2
II. Solvent effects on the quality of the polypyrrole films. . . . .	32
III. Anion effects on the properties of the polypyrrole films. . . . .	35
IV. Properties of 1M LiClO <sub>4</sub> -PC electrolyte at 25°C. . . . .	50
V. Properties of polypyrrole film doped with perchlorate. . . . .	51
VI. Properties of polypyrrole film as a function of its oxidation state. . . . .	53
VII. Kinetic parameter values used for polypyrrole. . . . .	54
VIII. Kinetic parameter values used for lithium. . . . .	56
IX. System of equations for cyclic voltammetry of polypyrrole. . .	72
X. Operating conditions used for cyclic voltammograms of polypyrrole. . . . .	74
XI. Electrochemical Characteristics of the 1 μm polypyrrole film in the 1M LiClO <sub>4</sub> -PC electrolyte. . . . .	76
XII. Fixed parameter values used for polypyrrole. . . . .	79
XIII. Sensitivity analysis on various physical parameters. . . . .	88
XIV. Sensitivity analysis on various electrochemical parameters. . .	89
XV. Sensitivity analysis on various operating conditions. . . . .	90
XVI. System of equations for charge/discharge behavior of lithium/polypyrrole secondary battery cell. . . . .	113
XVII. Operating conditions used for charge/discharge behavior of lithium/polypyrrole secondary battery cell. . . . .	114
XVIII. Electrochemical characteristic of one square centimeter lithium/polypyrrole secondary battery cell during discharge.	117

## LIST OF FIGURES

Figure	Page
1. Proposed stoichiometry of oxidized and neutral polypyrrole films . . . . .	12
2. Generally accepted mechanism for electrochemical polymerization of polypyrrole film. . . . .	14
3. Experimental cyclic voltammograms for a 20 nm polypyrrole film in 0.1M Et <sub>4</sub> NBF <sub>4</sub> -CH <sub>3</sub> CN electrolyte. . . . .	17
4. Scanning electron micrographs of polypyrrole film surface with different anions. . . . .	37
5. A schematic diagram of a single-compartment electrochemical cell with a rotating disk electrode. . . . .	59
6. A schematic diagram of modeling regions closed to the rotating disk electrode in the single-compartment electrochemical cell. . . . .	61
7. Experimental cyclic voltammograms for a 1 $\mu$ m polypyrrole film in 1M LiClO <sub>4</sub> -PC electrolyte at scan rates of 10 and 20 mV/sec. . . . .	75
8. Simulated cyclic voltammograms for a 1 $\mu$ m polypyrrole film in 1M LiClO <sub>4</sub> -PC electrolyte at scan rates of 10 and 20 mV/sec. . . . .	78
9. Decomposition of a cyclic voltammogram into its two components, the faradaic and capacitive current densities, at a scan rate of 20 mV/sec. . . . .	80
10. Dimensionless concentration profiles of the anion (ClO <sub>4</sub> <sup>-</sup> ) within the polypyrrole electrode region at a scan rate of 20 mV/sec. . . . .	82
11. Dimensionless faradaic charge profiles within the polypyrrole electrode region at a scan rate of 20 mV/sec. . . . .	84
12. Potential difference between solid and solution phases within the polypyrrole electrode region at a scan rate of 20 mV/sec. . . . .	86
13. The effects of maximal faradaic charge ( $Q_{f,oxd}$ ) on the cyclic voltammograms at a scan rate of 20 mV/sec. . . . .	91
14. The effects of double layer constant ( $a^*$ ) on the cyclic voltammograms at a scan rate of 20 mV/sec. . . . .	93

## LIST OF FIGURES (Continued)

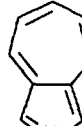
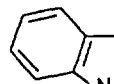
Figure	Page
15. The effects of anodic transfer coefficient ( $\alpha_{a1}$ ) on the cyclic voltammograms at a scan rate of 20 mV/sec. . . . .	94
16. The effects of exchange current per unit volume ( $a_{i_{o1,ref}}$ ) on the cyclic voltammograms at a scan rate of 20 mV/sec. . . . .	95
17. A schematic diagram of a typical monopolar Li/LiClO <sub>4</sub> -PC/PPy secondary battery cell. . . . .	101
18. A schematic diagram of modeling regions in Li/LiClO <sub>4</sub> -PC/PPy secondary battery cell. . . . .	103
19. Simulated charge and discharge behaviors of a typical Li/LiClO <sub>4</sub> -PC/PPy secondary battery cell at $i_{cell} = 0.2 \text{ mA/cm}^2$ . . . . .	116
20. Faradaic and capacitive current components within the polypyrrole positive electrode during charge at $i_{cell} = 0.2 \text{ mA/cm}^2$ . . . . .	118
21. Dimensionless concentration profiles of the anion (ClO <sub>4</sub> <sup>-</sup> ) across a typical cell during charge and discharge at $i_{cell} = 0.2 \text{ mA/cm}^2$ . . . . .	120
22. Dimensionless faradaic charge profiles across a typical cell during charge and discharge at $i_{cell} = 0.2 \text{ mA/cm}^2$ . . . . .	122
23. Solution potential profiles across a typical cell during charge and discharge at $i_{cell} = 0.2 \text{ mA/cm}^2$ . . . . .	124
24. The effect of the discharge rate on the cell discharge performance. . . . .	125
25. The effect of the thickness of the polypyrrole positive electrode on the cell discharge performance at $i_{cell} = 0.2 \text{ mA/cm}^2$ . . . . .	126
26. The effect of the thickness of the reservoir on the cell discharge performance at $i_{cell} = 0.2 \text{ mA/cm}^2$ . . . . .	127
27. The effect of the thickness of the separator on the cell discharge performance at $i_{cell} = 0.2 \text{ mA/cm}^2$ . . . . .	129

## I. INTRODUCTION

Electronically conducting polyheterocyclics are an interesting class of materials that have gained popularity in the last decade. Although most of the studies have been devoted to polypyrrole, extensive work on other polyheterocyclics such as polythiophene, polyfuran, polyazulene, polyindole, polycarbazole, and their derivatives, has been carried out by a number of investigators (1,2). Table I lists the structural and electrochemical analysis data for various conducting polyheterocyclics (1-3). The polyheterocycles derived from heterocyclic monomers are p-type conductors and are relatively stable in the air over extended periods of time. They possess high electronic conductivities as well as they can be employed as their own current collectors.

Electronically conducting polyheterocyclics have a number of potential technological applications because of their ability to switch between the conducting and nonconducting states. They can be used as energy storage devices, solar energy devices, electrochromic display devices, and electronic devices. One of the most promising applications is the development of new high-energy-density secondary batteries because of prospect for a long-term supply of inexpensive, lightweight, and noncorrodible electrode materials. In the design of high-energy-density batteries, conducting polymers fulfill the most important characteristic: a large amount of energy stored per unit weight. Another novel feature is that they can be fabricated into any desired shape, thereby providing unusual design flexibility.

Table I. Electronically conducting polyheterocycles.

Electronically Conductive Polyheterocycles	Structure of Monomer	Maximum Doping Level	Anion Content (% by wt)	Electronic Conductivity (/Ω-cm)
Polypyrrole		0.25 - 0.33	25 - 30	0.01 - 200
Polythiophene		0.06 - 0.30	7 - 25	10 - 20
Polyazulene		0.25	15 - 28	0.01 - 1
Polyindole		0.20 - 0.30	15 - 20	0.001 - 0.01
Polycarbazole	-	0.45	21	0.001 - 0.1
Polyfuran		-	26	-
Polypyrene	-	0.45	-	0.1 - 1

Among the recently available electronically conducting polyheterocyclics, polypyrrole has been received the most attention as a secondary battery electrode material because the electrochemical features of polypyrrole epitomize the polyheterocyclics in many important respects. Electrochemically synthesized polypyrrole can be produced from commercially available chemicals by a simple one-step electrochemical oxidation process. Polypyrrole has high conductivity and specific charge capacity, and exhibits a stable and reversible electrochemical redox behavior. There is no doubt that polypyrrole remains an interesting electrode material. However, the knowledge of electrochemical behavior and the application of polypyrrole published to date is still in the experimental stage and remains far from completion.

The main objectives of this study are to gain a better understanding of the dynamic behavior in electronically conducting polypyrrole films, and to provide guidance toward designs of new secondary batteries based on this polymer as a cathode material. To accomplish these objectives, two mathematical models are developed; one for simulating the cyclic voltammetric behavior of polypyrrole in a single-compartment cell, and one for simulating charge/discharge behavior of a lithium/polypyrrole (Li/PPy) secondary battery cell. Mathematical modeling is an integral part of the design and development of polymer batteries because it enables us to learn the cause and effect relationships, reveals phenomena in fine details, and suggests directions for improvements.

Simulation of cyclic voltammograms of polypyrrole film makes it possible to clarify the electrochemical reaction mechanism and charge transport phenomena. The model is used to study the effect of electrochemical parameters to characterize the electrochemical properties of polypyrrole. Thus, it is possible to obtain

values for the electrochemical parameters that would yield the best agreement between model predictions and experimental data. Based on the model of cyclic voltammogram and its estimated results, a mathematical model to simulate the charge/discharge behavior of lithium/polypyrrole secondary battery is then developed. This model is used to understand charge/discharge behavior and provide design criteria of new secondary batteries that utilize electronically conducting polypyrrole.

The treatment presented here is general and can be extended easily to account for other complex electroanalytical experiments (such as, chronoamperometry, chronopotentiometry, AC impedance, etc.) and other conducting polymers (such as, polyacetylene, polythiophene, polyparaphenylene, etc.) with the appropriate modifications in operating conditions and physical properties.

## II. LITERATURE SURVEY

The worldwide interest in electronically conductive polypyrrole films is readily gauged by the large number of publications in this field. This chapter reviews the historical background (4-24), the polymerization and structure (25-40), the physical and chemical properties (41-104), and potential technological applications (105-117).

### A. Historical Background

Polypyrrole was first chemically prepared as a powder by Angeli *et al.* (4,5) in 1916.  $H_2O_2$  was used as the oxidizing agent and gave a material which is commonly known as 'pyrrole black'. Pyrrole black is an amorphous powder and it is insoluble in organic solvents. Because of its undesirable properties, no further interest was shown in this material.

The electrochemical oxidation of pyrrole in aqueous sulfuric acid to produce a powdery, insoluble precipitate on a platinum electrode was first reported by Dall'Olio *et al.* (6) in 1968. Elemental analysis showed that the resulting polypyrrole consisted of 76% polypyrrole, the remainder being sulfate ions making this polymer cationic. Although this procedure represented the first electrochemical synthesis of a conducting polypyrrole, the undesirable physical properties and the relatively low room temperature conductivity ( $8 \Omega^{-1}cm^{-1}$ ) limited the interest generated by this synthetic route.

A new chapter in the evolution of electronically conducting polymers began with the discovery of the chemically synthesized pristine polysulfurnitride by Walatka *et al.* (7) in 1973. The resulting inorganic polymer itself behaves like

a metal over the entire temperature range from 4.2 to 300 K. The experimental information indicated that polysulfurnitride has a crystalline form and a quasi-one-dimensional structure. The conductivity of polysulfurnitride was reported as  $1000 \Omega^{-1}\text{cm}^{-1}$  and was attributed to impurity or defect scattering (8). This is also the first polymeric system known to exhibit superconductivity at a transition temperature below 0.3 K (8).

Attempts to find a covalent organic polymer, with high conductivity, lead to the discovery of polyacetylene in 1977 (9-11). The discovery of this semiconducting and metallic organic polyacetylene introduced new concepts in the field of the organic conducting polymers and intensified research in the synthesis and characterization of this class of compounds. Polyacetylene is one of the simplest linear conjugated polymers with a single-chain structure. It was found that exposure of films of either *cis*- or *trans*-polyacetylene to iodine, bromine, or arsenic pentafluoride vapor led to an oxidized form (p-type) while treatment with a solution of sodium naphthalide led to a reduced form (n-type). In 1979, it was discovered that p- or n-type polyacetylene could be accomplished electrochemically and that these processes were electrochemically reversible (12). Moreover, the oxidation or reduction of the film was accompanied by an increase in conductivity from  $10^{-8} \Omega^{-1}\text{cm}^{-1}$  for the neutral film to a value of up to  $10^3 \Omega^{-1}\text{cm}^{-1}$  for the oxidized film. These led naturally to the conclusion that polyacetylene and its various oxidized or reduced forms might act as promising charge storing materials for use in secondary batteries. Polyacetylene had been extensively investigated as an electrode material in secondary battery technologies (13,14). However, the main problem with using polyacetylene as an electrode material is its poor stability in the presence of oxygen and water (15).

The discovery of polyacetylene touched off a flurry of research directed towards the study and discovery of new conducting polymeric systems such as polypyrrole (16,17) and poly(paraphenylene) (18). In 1979, Diaz *et al.* (16,17) reported that the electronically conductive polypyrrole films could be produced by the anodic oxidation of pyrrole in acetonitrile with the presence of tetraethylammonium tetrafluoroborate. Resulting films could be cycled between the doped (oxidized) and undoped (neutral) states without loss of electroactivity. The doped films become good electronic conductors ( $100 \Omega^{-1} \text{cm}^{-1}$ ) whereas the undoped films are only moderate conductors ( $10^{-10} \Omega^{-1} \text{cm}^{-1}$ ). The film was continuous and could be peeled off the platinum substrate electrodes to yield free-standing, easily manageable films that were stable in air and had much higher electrical conductivities than achieved before (Dall'Olio *et al.*). The attractiveness of the polypyrrole system stems from several factors. The most important were undoubtedly the chemical and thermal stability of these polymers and their ease of preparation relative to polysulfurnitride and polyacetylene.

The successful synthesis of polypyrrole led to synthesis of similar electronically conducting polyheterocyclics. The most important are polypyrrole derivatives (19), polythiophene (20-23), and polythiophene derivatives (22-24). The discovery of these polymers was particularly significant since they are extremely stable in oxygen and moisture environments, even in their neutral state.

## B. Polymerization

Polypyrrole can be produced by either chemical or electrochemical synthesis. The chemical route generally leads to a conducting powder, whereas the electrochemical route yields a continuous film which is also conducting. Although the

chemical preparation of polypyrrole remains a desirable goal, presently, the electrochemical synthesis provides the only satisfactory route for producing these films.

### 1. Chemical Synthesis

Polypyrrole can be prepared by the chemical oxidation of the monomer with exposure to a wide variety of oxidizing conditions because of pyrrole's extremely high reactivities. For instance, polypyrrole has been prepared by oxidative pyrolysis of tetraiododopyrrole (25). In this case, varying degrees of oxidation are attained by varying the temperature of pyrolysis. The oxidized changes in the polymer are compensated by  $I_3^-$  formed from pyrolytically cleaved iodide. Oxidatively polymerized polypyrrole has also been synthesized by exposure of the monomer to mild oxidizing reagents such as potassium persulfate ( $K_2S_2O_8$ ) (25), and iron(III) (26). Salmon *et al.* (27) demonstrated chemically synthesized polypyrrole by a simple one step chemical oxidation of the monomer by a strong oxidant, such as  $Fe_3(ClO_4)_3$ , in various solvents. This chemically synthesized polypyrrole is a black and conducting powder which exhibits electronic and electrochemical properties similar to those of the electrochemically synthesized polypyrrole. Pyrrole also forms polymers under acidic conditions (28). In this case, however, the polymers contain alternating pyrrole and pyrrolidine units and therefore do not have an extended  $\pi$ -system.

In general, conducting polypyrrole by the chemical synthesis has two major limitations. First, the resulting polymer yields a finely divided precipitate which is completely insoluble in any solvent (26). Thus, the characterization of this polymer is very difficult because of those insolubility. Second, the presence of catalysts in many of the chemical synthesis allows for the introduction of

impurities into the polymer during synthesis. The electronic conductivities observed from these polymer are likely to be compromised by the presence of these impurities. For all these reasons, the discovery of an electrochemical synthesis route for the preparation of coherent polypyrrole films by Diaz *et al.* (16,17) in 1979 was regarded as an important break-through in the field of electronically conductive polymers.

## 2. Electrochemical Synthesis

Electrochemical synthesis is now the most commonly used synthetic approach for preparing electronically conductive polypyrrole films. The polymerization is carried out in a single-compartment electrochemical cell with the classic three-electrode configuration (2,29):

- a) working electrode; Pt, Au, or glass carbon,
- b) reference electrode; saturated calomel electrode (SCE),
- c) and auxiliary electrode; Pt, Li.

The electrolytic medium typically consists of an organic solvent (e.g., acetonitrile, propylene carbonate, etc.), a supporting electrolyte MX ( $M^+ = Et_4N^+$ ,  $Bu_4N^+$ ,  $Li^+$ ;  $X^- = ClO_4^-$ ,  $BF_4^-$ ,  $PF_6^-$ ,  $AsF_6^-$ ), and a pyrrole monomer (0.1M to 1M). The solvent, the monomer, and the supporting salt are generally purified by distillation or recrystallization just prior to electrolysis. The solutions are deoxygenated prior to electrolysis by nitrogen bubbling.

The electrochemical synthesis of polypyrrole is accomplished by anodic oxidation of pyrrole monomer from the electrolyte (17). Pyrrole is dissolved into the electrolyte solvent, along with a desired salt. Application of a constant potential (positive of +0.2 V versus SCE) to the electrode results in oxidation of the pyrrole monomer. As long as pyrrole monomer is being oxidized at the

electrode via the applied potential, the polymer grows continuously. In addition, the polymer can also be prepared by application of a constant current, usually on the order of  $0.2 \text{ mA/cm}^2$  (16,30,31). This method allows control over the total charge passed, and thereby, the film thickness. Third method involves cycling the potential over a range which polymerizes pyrrole at the anodic scan and reduces the polypyrrole products at the cathodic scan (32). This method exhibits an increase in current due to concomitant oxidation of the growing polymer at the electrode surface.

In general, electrochemical polymerization of pyrrole produces a strongly adhered, durable film with metal-like conductivity. The thickness of the resulting film can be controlled by the total charge passed through the cell. The resulting film is an oxidized conducting state because the aromatic dimer and higher molecular weight oligomers have lower oxidation potentials than the monomer. The conducting polycationic polymer consists of a densely packed insoluble material and is subsequently reduced chemically or electrochemically to the neutral polymer. The properties of polypyrrole film very much depend on the electrochemical environment. These effects will be discussed in a later section.

### C. Structure and Polymerization Mechanisms

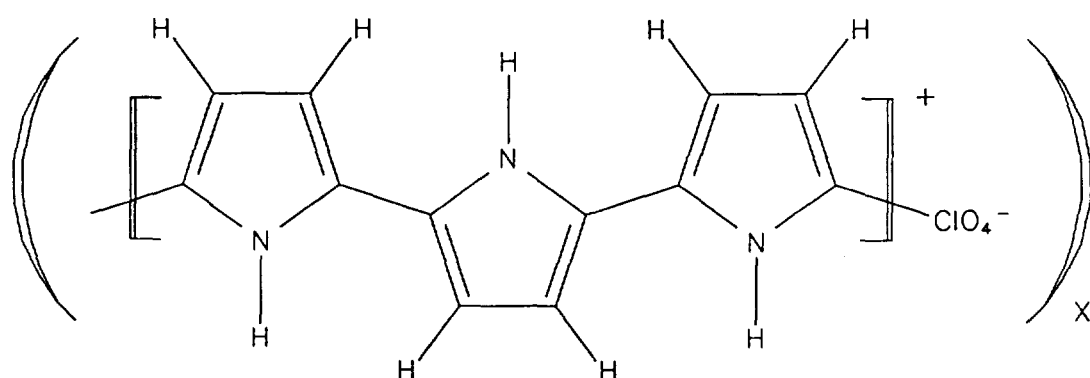
#### 1. Structure

All forms of polypyrrole reported so far are poorly crystalline and completely insoluble which means that much of our knowledge of the structure of these systems is obtained from a variety of indirect measurements.

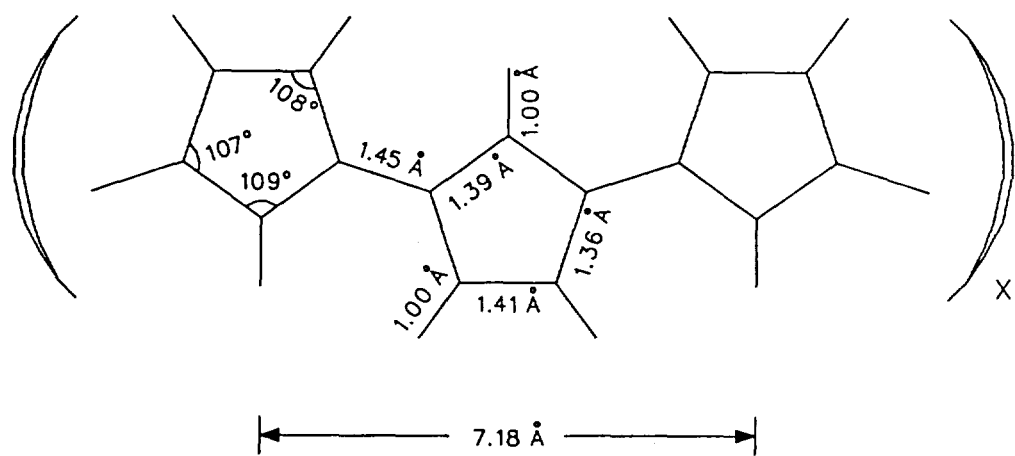
Generally accepted structure of oxidized and neutral polypyrrole films are shown in Fig. 1 (2,29). Polypyrrole films are primarily bonded *via*  $\alpha$ - $\alpha'$  linkages.

This is based largely on the demonstration that blocking  $\alpha$  and  $\alpha'$  positions seems to prevent the electrochemical polymerization of pyrroles (33). Also, the dominance of the  $\alpha$ - $\alpha'$  linkage in polypyrrole has been confirmed by  $^{13}\text{C}$  nuclear magnetic resonance spectrum analysis (29). However, analysis shows that the polymer is far from ideal, with less than two-thirds of the repeat units in this form (34). There is some involvement of the  $\beta$ -carbons in the chain bonding which could cause some crosslinking of the polymer (29).

Electrochemical synthesis of polypyrrole generates the film in the oxidized state, but the thin films can then be electrochemically cycled between the oxidized and neutral states by sweeping of the potential. The oxidized film (Fig. 1-A) has an extensively conjugated  $\pi$ -system, doped by oxidation so as to have unpaired electrons. Thus, the oxidized film contains anions, which are often referred to as dopants and act as counterions to balance the positive charge on the polymer and maintain electroneutrality. Determination of the amount of counterion in fully oxidized polypyrrole indicates the doping level and the amount of charge stored in the polymer. Diaz *et al.* (16) suggested approximately four pyrrole rings per tetrafluoroborate anion ( $\text{BF}_4^-$ ), while Street *et al.* (29) found three pyrrole rings per perchlorate anion ( $\text{ClO}_4^-$ ). The analysis of the inner structure of these polymers performed by scanning and transmission electron microscopy reveals that the doping process is inhomogeneous and the doping level must be considered as statistical (29). Electrochemical reduction of polypyrrole reduces the number of charged sites in the  $\pi$  structure of the polymer (Fig. 1-B). This results in the counterion leaving the film to maintain electroneutrality. There are no reports of doping with cations by the reduction of the neutral film.



A. Oxidized Polypyrrole Film



B. Neutral Polypyrrole Film

Fig. 1. Proposed stoichiometry of oxidized and neutral polypyrrole films.

## 2. Polymerization Mechanisms

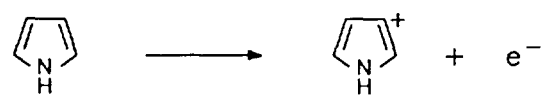
Although the mechanism of the electrochemical polymerization has been discussed by several group (2,29,35-37), a detailed mechanism has as yet to be unambiguously established. The generally accepted mechanism for the electrochemical polymerization of the polypyrrole film is radical coupling mechanisms as shown in Fig. 2 (36,37).

The first step in the electrochemical polymerization of pyrrole to polypyrrole is removal of one electron from the pyrrole monomer to form a positively charged radical cation by anodic oxidation (step 1). Since the radical cation species is unstable and highly reactive, it reacts immediately with a second radical cation of the monomer to give a dication (step 2). This dication then forms a neutral dimer by the elimination of two protons, which is more easily oxidized (step 3). Again, one electron is removed from dimer to form a positively charged radical dimer by anodic oxidation. The resulting cathonic dimer couples either with another cathonic dimer or radical cation to form a higher oligomer. Since dimers or higher oligomers are more easily oxidized than monomers, these could react further to build up the polymer chain (step 4).

The chain growth is terminated either when the radical cation of the growing chain becomes unreactive or, more likely, when the reactive end of the chain becomes sterically blocked (37). The final polymer chain bears a charge of unity for every three to four pyrrole rings, and this positive charge is counterbalanced by the anion which originates from the electrolyte salt. The deposition of polypyrrole on the surface of the electrode is described as a nucleation and growth mechanism very similar to the electrodeposition of metals (30,36)

Asavapiriyant *et al.* (30) concluded that the rate of polymerization is

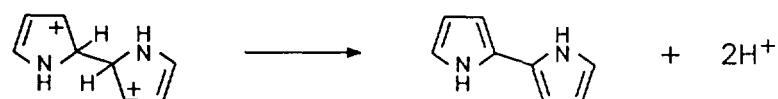
Step 1:



Step 2:



Step 3:



Step 4:



Fig. 2. Generally accepted mechanism for electrochemical polymerization of polypyrrole film.

controlled by the rate of electron transfer from the cyclic voltammetry and step potential experiments. However, Genies *et al.* (36) observed the coupling of the pyrrole radical cations to be the rate determining step. The role and positioning of the anion in the film remains one of the key questions in the electrochemical polymerization of conducting polypyrrole.

The radical coupling mechanism shown in Fig. 2 accounts for the following experimental observations regarding the polymerization reaction (35): a) electrochemical polymerization is a surface localized phenomenon. No evidence for polymerization in the bulk of the feed solution has been observed as expected from a polymerization mechanism where radical cations react with a neutral monomer, b) the polymerization of polypyrrole dimers (23) and trimers (38) has been demonstrated, c) the spectroelectrochemical experiments of Genies *et al.* (36) reveal that polypyrrole film deposition proceeds linearly with time. This observation is consistent with radical cation coupling as the rate limiting step of the polymerization reaction rather than diffusion, d) the elimination of the  $\alpha$  protons indicated by this mechanism is consistent with a decrease in the pH of the electrolyte solution during electrochemical polymerizations (29, 39). The loss of protons is commensurate with coupling of the radical cations as predicted, e) the number of electrons consumed in the polymerization of pyrrole, which has been estimated to be between 2.25 and 2.33 per pyrrole monomer, is consistent with the above mechanism. These numbers also agree with the number of anions found in the polymer films (40).

#### D. Electrochemical Properties

Electrochemically prepared polypyrrole films are electroactive and can be

switched between the neutral nonconducting state to the oxidized conducting state with a change of oxidation level. This change in oxidation level is accompanied by strong changes in both conductivity and spectral properties. The redox reaction is chemically reversible and can be driven repeatedly without loss of electroactivity. The conductivity of polypyrrole can change several orders of magnitude between the neutral and oxidized states. Because of the low oxidation potential of this polymer, it is very sensitive to oxygen in the atmosphere. Therefore, switching experiments must be performed in the absence of oxygen. Electrochemical switching between conducting and insulating states can be well presented by a cyclic voltammetry because thin films of the polymer exhibit well defined oxidation and reduction curves.

Typical cyclic voltammograms for a 20 nm polypyrrole film in 0.1M  $\text{Et}_4\text{NBF}_4-\text{CH}_3\text{CN}$  at scan rates of 10, 20, 40, 50, 60, 80, and 100 mV/sec are shown in Fig. 3 (40). At potentials negative of  $-0.3$  V versus SCE, the polypyrrole film is in its fully neutral nonconducting state. Anodic sweep of potential yields conversion of neutral polypyrrole to an oxidized, conducting state with increases in the capacitive background at potentials positive of  $-0.3$  V. At a potential  $+0.2$  V versus SCE, the oxidation reaction is completed and polypyrrole is in its fully oxidized conducting state. At potentials positive  $+0.2$  V versus SCE, polypyrrole film behaves like a capacitor and may be further charged. The large background capacitive currents in this region can be explained by that oxidized polypyrrole is porous to electrolyte with a high surface-to-volume ratio (41). If the potential is taken too positive, an irreversible loss of activity occurs. The loss of activity appears to occur gradually with increasing potential and has been attributed to a decrease in the conductivity of the film due to oxidation reactions

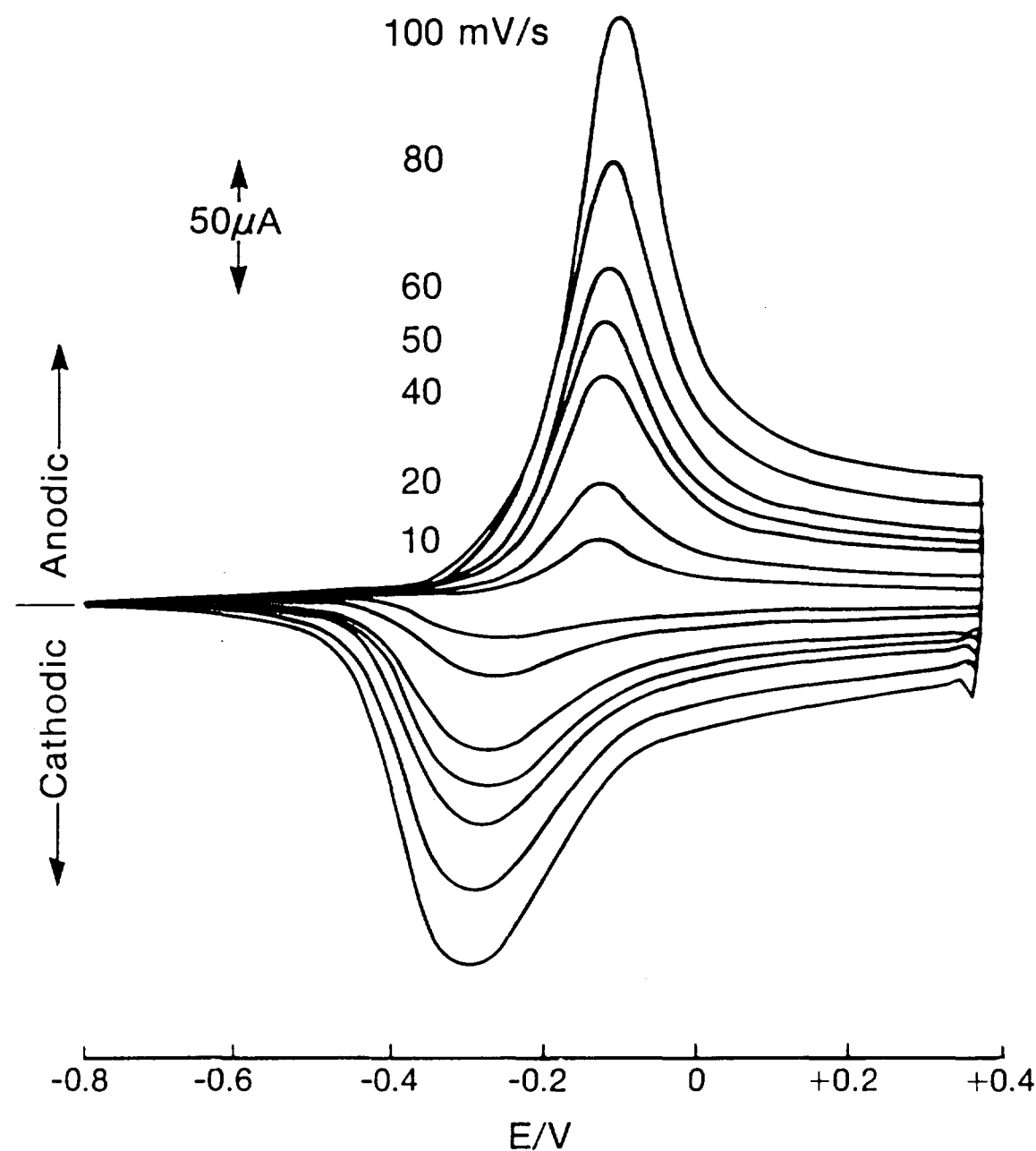


Fig. 3. Experimental cyclic voltammograms for a 20 nm polypyrrole film in 0.1M  $\text{Et}_4\text{NBF}_4\text{-CH}_3\text{CN}$  electrolyte.

which lead to loss of conjugation (30).

Cathodic sweep of potential yields conversion of oxidized polypyrrole to neutral, nonconducting state with decreases in the capacitive background current at potentials negative of +0.2 V. At a potential -0.5 V versus SCE, polypyrrole is again in its fully neutral state. Extending potentials to negative direction had little effect on the properties of polypyrrole films. This process can be done repeatedly with no evidence of decomposition of the polymer in the absence of oxygen.

The cyclic voltammograms of electronically conducting polypyrrole are not symmetrical. The shape of the anodic and cathodic current responses and the difference between anodic and cathodic peak potentials suggest that the electrochemical reaction of polypyrrole is quasi-reversible and that the reduction and oxidation kinetics may be limited by a slow ion diffusion in the film or by a slow electron transfer process. It has been observed that the cathodic peak is significantly broader than the anodic peak, and that the oxidation capacitive current is higher than the corresponding reduction current. The broadening of the observed cathodic peak is currently not well understood, but it could reflect the electrochemical nonequivalence of redox sites in the polypyrrole film. These effects can be explained on the basis of a large uncompensated resistance caused by the neutral polymer film (42). In the neutral state, polypyrrole has a high ionic resistance because of the presence of an ion gate. Both anodic and cathodic voltammograms are broader than expected for a Nernstian redox couple.

A distinctive color change accompanies the redox reaction involving polypyrrole polymer (30,40). The colors observed reflect the solid state electronic properties of the polymer in each of its redox states. Oxidized conducting polypyrrole

is brown-black due to the existence of interband electronic transitions. In contrast, neutral, nonconducting polypyrrole is light yellow due to the existence of a substantial band-gap. In the neutral state, yellow polypyrrole has a strong absorption band in the ultraviolet-blue range and the absorption in the visible range increases when the film is oxidized, giving the coating a brown color (43). The yellow color of polypyrrole during electrochemical cycling of the polymer between neutral and oxidized redox states indicates that the polymer is quantitatively reduced.

AC impedance measurements also have been used to characterize electrochemical properties of polypyrrole films, especially the nature and the origin of a large capacitance taking place in the oxidized polymer. Most of the experimental data obtained from these studies are analyzed in terms of an "equivalent circuit", an electrical circuit which is considered to model correctly the electrical behavior of the electrode interface when its calculated impedance, as a function of frequency, agrees with the experimentally determined impedance behavior.

AC impedance studies of polypyrrole by Burgmayer *et al.* (44,45) and Tanguy *et al.* (46,47) have employed relatively thick ( $\geq 5$  mm) films. Such films cannot be quantitatively addressed electrochemically, i.e., the as-synthesized oxidized polymer cannot be quantitatively reduced (3,36). Consequently, the extraction of mass transport and kinetic information from these data is not straight forward.

Bull *et al.* (41) examined the AC impedance behavior of thin polypyrrole films over a broad frequency band. They discussed results only in the potential region around +0.1 V versus SCE, where negligible faradaic processes occur, and did not consider mass transport in the analysis of these data. In this region, the

admittance can primarily be attributed to double layer charging. Penner *et al.* (48) demonstrated that both mass transport and structural information can be gleaned from AC impedance analysis. They interpreted the AC impedance data in the context of the limiting behavior of thin polypyrrole film for neutral and fully oxidized states.

Because of complexities in the switching process of polypyrrole film, these studies have employed only limiting cases of polypyrrole films, either at low doping level (where only faradaic reaction occurs) or at high doping level (where only double layer charging occurs). At intermediate states, significant concentrations of both oxidized and neutral polypyrrole are present in the film, which makes it a good electronic conductor. The electrochemical properties (such as, conductivity, diffusivity, differential capacitance, etc.,) are varied with oxidation state of polypyrrole film. Under these circumstances, the conventional equivalent circuits model is not adequate to describe the AC impedance responses of the polypyrrole film. Recently, Hauser *et al.* (49) presented a more realistic approach to the analysis of AC impedance data. Their approach, which is based on a mechanistic modeling approach as opposed to a circuit analog modeling approach for analysis of AC impedance data, shows the possibility to be adequate for conducting polymers.

The majority of conductivity ( $\sigma$ ) measurements have been carried out by Diaz *et al.* (33,50). These workers measured the room temperature conductivity, using a four-probe technique, and found values in the range  $10^{-3}$ - $200 \Omega^{-1} \text{cm}^{-1}$  depending on the nature of the anion present. The  $T^{\frac{1}{4}}$  temperature dependence of  $\log \sigma$  for fully oxidized polypyrrole has been observed between a temperature range of 10 to 220 K independent of the type of dopant anion as observed for

polyacetylene and other polyheterocycles (51-53). The dependency of electronic conductivity of polypyrrole on the nature of the anion present will be discussed in a later section.

The stability of polypyrrole is an important factor affecting its potential application. Among various aspects of the stability, the most important aspect is loss of conductivity as a function of time and exposure to various chemical environment. Erlandson *et al.* (54) and Cvetko *et al.* (55) studied the change in conductivity as a function of time and exposure to oxygen and water. These results show that the conductivity is fairly stable over time, but does depend on the polymerization conditions and the chemical environment. The presence of oxygen increases the degradation rate, while a mixture of oxygen and water vapor increases the rate even further. Diaz *et al.* (50) showed that polypyrrole was stable at elevated temperatures up to 200°C, depending on the nature of the anion. In addition, degradation due to electrolyte conditions, particularly the pH, is also important. Polypyrrole is also quite stable in the pH range 1 to 7 (39), but partially reversible loss of conductivity occurs above pH 7 because the nitrogen in the pyrrole rings tend to become deprotonated (17,56).

## E. Transport Properties

### 1. Electronic Transport

The origin of the electronic conductivity of polymers arises from a state of relative oxidation or reduction (57,58). In such states, the polymer loses (for oxidation) or gains (for reduction) electrons. The number of monomer units which gain or lose electrons is variable but a reasonable estimate is one electron per three monomer units (29).

Once the polymer is electronically charged, counterions from the solution enter the polymer fibril to produce electrostatic neutrality. It is these ions which are often referred to as dopants. However, this is not doping in the sense of semiconductor doping, where the dopant provides charge carriers. In conducting polymers, the charge carriers are generated within the polymer chain. On the other hand, it is convenient to refer to the counterions in the charged polymers as dopants.

Considering the polymer in terms of a semiconducting material and using the band structure model (59,60), oxidation and electron loss give rise to new energy states. Removal of one electron from a  $\pi$  bond leaves the remaining electron in a nonbonding orbital-different in energy from the valence and conduction states. These states are above the valence band and they give rise to the behavior of the polymer as though it were a heavily doped semiconductor.

The most commonly accepted conduction mechanism (57-60) is polaron and bipolaron formation upon oxidation. Oxidation of the polymer breaks one double bond, leaving a radical and a positive charge on the polymer chain which is commonly referred to as a polaron. Polarons converge into bipolaron when the polaron concentration gets high enough for the polarons to “feel” each other. The radical-cations are spread out through the adjacent  $\pi$  structure across approximately eight bond lengths, making contact with other radical cations. The combination of the two radicals (one from each polaron) forms a new  $\pi$  bond which is commonly referred to as a bipolaron. The bipolaron is more stable than the two radical-cation bonds at the same distance apart (i.e., the  $\Delta G$  of the bipolaron is greater than  $\Delta G$  of dissociations of the two polarons). The bipolarons are then free to hop along the polymer chain, which gives rise to the

electronic conductivity.

The electron hopping mechanisms proposed for the polyheterocyclics to date can be divided into three distinct categories: variants of Mott's variable range electron-hopping theory (61), polaron or bipolaron interchain hopping theory (62), and phonon-assisted hopping mechanisms (63). The essential features of these three mechanisms and several variants which have been recently proposed are discussed next.

i) Variable Range Hopping (VRH) Model – This model was proposed in 1969 to explain the electronic conductivity of crystalline semiconductors cooled to liquid helium temperatures so as to suppress band conduction (61). Currently, the VRH model is most often associated with the description of electron transport in amorphous semiconductor such as Ge, Si, III-V compound (53,64).

In conducting polyheterocycles, localized states (charge carriers) are introduced to the band-gap with the creation of polarons or bipolarons in addition to the electronic states present in the band-gap as a consequence of structural disorder in the polymer (53). In the application of the VRH model to the conducting polyheterocycles, carrier sites are assumed to be stationary, intersite distance are variable, and electron-hopping occurs in three dimensions. It should be noted that hopping is not assumed to be isoenergetic as it is in both of the other models discussed here. The rate of thermally-activated electron-hopping between localized sites is determined by the average difference in energy between them and by the extent of the wave function overlap.

The VRH theory predicts a  $T^{-\frac{1}{4}}$  temperature dependence of  $\log \sigma$ , as observed for polyacetylene and other polyheterocycles (53). However, several authors have noted that the density of electronic states at the Fermi level,

$N(E_F)$ , estimated from electron spin resonance (ESR) measurements are lower than that necessary to accommodate the  $\sigma$  values measured for both polypyrrole and polyacetylene (62,65). In addition, the thermoelectric power observed for polypyrrole or polyacetylene is not in agreement with model predictions.

On the basis of these data, Shen *et al.* (65) extended Mott's theory by considering localized states (bipolarons) which are mobile on a segment of conjugated polymer. Thus, electronic transport occurs as a composite process involving the "sliding" of a bipolaron on a conjugated polymer segment in conjunction with electron-hopping across defects and between chains. Better agreement for the thermoelectric power and values for  $N(E_F)$  were obtained with preliminary experimental data for polypyrrole samples prepared in aqueous electrolytes using this theory (65).

ii) Bipolaron Hopping Model – Polaron hopping mechanisms have previously competed with VRH theory to account for the mechanism of electronic transport in amorphous semiconductor (53,62). Chance *et al.* (62,66) have attempted to account qualitatively for electronic transport in the polyheterocycles at low doping levels with a model which considers interchain transport of charge via bipolaron hopping. They noted that interchain conduction pathways are likely to limit the macroscopically observed conductivity regardless of the mechanism proposed to account for intrachain charge transport (62,66). On this basis, it was assumed that ionization of an electronically conductive polymer yields localized charge carriers (solitons or bipolarons) which possess little intrachain mobility (62,66). A reduced potential energy barrier for the hopping process in *trans*-polyacetylene is achieved by coupling solitons to bipolarons (soliton pairs) which extend over just five lattice spaces (62). Consequently, bipolaron hopping is

assumed to account for interchain and intrachain charge transport in both *trans*-polyacetylene and in polymers like polypyrrole which do not possess a degenerate ground state and hence inherently possess bipolarons.

As compared to the Mott's mechanism, bipolaron hopping predicts truly spinless conductivity (62). However, the unique feature of this mechanism is the unusual conductivity versus % doping relation it predicts as a result of the fact that the bipolaron charge carriers cannot hop to other occupied sites in the polymer. Thus, the maximum contribution to the conductivity from bipolaron hopping occurs at intermediate doping levels, and reduced conductivity is predicted to result from doping in excess of this optimum level (62,66).

Unfortunately, comparison of this prediction is not possible in the case of polypyrrole since conductivity ( $\sigma$ ) versus concentration of bipolaron charge carriers data have not been reported for the polyheterocycles (62). However, satisfactory agreement with experimental data is obtained with the analogous bipolaron hopping expression for polyacetylene (62). The current expression of bipolaron hopping theory is relatively crude and entirely qualitative. Extensions are required before theoretically predicted thermoelectric power, Hall effect, and  $\log \sigma$  versus temperature relations can be done and compared with experimental measurements.

It should be noted that Chance *et al.* (66) proposed the bipolaron hopping mechanism to account for the electronic conductivity of a lightly doped system only. The argument is more advanced in that at moderate doping levels, the activation barrier for electron hopping is reduced by the overlap of charge carriers on the polymer chain and a delocalized conduction pathway develops.

iii) Soliton Hopping Model – Kivelson's three dimensional version (63), which

is a extension of the one-dimensional soliton hopping mechanism proposed by Su *et al.* (67), for transport in *trans*-polyacetylene also attempts to account for the mechanism of conduction at low doping levels. Since this model relies on the presence of both charged and uncharged carrier defects (solitons), its predictions are relevant to *trans*-polyacetylene only. In spite of this fundamental limitation, Pfluger *et al.* (53) have noted that this model may assist in the formulation of future models for phonon-assisted hopping between charged bipolaron sites in polyheterocycles because the transport data predicted with this model is in excellent agreement with experiment.

The Kivelson model assumes that the polymer is structurally disordered, and that localized electronic states are randomly distributed. The existence of significant numbers of both charged and neutral localized sites is also assumed in accordance with the observation of neutral solitons by ESR in lightly doped polyacetylene. It is likely that charged solitons are strongly pinned at low doping levels by electrostatically bound counterions whereas neutral solitons are highly mobile. Electronic transport is effected by the isoenergetic phonon-assisted hopping of electrons between charged and uncharged solitons.

Despite the success achieved by this model in predicting electronic transport data for *trans*-polyacetylene, the Kivelson model has generated considerable controversy. Ngai *et al.* (68) have questioned several of the assumptions inherent in the derivation of the Kivelson model. Chance *et al.* (66) have noted that a weakness of the Kivelson model is its dependence on an extrinsic factor, namely a substantial neutral soliton concentration, for the mechanism of conduction. In any case, elements of this model are likely to be employed in future electronic transport models appropriate for the polyheterocycles.

Despite numerous investigations in this area, the actual charge transport mechanisms by which these films conduct remain illusive.

## 2. Mass Transport

The unavailability of accurate values for the transport properties of electronically conducting polypyrroles has limited the characterization of these polymers. For example, the characterization of the ionic conductivity of polypyrrole membranes is limited by the absence of reliable permeability data. Diaz *et al.* (40,69) described polypyrrole as a densely packed, nonporous material principally on the basis of cyclic voltammetry of electroactive species. Noufi *et al.* (70), however, demonstrated both incorporation and mobility of  $\text{Fe}(\text{CN})_6^{3-}$  ions in polypyrrole. In addition, the photocorrosion of a polypyrrole coated semiconductor photoanode, although slowed by the polypyrrole film, seems to be associated with the permeability to solution species, since changes in solvent and electrolyte affect the rate of corrosion. Bull *et al.* (41) concluded from the AC impedance of oxidized polypyrrole films on solid electrodes that the polypyrrole films were quite permeable to solvent and electrolyte, and that the best description of the films behavior as an electronically conducting coating was as a porous electrode with electrochemical reactions occurring at both polypyrrole-solution interfaces and the solid electrode beneath the polypyrrole coating. This has been attributed to the large interfacial contact surface between the polymer and the electrolyte.

Additional evidence for the porosity of the polypyrrole film comes from the fact that electrochemical reactions occur at the substrate as in the oxidation of Si electrodes, although the reaction is considerably slower than with uncoated electrode (71,72). These observations suggest that polypyrrole cannot be considered simply as a nonporous metallic film. Burgmayer *et al.* (42) directly measured per-

meation rates for electrolytes through the polypyrrole membrane and concluded that the porosity characteristics lay somewhere between the limits suggested by Diaz *et al.* (40) and Bull *et al.* (41). They found the permeation rate of anion in the oxidized polypyrrole to be much faster than that in the neutral polypyrrole. This of course is the basis for the ion gate.

Based on these conclusions, attempts to estimate the apparent diffusion coefficients for counterions within the polypyrrole film have been conducted by several groups (73-76). Genies *et al.* (73) estimated the diffusion coefficient for  $\text{ClO}_4^-$  counterion in polypyrrole films as a function of the concentration of  $\text{LiClO}_4$  in the acetonitrile by using conventional chronocoulometry and chronoabsorptometry. The apparent diffusion coefficient was found between  $1.0 \times 10^{-10}$  and  $1.0 \times 10^{-9}$   $\text{cm}^2/\text{sec}$ , depending on the electrolyte concentration. However, the diffusion coefficient information derived from either of these experiments is unreliable because large capacitive current and uncompensated resistance effects in polypyrrole films were not considered.

Penner *et al.* (74) obtained apparent diffusion coefficients for  $\text{BF}_4^-$  within polypyrrole films in  $\text{Et}_4\text{NBF}_4$ /acetonitrile by use of a low amplitude current pulse technique. They found apparent diffusion coefficient values of  $4.0 \times 10^{-9}$  to  $8.0 \times 10^{-9}$   $\text{cm}^2/\text{sec}$ , depending on the polypyrrole film thickness. This analysis possesses several advantages for the determination of diffusion coefficients as compared to conventional chronocoulometry because the perturbation of the film redox state during the low amplitude current pulse experiment is extremely small.

Transient techniques have been also employed to estimate the apparent diffusion coefficient of  $\text{ClO}_4^-$  counterion in the polypyrrole films by Naoi *et. al* (75) and Panero *et al.* (76). The values found are in the range between  $2.0 \times 10^{-10}$

$\text{cm}^2/\text{sec}$  and  $3.0 \times 10^{-10} \text{ cm}^2/\text{sec}$ . The transient techniques, however, are not appropriate for the conducting polymers, unless proper account is taken of the influence of the polymer geometry.

The analysis shows that the values of the apparent diffusion coefficient of the counterions obtained with the doping process are larger than those obtained with the undoping process. It may be concluded that diffusion in polypyrrole film is a more complicated process than simply involving anions entering into the polymer as oxidation proceeds and leaving as reduction occurs. There is evidence from Kaufman *et al.* (77) and Chao *et al.* (78) that the diffusion process includes anions and cations. These results suggest that a realistic diffusion model should consider different mechanisms for the doping and undoping processes.

Another unsettled issue for transport properties of polypyrrole is the rate of electrochemical charge transport during redox reactions of the polymer itself and the effect of ion mobility on the rate. The shape sensitivity of the cyclic voltammogram suggests that the mobility of both the cation and the anion effect the kinetics of the polymer redox reaction but not the thermodynamics since the potentials corresponding to peak currents are essentially unshifted in various electrolytes (33,40). The rate at which polypyrrole can be charged and discharged between its oxidized and neutral states is very significant, especially in its application as an energy storage device. This rate is controlled primarily by the rate at which electrochemical charge can be propagated through the polymer. Unfortunately, because of its electronic conductivity, high surface area and associated large double layer charging currents, the usual method for investigating the rate of charge transport characterization (i.e., chronoamperometry) cannot be used for polypyrrole.

A few theoretical studies have been conducted on the characterization of the charge transport mechanisms within polypyrrole films. Feldberg (79) suggested a Butler-Volmer type reaction rate expression for the quasi-reversible switching behavior and a linear dependency of differential capacitance on doping level. However, this work failed to include the transport effect (diffusion and migration) of the counterion in the redox reaction rate. Pickup *et al.* (80) developed mathematical models, plane electrode and porous electrode models, for potential step chronoamperometry to study charging and discharging rate of polypyrrole film. They concluded that a porous electrode model has better prediction than a planar electrode model. However, their porous electrode model is not satisfactory because it is based on the assumption that faradaic reactions are negligible.

#### F. Dependency of Properties on Polymerization Conditions

It has been demonstrated that the microscopic structures and the properties of the polypyrrole films depend on polymerization conditions. Some of the variables which influence these properties and which can be controlled in the electrochemical environment are the substrate electrode material (71,81-85), solvent (1,16,17,42,51), electrolyte salt (1,33,36), driving force (31,86-90), pH (30), and temperature (55,87,88,91). Consequently, numbers of studies have been done to determine and optimize the polymerization conditions.

##### 1. Electrodes

The nature of the substrate electrode is critical in the preparation of polypyrrole films, particularly the adhesion of the film to the substrate. Since the films are produced by an oxidative process, it is important that the electrode does not oxidize concurrently with the aromatic monomer. For this reason,

most of the available films have been prepared using a platinum or a gold electrode. Metals such as silver, aluminum, indium, or iron, which oxidize more readily than the pyrrole monomer, would obviously not be good choices for the electrode (81). Polypyrrole films can also be prepared using a variety of semiconducting materials, including tin oxide, n-type polycrystalline silicon (71), gallium arsenide (82), cadmium sulfide and cadmium selenide (83), and graphite (84). Polymerizations on platinum and glassy carbon electrodes produce better adhering films than on tin oxide or single crystal n-type silicon (85).

## 2. Solvents

The polymerization reaction proceeds via radical cation intermediates. Therefore, the progress of this reaction will be sensitive to the nucleophilicity of the environment in the region near the electrode surface. This then places some limitations on the choice of solvent and electrolyte. For this reason, most of the reported studies have been performed in poor nucleophilic aromatic solvents. The effect of these solvents on the quality of polypyrrole films is shown in Table II (1). Among these, acetonitrile has been the most commonly used solvent, although a wide variety of other aromatic solvents can be used as long as the nucleophilic character of the solvent is poor. However, certain nucleophilic aromatic solvents (such as, dimethylformamide) and hydroxylic solvents can also be used to prepare good films if the nucleophilicity of the solution can be reduced using protic acids.

The ionic conductivity of polypyrrole film can be influenced by electrolytic conditions. Burgmayer *et al.* (42) investigated the effect on the ionic conductivity of polypyrrole, by varying type of solvent and electrolyte in the electropolymerization and assessing the results with measurement of in-phase impedance. The

Table II. Solvent effects on the quality of the polypyrrole films.

Solvent/Electrolyte	Film Quality	Electronic Conductivity ( $\Omega^{-1}\text{cm}^{-1}$ )
Acetonitrile/0.1M TEAT <sup>†</sup>	Good	50.0
Acetonitrile/0.1M Toluenesulfonic Acid	Good	50.0
Acetonitrile/0.1M TEAT+1M Pyridine	No	-
Methylene Chloride/0.1M TBAT <sup>‡</sup>	Good	50.0
Butanone/0.1M TBAT	Good	40.0
Propylene Carbonate/0.1M TBAT	Good	50.0
Dimethylformamide/0.1M TEAT	No	-
Dimethylformamide/0.1M Toluenesulfonic Acid	Good	20.0
Dimethylsulfoxide/0.1M TEAT	No	-
Hexamethylphosphoramide/0.1M TEAT	No	-
Ethanol/0.1M TBAT	Bad	0.2
Ethanol/0.1M Toluenesulfonic Acid	Good	3.0
Ethanol/0.1M Sulfuric Acid	Good	3.0
Ethanol/0.1M Phosphoric Acid	No	-
Ethanol/0.1M Hydrochloric Acid	Bad	-

<sup>†</sup>TEAT(Tetrachylammonium Tetrafluoroborate)

<sup>‡</sup>TBAT(Tetrabutylammonium Tetrafluoroborate)

results showed that a solvent can alter the ionic conductivity of the resulting polymer. The change in ionic conductivity must reflect a microscopic structural change in the polymer that ensued during electropolymerization. Also, they observed that the electropolymerizing polymer film grows approximately two times faster in water than in acetonitrile. According to their results, the original choice of perchlorate in acetonitrile solvent gave a polypyrrole film with the lowest oxidized ionic resistance, which means the most desirable response. In contrast, ionic conductivity changes in counterions have much smaller effect.

Water content in the electrolyte also influences the performance of polypyrrole film. Diaz *et al.* (16,17,51) reported that films grown in anhydrous acetonitrile have a rough surface with dendrite-like structure as shown by scanning electron microscopy, while presence of as little as 1% H<sub>2</sub>O or other hydroxylic solvents led to much smoother and more adherent films.

### 3. Electrolytes

With regards to the electrolyte salt, the main considerations are the solubility, degree of dissociation, and the nucleophilicity (1). Most of the salts used are tetraalkylammonium salts, because they are soluble in arotic solvents and dissociate quite easily. Although some lithium salts are soluble in arotic solvents, these salts are highly aggregated. Most sodium and potassium salts show poor solubility in arotic solvents.

The stability of the incipient cation of the electrolyte salt is an important factor to be taken into consideration for the formation of the polymer film. Film formation results from pyrrole cation intermediates with moderate stability favoring the radical coupling reaction. The more stable cations of the electrolyte salt diffuse away from the electrode surface and produce soluble products. The

very reactive cations of the electrolyte salt react indiscriminately with solvent and other nucleophiles in the region of the electrode surface thereby, minimizing the polymer forming reaction.

The electrochemically synthesized conducting polypyrrole films contain 10-35% anions (by weight) which are affiliated with the cationically charged polymer chains to produce electrostatic neutrality (33). The amount of anion found in each film is governed by the doping level of the polymer and it is characteristic of each film. The anions listed in Table III are poor nucleophiles commonly used in the preparation of good quality films. Common counterions to produce good polypyrrole film in nonaqueous solvents includes  $\text{BF}_4^-$ ,  $\text{ClO}_4^-$ , and  $\text{PF}_6^-$ . Sulfonates are commonly used anions in aqueous solvents. The doping level of polypyrrole is 0.25-0.32 per pyrrole unit, corresponding to one anion for every 3-4 pyrrole units. The doping level is an intrinsic characteristic of the polymer and is not sensitive to the nature of the anion. However, the anion does influence both the structural properties and the electroactivities of the films. The size and electronic structure of the anion affect both the conductivity and the structural properties of polypyrrole. In addition, good films are typically not produced when the anion is a halide, because halides are fairly nucleophilic and easily oxidized. Highly nucleophilic anions, such as hydroxide, alkoxide, cyanide, acetate, and benzoate do not produce good quality films either but instead lead to soluble products.

The anion influences the electrical properties of the films which are in the oxidized form (33). Because the counterion acts to separate polymer chains within the bulk, a larger counterion creates a larger chain separation, and therefore, a larger distance over which charge must hop to get from one chain to

Table III. Anion effects on the properties of the polypyrrole films.<sup>†</sup>

Doped Anion	Maximal Doping Level	Density (g/cm <sup>3</sup> )	Electronic Conductivity (Ω <sup>-1</sup> cm <sup>-1</sup> )
Tetrafluoroborate (BF <sub>4</sub> <sup>-</sup> )	0.32	1.48	30-100
Hexafluoroarsenate (PF <sub>6</sub> <sup>-</sup> )	0.32	1.48	30-100
Hexafluorophosphate (AsF <sub>6</sub> <sup>-</sup> )	0.32	1.48	30-100
Perchlorate (ClO <sub>4</sub> <sup>-</sup> )	0.30	1.51	60-200
Hydrogensulfate (HSO <sub>4</sub> <sup>-</sup> )	0.30	1.58	0.3
Fluorosulfonate (FSO <sub>3</sub> <sup>-</sup> )	-	1.47	0.01
Trifluoromethylsulfonate (CF <sub>3</sub> SO <sub>3</sub> <sup>-</sup> )	0.31	1.48	0.3-1
p-Bromobenzenesulfonate (BrC <sub>6</sub> H <sub>4</sub> SO <sub>3</sub> <sup>-</sup> )	0.33	1.58	50
p-Toluenesulfonate (CH <sub>3</sub> C <sub>6</sub> H <sub>4</sub> SO <sub>3</sub> <sup>-</sup> )	0.32	1.37	20-100
Trifluoroacetate (CF <sub>3</sub> COO <sup>-</sup> )	0.25	1.45	12

<sup>†</sup>Tetraalkylammonium salts used

the next. The dependence of room temperature conductivity on the nature of the anion present in the electrolyte is shown in Table III (33). In general, the films with perfluoride or perchlorate anions are more conducting than the films with the sulfonate and carboxylate anions. Exceptions are films containing aromatic sulfonate anions.

The size and shape of the counterion also affect the structural and mechanical properties of polypyrrole films. As shown in Fig. 4, the topology of the surface is dramatically different for polypyrrole films containing various anions. The difference observed between the surfaces are not reflected in the packing structure of the bulk material. Therefore, all the films have similar flotation densities which fall in the range 1.45-1.51 g/cm<sup>3</sup>. In a similar manner, the mechanical properties of the films change with the type of anion in the electrolyte. Polypyrrole films containing toluenesulfonate, perchlorate, and fluoroborate anions are hard and strong films and stretch very little (4-5% elongation at break). However, the films containing toluenesulfonate anion are stronger and have a tensile strength 30-40% higher than for other films. The values of conductivity, elongation, and module are similar for these films.

The temperature sensitivity of the electrical properties of the films is also influenced by the nature of the anion. Film with fluoroborate, fluorophosphate, perchlorate, nitrate, and toluenesulfonate anions can be heated to approximately 160°C in air before they begin to decompose. Furthermore, the change in conductivity with temperature is very mild, 10-50% per 100°. Films with toluenesulfonate and trifluoroacetate anions can be heated to 280°C before they begin to decompose. The conductivity of the latter films increases by a factor of 3-5% per 100° increase in temperature, with the less conducting film showing

the biggest change.

Anions also show a strong influence on electroactivity. Several authors (33,36) have investigated the sensitivity of cyclic voltammetric behavior to the use of different counterions in electrochemical polymerization. Since the rate of switching is limited by the mobility of the anion in and out of the film, the switching rates are very sensitive to the anion. This rate dependency on the anion gives rise to very complicated cyclic voltammograms which represent the combined faradaic and capacitive currents. Anions influence only the kinetics of the reaction and not the switching potential.

#### 4. Driving Forces

It has been shown that polypyrrole can be electrochemically synthesized by controlled potential or controlled current (31,86-90). The conductivity, polymer structure, stability, and electroactivity are found to be a function of the choice of driving force (current or potential) and the magnitude of that on the polymerization.

The effects of the driving force on the electronic conductivity of polypyrrole films have been investigated by several groups (86-88). Hahn *et al.* (86) investigated a conductivity of polypyrrole films as a function of applied current density. Their analysis show a maximum conductivity of polypyrrole films prepared at constant current density of  $0.75 \text{ mA/cm}^2$ . Maddison *et al.* (87) also investigated a maximum conductivity for polypyrrole films as function of current density, but found at a current density of  $2.8 \text{ mA/cm}^2$ . In contrast to the acetonitrile used by Hahn *et al.*, they utilized an aqueous electrolyte. Satoh *et al.* (88) examined the effect of applied potential on the electronic conductivity. Their results show a maximum conductivity at potential of +0.6 V versus SCE,

where a value of  $500 \Omega^{-1} \text{cm}^{-1}$  is obtained. The conductivities of films prepared at potentials above or below +0.6 V versus SCE rapidly fell to below  $100 \Omega^{-1} \text{cm}^{-1}$ .

The applied potential or current on polymerization also affects the structural of polypyrrole films. Polypyrrole films formed at a relatively high anodic potential or current (89,90) were observed to have a porous morphology. Anions incorporated in the polypyrrole film lattice were found to accompany a smooth doping and undoping reaction because of their rough polymer structure. Although polypyrrole films so obtained may show a high charging-discharging efficiency, they have defects in mechanical strength and in the degree to which they adhere to the substrate.

Otero *et al.* (31) prepared polypyrrole films from acetonitrile solution containing lithium perchlorate under varying conditions of potential control: constant potential, square wave potential step, and potential sweep methods. The resulting films were analyzed by scanning electron microscopy. The square wave potential step method produced polypyrrole films having a smoother surface, that adhered more strongly to the platinum substrate. These characteristics increased with a decrease in the step duration, that is, a more rapid cycling of the potential resulted in smoother, more adherent films.

## 5. Others

Other factors which have been shown to affect the properties of polypyrrole films include the pH of the electrolyte used for synthesis, and the temperature under which the synthesis is carried out. In acid solution, the polypyrrole films become rougher and even take on a powdery appearance (6,30). In alkaline solution, only thin films may be grown and this may imply that a very compact film free of pores (essential at least for anion movement in the film) is formed

(30). Satoh *et al.* (88) investigated the effects of polymerization temperature of the electrolyte, and observed a maximum conductivity of polypyrrole films grown at a temperature of 10°C.

#### G. Modifications of Properties

Further encouraging features of the pyrrole polymer system were the degrees of freedom available to modify the electrical and physical properties by resorting to particular anions, derivatives, or copolymers in order to achieve any desired matrix of polymer properties. Several strategies directed at improving the properties of polypyrrole have been proposed recently (92-104).

There is now abundant experimental evidence to support the contention that the rate of polypyrrole redox reaction is limited by the mass transport of charge compensating ions in the polymer phase (36,40,41). The amorphous morphology of the polypyrrole, to compare polyacetylene, produces slower counterion transfer rates and results in slow electrochemical kinetics (i.e., low current density). Application of polypyrrole as a battery material requires that polypyrrole charge and discharge quickly (69). To synthesize conducting polymer films with a well-defined morphology generally involves the formation of a polypyrrole film within a somewhat porous host membrane, and a subsequent dissolution of the host membrane. Penner *et al.* (92) introduced a fibrillar-microporous morphology, in which polymer chains are organized into narrow fibers surrounded by micropores. Nuclepore polycarbonate membranes, which are soluble in dichloromethane, were used as the porous host membranes. An interesting and potentially useful attribute of this approach is that the conducting element can be grown to any desired diameter and thickness within the host material. Naoi *et al.* (75,93)

reported the superiority of the charging-discharging performance of lithium batteries employing modified polypyrrole with nitril rubber. The polypyrrole film formed with the aid of nitril rubber showed a highly enhanced anion doping-undoping process because it has a rough, porous structure in the direction perpendicular to the current collector substrate. Thus, it should be possible to improve the performance of polymer based devices by employing such transport optimized films.

The other class of techniques investigated is the formation of composites. De Paoli *et al.* (94,95) have prepared poly(vinyl chloride)-polypyrrole composite membranes by electropolymerizing pyrrole inside a poly(vinyl chloride) film on an electrode surface. Although these composites had the desirable mechanical properties of the poly(vinyl chloride) host and the high conductivity of the polypyrrole, poly(vinyl chloride) is not the ideal host material because it is neither porous nor conductive. Lindsey *et al.* (96) have demonstrated that polypyrrole can be deposited within the matrix of several swellable polymers to form a conducting composite. This composite membrane shows conductivities as high as  $10 \Omega^{-1}\text{cm}^{-1}$  and excellent mechanical properties which make the membrane easier to fold without cracking.

Fan *et al.* (97) prepared polypyrrole film in matrices of Nafion and clay (hectorite) by electropolymerization. These films display higher electronic conductivity and stability than films made of polypyrrole alone. Penner *et al.* (98) showed that electronically conducting composite membranes can be prepared by electropolymerizing pyrrole within Nafion-impregnated Gore-Tex (NiGT), which has an open-end porous structure. The electronic conductivity of the polypyrrole doped NiGT membrane is essentially identical to the conductivity of polypyrrole.

Novák *et al.* (99,100) prepared polypyrrole and polyethylene oxide composite polymer film. This composite polymer shows enhanced coulomb capacity and poor charge retention as compared to polypyrrole itself.

Copolymer formation is another technique for the production of conducting membranes. A variety of copolymers can be prepared by varying the nature, number, and ratios of polymers that are copolymerized with polypyrrole. Nazzal *et al.* (101) had prepared pyrrole and styrene copolymer films. The films vary in their properties, depending on the ratio of styrene to pyrrole. Films with a high concentration of styrene had electrical conductivities of about  $10 \Omega^{-1}\text{cm}^{-1}$  with mechanical properties similar to polystyrene. On the other hand, films with a low concentration of styrene had higher conductivities, about  $50 \Omega^{-1}\text{cm}^{-1}$ , with mechanical properties similar to polypyrrole tetrafluoroborate.

Also, attempts have been made to copolymerize different kinds of heterocyclic compounds, and electrochemical properties of the resulting copolymers have briefly been studied. So far copolymers of pyrrole and N-methyl pyrrole (19), pyrrole and phenol (102), pyrrole and terthienyl (103), and pyrrole and thiophene (104) have been prepared by electrolytic oxidation of mixtures of monomers.

Consequently, by appropriate choice of the polymerization condition or composite formation, satisfactory electrochemical and mechanical properties can be achieved for a particular application of polypyrrole.

#### H. Applications

Commercially significant applications of electronically conducting polypyrrole films are most likely to stem from their unique properties and characteristics, the exact combination of which is not offered by any other material. These ap-

plications are on the area of energy storage (105-110), solar energy conversion (85,111-116), electrochromic display devices (40,43,50,117), etc.

### 1. Energy Storage Devices

The most common application of these polymer films has been in the area of energy storage and distribution. The main properties of polypyrrole films which make them attractive as electrode materials in the high-energy-density secondary battery technologies are ease of preparation, electrochemical redox behavior, high electrical conductivity, and ease of property modification. These polymers also offer flexible design characteristics.

Indeed, lithium/polypyrrole rechargeable batteries are under study in various laboratories with some encouraging preliminary results (105-110). They have demonstrated the charge/discharge behavior of lithium/polypyrrole cells and reported a open circuit voltage of 3.0-4.0 V, an energy density of 50-200 Wh/kg, and a power density of 200 W/kg. These results indicate that conducting polypyrrole films can be used as positive electrodes in rechargeable lithium organic electrolyte batteries, with good promise of long cycleability and high charge/discharge efficiency.

However, there are some major problems which appear to limit the applicability of these polymer electrode. The morphology of polypyrrole, which is relatively amorphous compare to polyacetylene, has been a major stumbling block in the development of the polypyrrole secondary battery system. The morphology of polypyroles determines the facility of counterion transport and the rate of the electrochemical reaction of the dopants within polypyrrole film (105,106). Other problems are the lack of stability even in hermetically sealed environments, the poor stability of the organic solvent against a high open circuit voltage, the self

discharge of the polymer in the electrolytic medium, and their cost compared to alternative battery systems.

## 2. Solar Energy Devices

The conducting polymer can serve as an enhancer of properties for the basic components in solar energy cells and photoelectric devices. It is of significant importance to enhance the stability against the photodegradation of semiconductor photoanodes in electrochemical photovoltaic cells. The polypyrrole films can be grown on n-type semiconductor electrodes (such as, Si, GaAs, CdS, CdSe, and CdTe) in the photoelectrochemical cells by photo assisted electrochemical oxidation of the pyrrole monomer (71,82,85,111-115). Cooper *et al.* (116) showed that thin layer of polypyrrole deposited on n-type photoanodes can efficiently transfer charge over large distances and effectively inhibit the dissolution or oxidation of the n-type semiconductor, thus extending lifetime of photoelectrochemical cells.

A problem encountered with this application is that the film does not adhere to the electrode surface over a long period of time. Efforts are being made to solve this problem. For example, Fan *et al.* (112) and Skotheim *et al.* (113) reported an improvement in film adhesion by metallizing the Si surface prior to polymerization of the pyrrole. Other methods of improving the film adhesion include chemical binding of the film to the electrode (85,115).

## 3. Electrochromic Display Devices

Electrochromic effect is defined as a change of the visible absorption coefficient (a color change) induced in a material by the passage of a charge (an applied electric field or current). It has been demonstrated by many laboratories that polypyrrole films are brown-black in the doped state and light yellow in

the undoped state. A color change proceeds as a result of the insertion of ions from an electrolyte and electrons from an electrode. In the neutral state, yellow polypyrrole has a strong absorption band in the ultraviolet-blue range and the absorption in the visible range increases when the film is oxidized, giving the coating a brown color (40,50,117). This feature makes electronically conducting polypyrrole an attractive candidate for electrochromic display.

Response times are less than 100 msec and are acceptable, but lifetime is a problem ( $10^5$  cycles is the best) and does not compete with the lifetime obtained with inorganic electrochromic materials such as tungsten oxide ( $10^6$  cycles). Further improvements in contrast ratio, switching speed, and long-term stability are required before polypyrrole can gain general acceptance for use in display devices (43).

#### 4. Others

Recently, applications of organic conducting polymers, polypyrrole, poly-thiophene, etc., to electronic devices have been investigated by several workers; some devices are totally organic and the others are partially organic (118-121). Characteristics of these polymers, which are often very different from those of inorganic materials, enable us to fabricate new types of electronic devices which are superior to the conventional ones. By utilizing these polymers, memory devices (45,118,119), p-n junctions (120), and molecular based transistors (121) have been fabricated. Moreover, organic conducting polymers can be made with various kinds of functional molecules incorporated in their matrices, such as organic dyes, metal-organic compounds, biomolecules, etc.

Conducting pyrrole polymers have also found application in catalysis. Bull *et al.* (84) incorporated tetrasulfonated iron phthalocyanine anion in polypyrrole

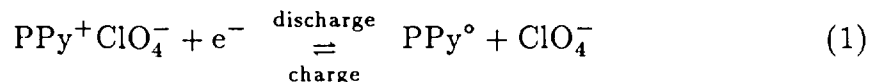
film and demonstrated that the films catalyzed the reaction of oxygen on glassy carbon electrodes, at potentials 250-800 mV less negative than at bare glassy carbon or glassy carbon electrodes coated with polypyrrole containing noncatalytic ions.

Polypyrrole membranes offer a lower resistance to ion transport when the polymer is in the neutral state and a higher resistance when in the oxidized state (44,45). For these reasons, they have been employed as electronically control ion-gates.

### III. MATHEMATICAL TREATMENT OF MATERIALS

#### A. Electrochemistry

The electrochemical reaction occurring at the polypyrrole electrode is known to be a doping-undoping process. That is, the polypyrrole itself loses electrons and gains dopants in its structure during the doping process, while it gains electrons and releases dopants during the undoping process



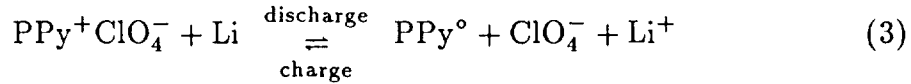
where  $\text{PPy}^\circ$  and  $\text{PPy}^+$  are the neutral and oxidized forms of polypyrrole. The counterion ( $\text{ClO}_4^-$ ) is incorporated into the solid structure of polypyrrole to produce electrostatic neutrality and is referred to as the dopant.

It is noted that the oxidized polypyrrole is generally believed to be comprised of localized defect states in the form of polarons (radical cations) at low doping levels and bipolarons (dication) at high doping levels. Of course, the doping process is inhomogeneous and must be considered as statistical. To avoid these complexities and inhomogeneities, a volume averaged doping level (i.e., the ratio of one doped anion to the number of pyrrole monomer units) is used to describe the doping (oxidation) state of polypyrrole without regards to the actual amount of polaron and bipolaron in the local polymer chain.

The electrochemical reaction at the lithium electrode is known to be the dissolution and deposition of the lithium cation as follows:



Therefore, the overall reaction within the lithium/polypyrrole secondary battery cell becomes



These equations can be written in Newman's general notation (122) as

$$\sum_i s_{j,i} M_i^{z_i} = n_j e^- \quad (4)$$

where  $s_{j,i}$  represents stoichiometric coefficient of species  $i$  for reaction  $j$ ,  $M_i$  represents the symbol for the chemical formula of species  $i$ ,  $z_i$  represents the charge number of species  $i$ , and  $n_j$  represents number of electrons transferred for reaction  $j$ . It should be noted that  $s_{j,i}$  has a positive or negative value depending on whether species  $i$  is an anodic or a cathodic reactant, respectively. That is, according to Eqs. [1] and [2]

$$\begin{aligned} s_{1,\text{Li}^+} &= 0 \\ s_{2,\text{Li}^+} &= -1 \\ s_{1,\text{ClO}_4^-} &= +1 \\ s_{2,\text{ClO}_4^-} &= 0 \end{aligned} \quad [5]$$

From the discussion above, it can be seen that the cation and anion of the electrolyte are responsible for the electrons produced or consumed at the electrode, such that

$$\sum_i s_{j,i} z_i = -n_j \quad (6)$$

## B. Properties of 1M LiClO<sub>4</sub>-PC Electrolyte

The electrolyte in this study consists of 1M LiClO<sub>4</sub> in propylene carbonate and is referred to as a binary electrolyte because it is assumed that LiClO<sub>4</sub>

dissociates in propylene carbonate into charged  $\text{Li}^+$  and  $\text{ClO}_4^-$  species (123). Propylene carbonate is chosen as a solvent because it is a polar nonaqueous solvent which is stable, nontoxic, and can easily be purified. Because of its high dielectric constant, it can serve as a good solvent for different inorganic salts.

Various measurements of the physical and structural properties of 1M  $\text{LiClO}_4\text{-PC}$  were conducted by Keller *et al.* (123). Among those properties, the imports are density ( $\rho_s$ ), viscosity ( $\mu$ ), equivalent molar conductance ( $\Lambda$ ), and transference number ( $t_i$ ). The density and viscosity were determined by a pycnometer and a viscometer with an accuracy of three decimal places. The equivalent molar conductance was calculated by a graphical extrapolation of the equivalent conductance plotted vs. the square root of the concentration and was reported as  $5.640 \text{ cm}^2/\Omega\text{-mol}$ . The transference number of a  $\text{Li}^+$  was reported as 0.19 by the Hittorf method.

The necessary parameter values, which are currently not available from literature or experimental work, can be obtained from experimental measurements and theoretical relationships. The kinematic viscosity ( $\nu$ ) can be obtained by (122)

$$\nu = \frac{\mu}{\rho_s} \quad (7)$$

The ionic equivalent conductance of species  $i$  ( $\lambda_i$ ) in a binary electrolyte can be obtained by (122)

$$\lambda_i = t_i \Lambda \quad (8)$$

and is related to the ionic mobility of species  $i$  ( $u_i$ ) as follows (122):

$$u_i = \frac{\lambda_i}{|z_i|F^2} \quad (9)$$

The ionic diffusion coefficient for species  $i$  ( $D_i$ ) can be then obtained by the

Nernst Einstein equation (122)

$$D_i = RT u_i \quad (10)$$

The physical and transport properties of 1M LiClO<sub>4</sub>-PC electrolyte discussed above are summarized in Table IV.

### C. Properties of Polypyrrole

Despite extensive work at a large number of laboratories (25-117), properties of the polypyrrole film are far from being understood. This is because of its complexity in the switching process and high reactivity toward air and moisture. Only a few measurements of the properties have been reported, and these are

Table IV. Properties of 1M LiClO<sub>4</sub>-PC electrolyte at 25°C.

#### A. Experimental Measurements.<sup>†</sup>

Density ( $\rho_s$ )	1.254 g/cm <sup>3</sup>
Viscosity ( $\mu$ )	70.80 mg/cm-sec
Equivalent Conductance ( $\Lambda$ )	5.640 cm <sup>2</sup> /Ω-mol
Transference Number of Li <sup>+</sup> ( $t_+$ )	0.190
Transference Number of ClO <sub>4</sub> <sup>-</sup> ( $t_-$ )	0.810

<sup>†</sup> Obtained from Ref. (123)

#### B. Theoretical Calculations.<sup>‡</sup>

Kinematic viscosity ( $\nu$ )	0.056 cm <sup>2</sup> /sec
Ionic Conductance of Li <sup>+</sup> ( $\lambda_+$ )	1.072 cm <sup>2</sup> /Ω-mol
Ionic Conductance of ClO <sub>4</sub> <sup>-</sup> ( $\lambda_-$ )	4.568 cm <sup>2</sup> /Ω-mol
Ionic Mobility of Li <sup>+</sup> ( $u_+$ )	$1.151 \times 10^{-9}$ cm <sup>2</sup> -mol/J-sec
Ionic Mobility of ClO <sub>4</sub> <sup>-</sup> ( $u_-$ )	$4.907 \times 10^{-10}$ cm <sup>2</sup> -mol/J-sec
Diffusion Coefficient of Li <sup>+</sup> ( $D_+$ )	$2.853 \times 10^{-7}$ cm <sup>2</sup> /sec
Diffusion Coefficient of ClO <sub>4</sub> <sup>-</sup> ( $D_-$ )	$1.216 \times 10^{-6}$ cm <sup>2</sup> /sec

<sup>‡</sup> Calculated using relationship given by Ref. (122)

limited to the fully oxidized or neutral states as summarized in Table V (33). The necessary parameter values at the intermediate state, which are currently not available from the literature or experimental work, can be approximated as functions of the doping level,  $\lambda$  (i.e., the ratio of one doped anion to the number of pyrrole monomer units).

It is convenient to define the fractional doping level of polypyrrole film,  $\theta$ , as a function of the doping level as follows:

$$\theta = \frac{\lambda}{\lambda_{\max}} \quad (11)$$

where  $\lambda_{\max}$  represents the doping level of fully oxidized state. Since  $\theta$  varies linearly with the amount of oxidized polypyrrole,  $\theta$  can be expressed by the local faradaic charge of the polypyrrole film,  $Q_f$ , as follows:

$$\theta = \frac{Q_f - Q_{f,\text{red}}}{Q_{f,\text{oxd}} - Q_{f,\text{red}}} \quad (12)$$

where the subscripts, oxd and red, represent the fully oxidized and neutral states. It is noted that  $\theta = 0$  for a fully neutral state of polypyrrole with a minimal faradaic charge,  $Q_{f,\text{red}}$ , and  $\theta = 1$  for a fully oxidized state of polypyrrole with a maximal faradaic charge,  $Q_{f,\text{oxd}}$ .

The microscopic structures and the properties of the polypyrrole film at intermediate state can be considered as functions of  $\theta$  as summarized in Table

Table V. Properties of polypyrrole film doped with perchlorate.

Properties	Oxidized State	Neutral State
Doping Level ( $\lambda$ )	0.30	0.00
Density ( $\rho$ )	1.51 g/cm <sup>3</sup>	-
Conductivity ( $\sigma_p$ )	200.0 /Ω-cm	1.0×10 <sup>-5</sup> /Ω-cm

VI. The porosity of the polypyrrole film,  $\epsilon_p$ , is governed by a material balance on the solid phase because the density of the polypyrrole changes with doping level due to the amount of doped anion, and can be expressed in terms of  $\theta$  as follows:

$$\epsilon_p = \theta\epsilon_{\text{oxd}} + (1 - \theta)\epsilon_{\text{red}} \quad (13)$$

where  $\theta$  represents the amount of oxidized polypyrrole and  $(1 - \theta)$  represents the amount of neutral polypyrrole. The electronic conductivity of polypyrrole film ( $\sigma_p$ ) is also obtained in a same manner:

$$\sigma_p = \theta\sigma_{\text{oxd}} + (1 - \theta)\sigma_{\text{red}} \quad (14)$$

The faradaic charge ( $Q_f$ ) at the intermediate state can be expressed as a function of the electrochemical reaction rate which is discussed next in detail.

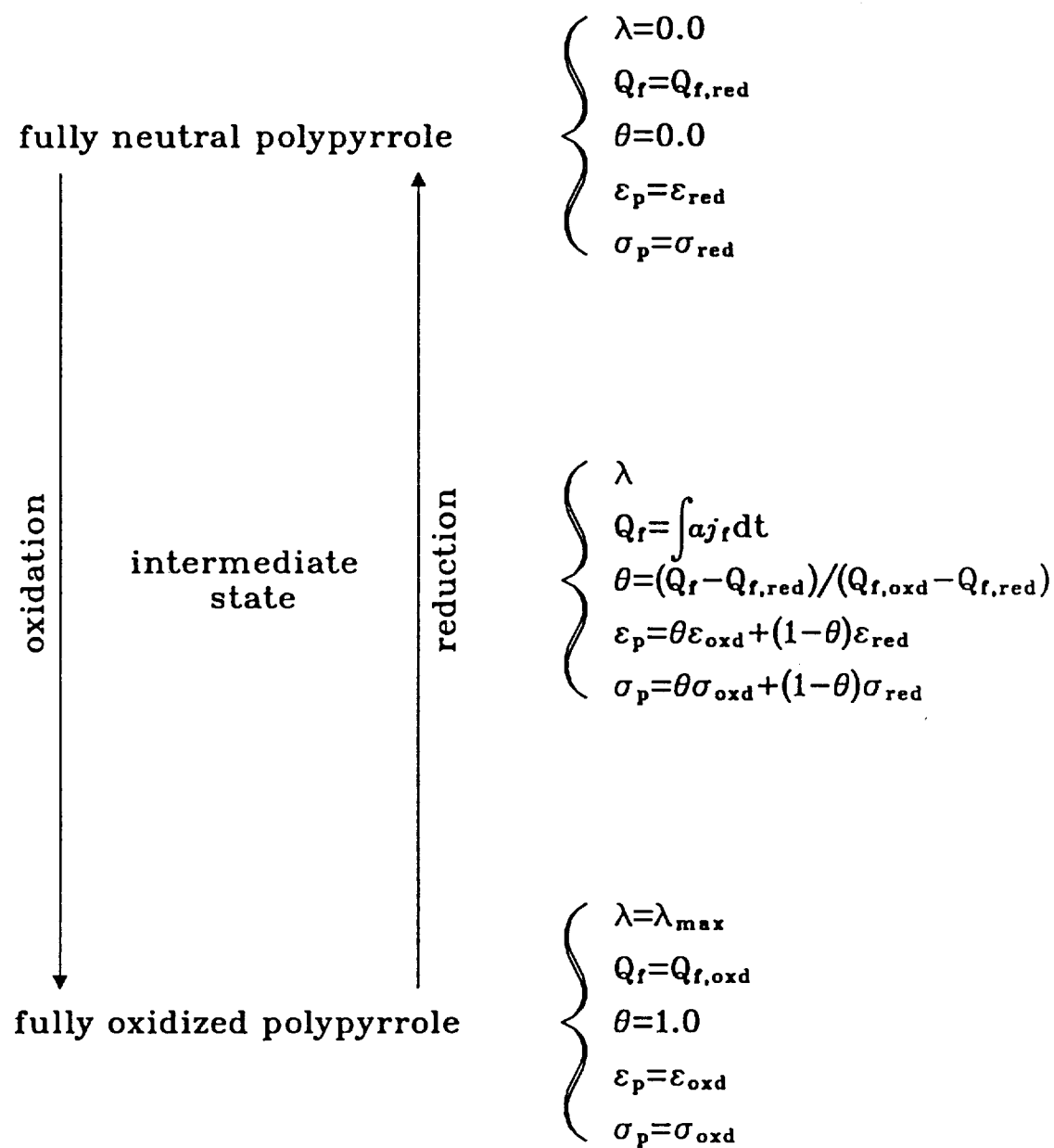
#### D. Electrochemical Reaction Rate of Polypyrrole

The reaction at the polypyrrole electrode described in Eq. [1] is assumed to be a pseudo-homogeneous reaction. The reaction rate during charge/discharge is controlled primarily by the available electroactive area and the transport (diffusion and migration) of the counterion to the electrode surface. This rate can be expressed by the local faradaic transfer current per unit volume (current transferred per unit volume of polypyrrole electrode by electrochemical reaction [1]), which is assumed to be represented by the Butler-Volmer equation as

$$aj_f = ai_{\text{o1,ref}} \left\{ \left(1 - \theta\right) \left( \frac{c_-}{c_{-,ref}} \right) \exp\left(\frac{\alpha_{\text{a1}} F}{RT} \eta_1\right) - \theta \exp\left(\frac{-\alpha_{\text{c1}} F}{RT} \eta_1\right) \right\} \quad (15)$$

where  $a$  is the specific interfacial area per unit volume,  $i_{\text{o1,ref}}$  is the exchange current density for reaction [1] at a given reference concentration ( $c_{\text{i,ref}}$ ),  $\alpha_{\text{a1}}$

Table VI. Properties of polypyrrole film as a function of its oxidation state.



and  $\alpha_{c1}$  are anodic and cathodic transfer coefficients, and  $\eta_1$  is the overpotential for the reaction [1]. The term  $a(1 - \theta)$  represents the available electroactive area for oxidation (amount of neutral polypyrrole sites) and  $a\theta$  represents the available electroactive area for reduction (amount of oxidized polypyrrole sites). Anodic and cathodic current components are taken to be positive and negative, respectively. Note also that  $\alpha_{a1} + \alpha_{c1} = n_1$ .

The overpotential is defined as

$$\eta_1 = (\Phi_1 - \Phi_{ref}) - (\Phi_2 - \Phi_{ref}) - U_1 \quad (16)$$

where  $\Phi_1$  is the potential in the solid phase,  $\Phi_2$  is the potential in the solution phase,  $\Phi_{ref}$  is the reference potential, and  $U_1$  is the theoretical open circuit potential for reaction [1] at the given concentration ( $c_i$ ).  $U_1$  is given by

$$U_1 = U_{1,ref} - \frac{RT}{n_1 F} \ln\left(\frac{\theta}{1-\theta}\right) \quad (17)$$

where  $U_{1,ref}$  is the open circuit potential for reaction [1] at a given reference concentration ( $c_{i,ref}$ ). It can be seen that the local transfer current predicted by the Butler-Volmer kinetic expression, Eq. [15], depends on the difference between the potential of the solid phase ( $\Phi_1$ ) and that of the adjacent solution within the porous electrode ( $\Phi_2$ ). The kinetic parameter values used to simulate the electrochemical reaction rate of the polypyrrole film are summarized in Table

Table VII. Kinetic parameter values used for polypyrrole.

Exchange Current Density ( $a i_{o1,ref}$ )	10.0 A/cm <sup>3</sup> <sup>†</sup>
Anodic Transfer Coefficient ( $\alpha_{a1}$ )	0.7 <sup>†</sup>
Cathodic Transfer Coefficient ( $\alpha_{c1}$ )	0.3 <sup>†</sup>
Open Circuit Potential ( $U_{1,ref}$ )	3.087 V (vs. Li)
Number of Electron ( $n_1$ )	1

<sup>†</sup> Estimated values

VII. The estimated value of each parameter was obtained by statistical comparison between the experimental results and model predictions and is discussed in a later section.

#### E. Electrochemical Reaction Rate of Lithium

$\text{Li}/\text{Li}^+$  electrode is quite stable in  $\text{LiClO}_4\text{-PC}$  solutions in the absence of impurities in the electrolyte (124). Micropolarization tests on a lithium rod about the equilibrium potential indicate only ohmic losses. Lithium deposits at (nearly) 100% faradaic efficiency. The lithium electrode also exhibits a reversible Nernstian behavior (125).

The rate of electrochemical reaction at the lithium electrode in Eq. [2] during charge and discharge processes is controlled primarily by the transport (diffusion and migration) of lithium cations and can be approximated by the Butler-Volmer equation as follows:

$$j_2 = i_{o2,\text{ref}} \left\{ \exp\left(\frac{\alpha_{a2}F}{RT}\eta_2\right) - \exp\left(\frac{-\alpha_{c2}F}{RT}\eta_2\right) \right\} \quad (18)$$

where  $j_2$  is local faradaic transfer current density for reaction [2],  $i_{o2,\text{ref}}$  is the exchange current density for reaction [2] at a given reference concentration ( $c_{i,\text{ref}}$ ),  $\alpha_{a2}$  and  $\alpha_{c2}$  are the transfer coefficients for the anodic and the cathodic reactions, and  $\eta_2$  is the overpotential for reaction [2]. Again  $\alpha_{a2} + \alpha_{c2} = n_2$ .

The overpotential is defined as

$$\eta_2 = (\Phi_1 - \Phi_{\text{ref}}) - (\Phi_2 - \Phi_{\text{ref}}) - U_2 \quad (19)$$

where  $U_2$  is the theoretical open circuit potential for reaction [2] at the given concentration ( $c_i$ ) and is given by

$$U_2 = U_{2,\text{ref}} - \frac{RT}{n_2 F} \ln\left(\frac{c_i}{c_{i,\text{ref}}}\right) \quad (20)$$

where  $U_{2,\text{ref}}$  is the open circuit potential for reaction [2] at a given reference concentration ( $c_{i,\text{ref}}$ ).

The kinetic parameter values used to simulate the electrochemical reaction rate of the lithium electrode are summarized in Table VIII. Li/Li<sup>+</sup> has a high exchange current density ( $i_{o2,\text{ref}}$ ) in 1M LiClO<sub>4</sub>-PC solution of the order of 2-5 mA/cm<sup>2</sup> for a smooth surface, and a value for the cathodic transfer coefficient ( $\alpha_{c2}$ ) in the range 0.66 to 0.72 (126).

Table VIII. Kinetic parameter values used for lithium.

Exchange Current Density ( $i_{o2,\text{ref}}$ )	0.002 A/cm <sup>2</sup> <sup>†</sup>
Anodic Transfer Coefficient ( $\alpha_{a2}$ )	0.3 <sup>†</sup>
Cathodic Transfer Coefficient ( $\alpha_{c2}$ )	0.7 <sup>†</sup>
Open Circuit Potential ( $U_{2,\text{ref}}$ )	0.0 V (vs. Li)
Number of Electron ( $n_2$ )	1

<sup>†</sup> Obtained from Ref. (126)

#### IV. CYCLIC VOLTAMMETRY

In recent years, considerable research effort has been expended on the characterizations of electronically conducting polypyrrole films (25-117). As the results of these studies, electronically conductive polypyrrole films have been approved as potential materials which have technological applications in the area of conductors, organic batteries, and display devices. However, many questions still remain about properties of polypyrrole. Among those unsettled problems, the electronic and ionic charge transport mechanisms within the polypyrrole films have been fundamentally important since the rate of the polymer redox reaction under most circumstances is controlled by these factors. Thus, an understanding of charge transport in these polymers is a prerequisite to further technological applications.

Among the available electroanalytical techniques, the cyclic voltammetry technique has been widely used to understand the electroactivity and the electrochemical properties of polypyrrole films because it can better describe the characteristics of the switching behavior between conducting and nonconducting states (40-43). General experimental cyclic voltammograms of polypyrrole film approximate the behavior of a quasi-reversible couple with the distinct characteristic of a large capacitive background current.

In this chapter, experimental and simulated cyclic voltammetry of 1  $\mu\text{m}$  polypyrrole doped with perchlorate are performed in 1M LiClO<sub>4</sub>-PC solution. Both results are obtained from identical conditions and compared with each other to clarify the electrochemical reaction mechanisms and charge transport phenomena within the polypyrrole films.

In the mathematical modeling, the current density responses are analyzed in terms of the faradaic and capacitive current components associated with the electrochemical switching of a polypyrrole film between the insulating and conducting states (79). The model is used to characterize dynamic behavior (i.e., the relationship between polymer morphology, charge transport, and electrochemical characteristics) within the polypyrrole films by studying the effects of various parameters.

#### A. Experimental Descriptions

A single-compartment electrochemical cell used for the experiments is schematically presented in Fig. 5. The cell contains a platinum rotating disk electrode coated with polypyrrole film as a working electrode, a platinum counter electrode, a saturated calomel reference electrode (SCE), and a 1M LiClO<sub>4</sub>-PC electrolyte. A rotating disk electrode (RDE) is used here because of its well-defined hydrodynamics (127,128). A luggin capillary tip of the reference electrode is placed as close as possible to the center of the polypyrrole working electrode surface. This enables one to minimize ohmic loss and to use the reference electrode to detect the solution potential near the working electrode. The system is deoxygenated throughout experiments by nitrogen bubbling. The electrodeposition of thin polypyrrole film on the surface of platinum disk electrode is discussed in Appendix A.

Cyclic voltammetry is accomplished using an EG&G Princeton Applied Research (PAR) Model 173 potentiostat/galvanostat in conjunction with a PAR Model 175 programmer, and resulting current density responses are recorded on an IBM AT personal computer.

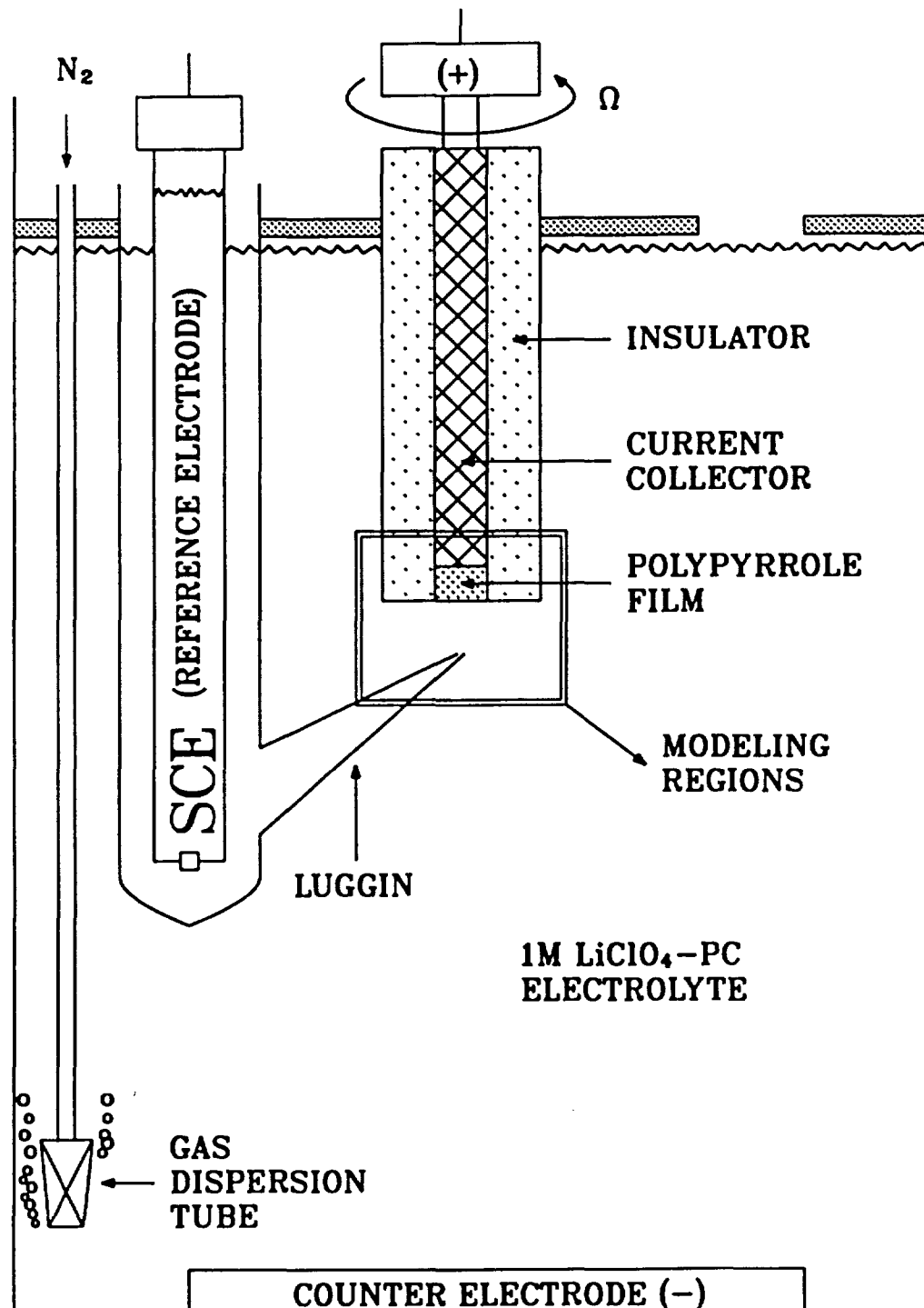


Fig. 5. A schematic diagram of a single-compartment electrochemical cell with a rotating disk electrode.

## B. Model Descriptions

The model presented here is for predicting the cyclic voltammetric behavior of the polypyrrole films doped with perchlorate. The modeling regions close to the rotating disk electrode, which are relevant to the development of the model equations, are schematically presented in Fig. 6.

The modeling regions consist of two main regions, two boundaries, and one inter-regional interface, and must be modeled simultaneously. These are the boundary interface between a platinum current collector and the polypyrrole electrode ( $y = 0$ ); the polypyrrole electrode region of width  $\delta_{pp}$ ; the inter-regional interface between the polypyrrole electrode and an electrolyte diffusion layer ( $y = y_{pp}$ ); the electrolyte diffusion layer of width  $\delta_{dl}$ ; and the boundary at a bulk electrolyte solution ( $y = y_{dl}$ ).

In all of the regions, the dependent variables are: the concentration of  $\text{Li}^+$  ( $c_+$ ), the concentration of  $\text{ClO}_4^-$  ( $c_-$ ), the local faradaic charge per unit volume ( $Q_f$ ), the potential of the solid phase ( $\Phi_1$ ), and the potential of the solution phase ( $\Phi_2$ ). Because the cyclic voltammetry controlled by sweeping potential at a constant scan rate, values for these unknowns depend on the perpendicular distance from the platinum current collector of the polypyrrole electrode ( $y$ ) and applied potential ( $E$ ), and they are obtained by solving the system of governing equations and assumptions for each region of the cell described next in detail.

### 1. Governing Equations – Polypyrrole Electrode Region

Polypyrrole electrode region has a porous structure and consists of a solid phase of polypyrrole and a solution phase of an organic electrolyte that penetrates the void spaces in the porous structure as shown in Fig. 6. It is assumed that the polypyrrole film and the void space are continuous to conduct electronically and

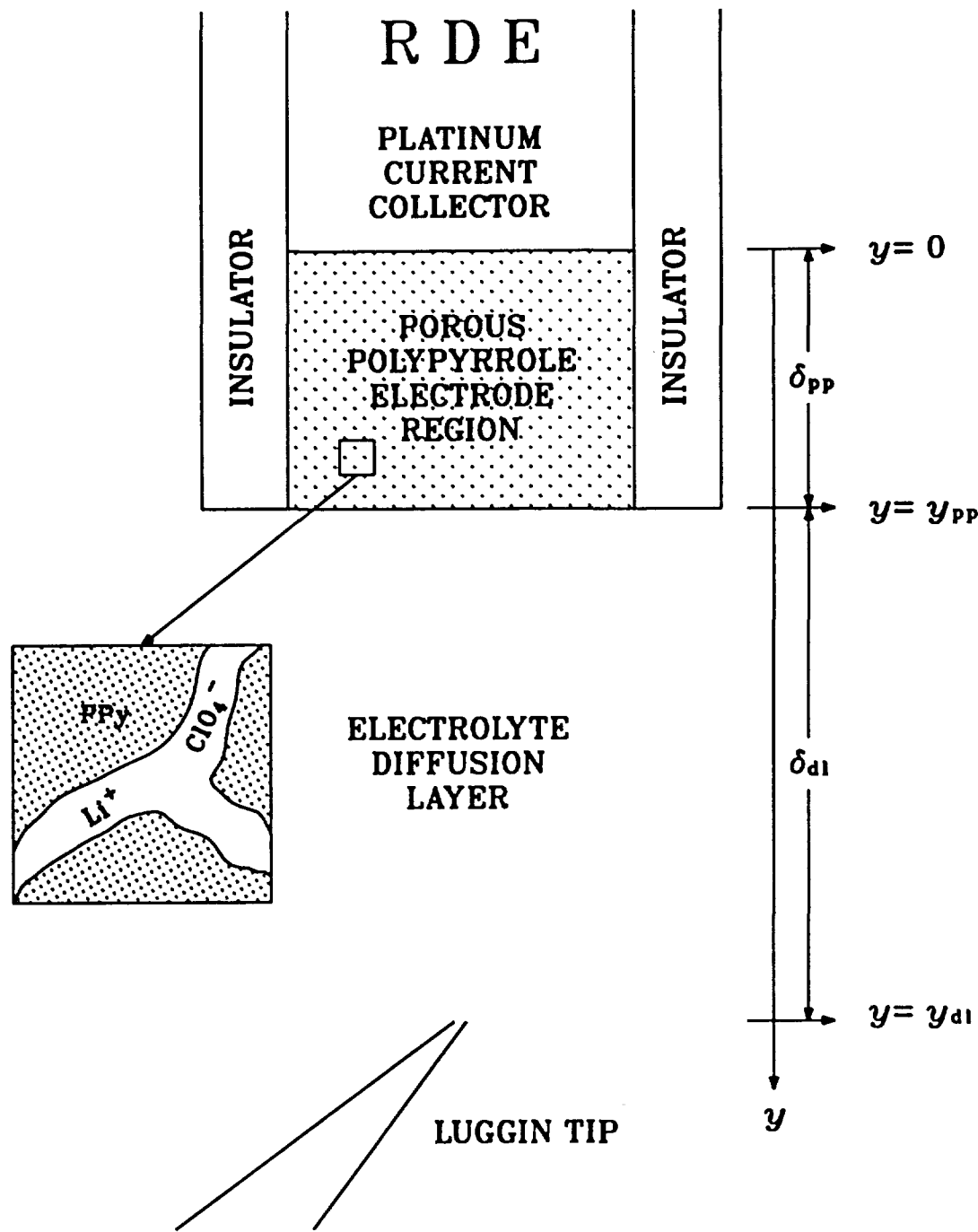


Fig. 6. A schematic diagram of modeling regions closed to the rotating disk electrode in the single-compartment electrochemical cell.

ionically (51). The solid polypyrrole has a non-homogeneous structure because of its impurities and structural defects (such as, crosslinking, reticulation, etc.). To account for the non-homogeneous nature of microscopic structure of polypyrrole, a porous electrode theory, where the details of the pore geometry are ignored and the entire porous structure is regarded as a single pseudo-homogeneous mixture, has been employed (129). That is, macroscopic properties and volume averaging technique are used to describe physically the porous material in terms of simple measurable parameters without regards to the actual geometrical details of the pore structure. An extensive discussion of volume averaging technique has been given by Dunning (130), Trainham (131), and Whitaker (132).

Two of macroscopic properties used here are a porosity ( $\epsilon_p$ ) and a tortuosity ( $\tau$ ). The porosity represents the void volume fraction occupied by the electrolyte within the volume element. The tortuosity represents structural defects of polymer chain. Here, the tortuosity is assumed to be related simply to the porosity as follows (133):

$$\tau = \epsilon_p^{-ex} \quad (21)$$

where ex is a proportional constant.

The properties of the electrolyte occupied the void spaces of the porous polypyrrole electrode (diffusivity, mobility, conductivity, etc.) must be modified to account for the porous nature of this region. The effective diffusivity ( $D_{i,p}$ ) and mobility ( $u_{i,p}$ ) of species i within the porous structure are related to the free stream diffusivity ( $D_i$ ) and mobility ( $u_i$ ) as follows (133):

$$D_{i,p} = D_i \epsilon_p^{1+ex} \quad (22)$$

$$u_{i,p} = u_i \epsilon_p^{1+ex} \quad (23)$$

The effective solution conductivity ( $\kappa_p$ ) within the porous structure is also related to the free stream solution conductivity ( $\kappa$ ) as follows:

$$\kappa_p = \kappa \epsilon_p^{1+ex} \quad (24)$$

and free stream solution conductivity ( $\kappa$ ) can be expressed as

$$\kappa = F^2 \sum_i z_i^2 u_i c_i \quad (25)$$

where  $c_i$  represents the concentration of species i.

#### Material Balance for Dissolved Species

The differential material balance equation in the solution phase is formulated for a dissolved species i in terms of average quantities as follows (129):

$$\frac{\partial(\epsilon_p c_i)}{\partial t} = -\nabla \cdot \mathbf{N}_{i,p} + R'_{1,i} \quad (26)$$

where  $c_i$  represents the concentration of species i per unit volume of electrolyte within the porous matrix,  $\epsilon_p c_i$  represents the average concentration per total unit volume including the solid polymer phase and the electrolyte that occupies the space within the matrix,  $\mathbf{N}_{i,p}$  represents the flux of species i within the porous region, and  $R'_{1,i}$  represents the consumption or production rate of species i.

The flux of species i within the porous polypyrrole electrode region ( $\mathbf{N}_{i,p}$ ) is due to migration in the electric field and diffusion in the concentration gradient, and is expressed as follows (129):

$$\mathbf{N}_{i,p} = -z_i u_{i,p} F c_i \nabla \Phi_2 - D_{i,p} \nabla c_i \quad (27)$$

where  $\Phi_2$  is the potential in the solution phase within the porous region. It is assumed that there is no convective flow within the porous region. That is, there

is no bulk flow through the pores and fresh feed must diffuse and migrate to the reactive sites within the porous region. This assumption seems reasonable as long as the thickness of the porous electrode ( $\delta_{pp}$ ) is much less than the electrolyte diffusion layer ( $\delta_{dl}$ ).

The consumption or production rate of species i within porous polypyrrole electrode region ( $R'_{1,i}$ ) is due to both the electrochemical reaction [1] and double layer charging. For oxidation, anions are doped to the polypyrrole structure by the electrochemical reaction [1]. Also, anions are attracted to the polypyrrole electrode surface for the double layer charging, while cations are repelled. For reduction, opposite effect hold. Anions are undoped from the polypyrrole structure by the electrochemical reaction [1] and are repelled because of double layer effects. Thus,  $R'_{1,i}$  becomes

$$R'_{1,i} = -\frac{s_{1,i}aj_1}{n_1 F} \quad (28)$$

The term,  $aj_1$ , represents the local transfer current per unit volume (i.e., current passed per unit volume of electrode, A/cm<sup>3</sup>) and is discussed below in detail. No homogeneous and heterogeneous chemical reactions are considered here.

A one dimensional material balance equation for species i can be obtained by combining the normal component of Eqs. [26], [27], and [28] as follows:

$$\frac{\partial(\epsilon_p c_i)}{\partial t} = z_i F \frac{\partial}{\partial y} \left( u_{i,p} c_i \frac{\partial \Phi_2}{\partial y} \right) + \frac{\partial}{\partial y} \left( D_{i,p} \frac{\partial c_i}{\partial y} \right) - \frac{s_{1,i}aj_1}{n_1 F} \quad (29)$$

### Charge Balance

The local charge accumulated within the porous polypyrrole electrode per unit volume,  $Q$ , is defined to be the sum of the local faradaic and capacitive charges per unit volume,  $Q_f$  and  $Q_c$ , as follows:

$$Q = Q_f + Q_c \quad (30)$$

The rate of accumulation of the local faradaic charge within the porous polypyrrole electrode per unit volume ( $Q_f$ ) is assumed to be related to the local faradaic transfer current per unit volume ( $aj_f$ ) as follows:

$$\frac{\partial Q_f}{\partial t} = aj_f \quad (31)$$

Combining Eqs. [15] and [31] shows that

$$\frac{\partial Q_f}{\partial t} = ai_{o1,\text{ref}} \left\{ \left( 1 - \theta \right) \left( \frac{c_-}{c_{-,\text{ref}}} \right) \exp \left( \frac{\alpha_{a1} F}{RT} \eta_1 \right) - \theta \exp \left( \frac{-\alpha_{c1} F}{RT} \eta_1 \right) \right\} \quad (32)$$

The flow of current through a porous polypyrrole electrode results in charging of the double layer within the pores of the polypyrrole electrode in a manner consistent with that proposed by Feldberg (79). That is, the amount of local capacitive charge that goes to charging the double layers within the pores of the polypyrrole electrode,  $Q_c$ , is related to the amount of the local faradaic charge added to the polymer electrode by the electrochemical reaction:

$$Q_c = a^* (\eta_1 - \eta_{1,\text{pzc}}) Q_f \quad (33)$$

where  $a^*$  is a double layer constant assumed to be independent of potential and  $\eta_{1,\text{pzc}}$  is the total overpotential across the double layer within polypyrrole electrode at the point of zero charge (PZC) which is given by

$$\eta_{1,\text{pzc}} = \left\{ (\Phi_1 - \Phi_{\text{ref}}) - (\Phi_2 - \Phi_{\text{ref}}) - U_{1,\text{ref}} \right\}_{\text{pzc}} \quad (34)$$

The local capacitive transfer current per unit volume,  $aj_c$ , associated with the charging of the double layer is defined as follows:

$$aj_c = \frac{\partial Q_c}{\partial t} \quad (35)$$

Differentiating Eq. [33] yields

$$aj_c = a^* \left( Q_f \frac{\partial \eta_1}{\partial t} + (\eta_1 - \eta_{1,\text{pzc}}) aj_f \right) \quad (36)$$

with the assumption that  $\Phi_{\text{ref}} = (\Phi_{\text{ref}})_{\text{pzc}}$ .

### Transfer Current Balance

The local transfer current per unit volume,  $aj_1$ , is consists of two terms (41,79,80):

$$aj_1 = aj_l + aj_c \quad (37)$$

and is defined by the current transferred from the solution phase to the solid phase as follows:

$$aj_1 = \nabla \cdot i_2 = -\nabla \cdot i_1 \quad (38)$$

It is assumed that the superficial current density in the solid phase ( $i_1$ ) is due to the movement of electrons and is governed by Ohm's law (122)

$$i_1 = -\sigma_p \frac{\partial \Phi_1}{\partial y} \quad (39)$$

and the superficial current density in the solution phase ( $i_2$ ) is due to the movement of charged species (122)

$$i_2 = F \sum_i z_i N_{i,p} \quad (40)$$

Substituting the  $y$  component of Eq. [27] into Eq. [40] yields

$$i_2 = -\kappa_p \frac{\partial \Phi_2}{\partial y} - F \sum_i z_i D_{i,p} \frac{\partial c_i}{\partial y} \quad (41)$$

The second term on the right in Eq. [41] represents the concentration potential; this term will disappear if the ionic diffusion coefficients are all the same, which is not the case here.

Combining Eqs. [38], [39], and [41] yields the one dimensional local transfer current balance within the porous polypyrrole electrode region:

$$\begin{aligned} aj_1 &= \frac{\partial}{\partial y} \left( \sigma_p \frac{\partial \Phi_1}{\partial y} \right) \\ &= -\frac{\partial}{\partial y} \left( \kappa_p \frac{\partial \Phi_2}{\partial y} \right) - F \sum_i z_i \frac{\partial}{\partial y} \left( D_{i,p} \frac{\partial c_i}{\partial y} \right) \end{aligned} \quad (42)$$

### Electroneutrality

Assuming that the double layer at the pore wall is extremely thin relative to the pore dimension, the electrolyte within the pores can be considered electronically neutral. Thus, the electroneutrality condition can be applied as follows:

$$\sum_i z_i c_i = 0 \quad (43)$$

### 2. Governing Equations – Solution Diffusion Layer

Mass transfer in the diffusion layer is governed by the following differential material balance equation for species i:

$$\frac{\partial c_i}{\partial t} = -\nabla \cdot \mathbf{N}_i \quad (44)$$

and  $\mathbf{N}_i$ , the flux of species i, is due to migration in the electric field, diffusion in the concentration gradient, and convection in the flow field

$$\mathbf{N}_i = -z_i u_i F c_i \nabla \Phi_2 - D_i \nabla c_i + c_i \mathbf{v} \quad (45)$$

where  $\mathbf{v}$  represents electrolyte velocity vector. Only the axial component of the flux is considered in the model and the velocity component in that direction depends only on the normal distance from the polypyrrole electrode surface ( $y = y_{pp}$ ) with the no-slip condition (134)

$$v_y = -a' \Omega \sqrt{\frac{\Omega}{\nu}} (y - \delta_{pp})^2 \quad (46)$$

where  $a'$  represents a rotating disk electrode constant,  $\Omega$  represents a disk rotation speed, and  $\nu$  represents a kinematic viscosity. Combining Eqs. [44], [45], and [46]

yields the one dimensional material balance for species  $i$  within the electrolyte diffusion layer (122):

$$\frac{\partial c_i}{\partial t} = \frac{z_i D_i F}{RT} \frac{\partial}{\partial y} \left( c_i \frac{\partial \Phi_2}{\partial y} \right) + D_i \frac{\partial^2 c_i}{\partial y^2} + a' \Omega \sqrt{\frac{\Omega}{\nu}} (y - \delta_{pp})^2 \frac{\partial c_i}{\partial y} \quad (47)$$

Since the solid electroactive material does not exist in the diffusion layer, the local faradaic charge ( $Q_f$ ) and the solid potential ( $\Phi_1$ ) are dummy variables treated as constants and are set arbitrarily equal to zero

$$Q_f = 0 \quad (48)$$

$$\Phi_1 = 0 \quad (49)$$

It is assumed that the electrolyte in the diffusion layer is electrically neutral, so that the solution potential profiles obey the condition of electroneutrality, Eq. [43].

### 3. Boundary and Interface Conditions

To complete the system of equations for the model, the boundary conditions at each end of the cell and inter-regional interface must be specified for the dependent variables:  $c_+$ ,  $c_-$ ,  $Q_f$ ,  $\Phi_1$ , and  $\Phi_2$ . Boundary and interface conditions for these dependent variables are specified in the order of the platinum current collector to the bulk solution.

The polypyrrole electrode is bounded by a platinum current collector on one face ( $y = 0$ ) and by the electrolyte diffusion layer on the other ( $y = y_{pp}$ ). At the current collector/polypyrrole electrode interface ( $y = 0$ ), the net normal component of the flux of each species  $i$  towards or away from the electrode is assumed to be equal to the rate of consumption or production by the

electrochemical reaction [1] and double layer charging ( $R'_{1,i}$ ). Thus

$$-z_i u_{i,p} F c_i \frac{\partial \Phi_2}{\partial y} - D_{i,p} \frac{\partial c_i}{\partial y} = -\frac{s_{1,i} a j_1}{n_1 F} \quad (50)$$

The rate of accumulation of the local faradaic charge within the polypyrrole electrode per unit volume ( $Q_f$ ) is obtained from the local faradaic transfer current per unit volume ( $a j_f$ ) as shown by Eq. [32]. The solid potential at this point expressed as a difference between the applied potential ( $E$ ) and reference electrode potential ( $\Phi_{ref}$ )

$$\Phi_1 = E + \Phi_{ref} \quad (51)$$

It is assumed that no potential drop exists between the lead of reference electrode and the solution in the luggin tip, which is a reasonable because no appreciable current flows through the reference electrode. The applied potential ( $E$ ) is varied between positive and negative potential limits under the constant scan rate ( $v_s$ ) by potentiostat as follows:

$$\begin{aligned} E &= E_{neg} + v_s t && \text{(For Anodic Scan)} \\ &= E_{pos} - v_s t && \text{(For Cathodic Scan)} \end{aligned} \quad (52)$$

At this point, because all of the current leaves the cell *via* the current collector, the superficial current density in the solution phase ( $i_2$ ) can be set equal to zero, so that

$$-\kappa_p \frac{\partial \Phi_2}{\partial y} - F \sum_i z_i D_{i,p} \frac{\partial c_i}{\partial y} = 0 \quad (53)$$

At the polypyrrole electrode/electrolyte diffusion layer interface ( $y = y_{pp}$ ), the flux of each species  $i$  across the two regions must be continuous, which can be written as follows:

$$-z_i u_{i,p} F c_i \frac{\partial \Phi_2}{\partial y} - D_{i,p} \frac{\partial c_i}{\partial y} = -z_i u_i F c_i \frac{\partial \Phi_2}{\partial y} - D_i \frac{\partial c_i}{\partial y} \quad (54)$$

Because the solid electrode phase ends at this point and all of the current is in the solution phase, the gradient of the local faradaic charge ( $Q_f$ ) and the solid potential ( $\Phi_1$ ) can be set equal to zero

$$\left. \frac{\partial Q_f}{\partial y} \right|_{y_{pp}} = 0 \quad (55)$$

$$\left. \frac{\partial \Phi_1}{\partial y} \right|_{y_{pp}} = 0 \quad (56)$$

The superficial current density in the solution phase ( $i_2$ ) must be also continuous across the two regions, so that

$$-\kappa_p \frac{\partial \Phi_2}{\partial y} - F \sum_i z_i D_{i,p} \frac{\partial c_i}{\partial y} = -\kappa \frac{\partial \Phi_2}{\partial y} - F \sum_i z_i D_i \frac{\partial c_i}{\partial y} \quad (57)$$

In the bulk solution ( $y = y_{dl}$ ), the concentration of each species  $i$  is set equal to the bulk concentration ( $c_{i,ref}$ ), which is maintained constant by excess electrolyte and rapid mixing

$$c_i = c_{i,ref} \quad (58)$$

and the solution potential is set equal to that of the reference electrode ( $\Phi_{ref}$ )

$$\Phi_2 = \Phi_{ref} \quad (59)$$

Note that this requires assuming that no potential drop exists between the reference electrode lead and the solution in the luggin tip, which is a reasonable assumption since no appreciable current flows through the reference electrode. Since no electroactive solid material exist at this point, the local faradaic charge ( $Q_f$ ) and the solid potential ( $\Phi_1$ ) are dummy variables treated as constants and are set arbitrarily equal to zero.

#### 4. Initial Conditions

Initial conditions are necessary for the variables which depend explicitly on time. For convenience, it is assumed that the polypyrrole electrode is in its fully neutral state and is ready to be oxidized. Consequently, the local faradaic charge per unit volume ( $Q_f$ ) is initially set equal to  $Q_{f,red}$ , a minimal charge state, throughout the porous polypyrrole electrode region. Therefore, porosity ( $\epsilon_p$ ) and conductivity ( $\sigma_p$ ) of the polypyrrole electrode are initially set equal to  $\epsilon_{red}$  and  $\sigma_{red}$ , values at this neutral state, throughout the porous polypyrrole electrode region. In the diffusion layer, these variables are treated as dummy variables and are arbitrarily set equal to zero.

The concentration of each species  $i$  throughout the cell is set equal to its bulk concentration:

$$c_i = c_{i,ref} \quad (60)$$

The conductivity of the electrolyte ( $\kappa$ ) can be obtained by combining Eqs. [25] and [60]. The other dependent variables ( $\Phi_1$  and  $\Phi_2$ ) do not require initial conditions and are arbitrarily set equal to zero at  $t = 0$  for all  $y$ .

#### 5. Solution Method

The governing equations and boundary conditions for the determination of the quantities  $c_+$ ,  $c_-$ ,  $Q_f$ ,  $\Phi_1$ , and  $\Phi_2$  in all of the regions of the cell have been summarized in Table IX. It is noted that the numbers in the tables refer to the equation numbers in the text. The system of equations are put into finite difference form and solved as function of time ( $t$ ) and position ( $y$ ) by using a numerical technique referred to as Newman's pentadiagonal block matrix equation solver (135) and implicit stepping (136).

Table IX. System of equations for cyclic voltammetry of polypyrrole.

## A. Governing equations.

Variables	Polypyrrole Electrode Region	Electrolyte Diffusion Layer
$c_+$	29	47
$c_-$	29	47
$Q_f$	32	48
$\Phi_1$	42	49
$\Phi_2$	43	43

## B. Boundary and interface conditions.

Variables	$y = 0$	$y = y_{pp}$	$y = y_{dl}$
$c_+$	50	54	58
$c_-$	50	54	58
$Q_f$	32	55	48
$\Phi_1$	51	56	49
$\Phi_2$	53	57	59

The whole cell is divided into  $NJ$  mesh points with  $J = 1$  designated to be the boundary of the platinum current collector and polypyrrole electrode,  $J = NJ1$  designated to be the inter-regional interface of the polypyrrole electrode and electrolyte diffusion layer, and  $J = NJ$  to be the bulk solution. Mesh point spacings are different in different regions because of the difference in the thickness of each region and the number of nodal points used.

Second order finite-difference approximations of the derivatives for an internal mesh point can be written as

$$\frac{\partial^2 C_k(J)}{\partial y^2} \approx \frac{C_k(J-1) - 2C_k(J) + C_k(J+1)}{(\Delta y)^2} \quad (61)$$

$$\frac{\partial C_k(J)}{\partial y} \simeq \frac{-C_k(J-1) + C_k(J+1)}{2(\Delta y)} \quad (62)$$

and for a boundary node as

$$\frac{\partial C_k(J)}{\partial y} \simeq \frac{-3C_k(J) + 4C_k(J+1) - C_k(J+2)}{2(\Delta y)} \quad (63)$$

$$\frac{\partial C_k(J)}{\partial y} \simeq \frac{C_k(J-2) - 4C_k(J-1) + 3C_k(J)}{2(\Delta y)} \quad (64)$$

where  $\Delta y$  denotes the distance between node points, and  $C_k(J)$  represents the  $k^{\text{th}}$  unknown at node  $J$ .

The accuracy of the finite difference approximations of the above derivatives is  $(\Delta y)^2$ . Equation [63] (a forward difference form) is used at  $J = 1$ ; and Eq. [64] (a backward difference form) is used at  $J = NJ$ . For the inter-regional boundaries, Eq. [63] is used on the upper region (higher region number) side, and Eq. [64] is used on the lower region side. Note that to maintain  $(\Delta y)^2$  accuracy five node points, pentadiagonal block matrix equation solver are used at an inter-regional boundary node point (135).

For the time derivatives, implicit stepping is used (136):

$$\frac{\partial C_k(J)}{\partial t} \simeq \frac{C_k(J)|_{t+\Delta t} - C_k(J)|_t}{\Delta t} \quad (65)$$

where  $C_k(J)|_t$  refers to the known value obtained from the previous time step, and  $C_k(J)|_{t+\Delta t}$  represents the unknown value to be determined at  $t + \Delta t$ .

### C. Results and Discussion

The values used for the operating conditions in the cyclic voltammograms are given in Table X. The applied potential ( $E$ ) sweeps between  $-0.8$  V and  $+0.8$  V under the constant scan rates ( $v_s$ ) of 10 and 20 mV/sec at room temperature. The

scan rate and the potential interval are selected to obtain a complete oxidation and reduction of the polymer within the stability range of the electrolyte. The rotating speed of disk electrode ( $\Omega$ ) is arbitrarily chosen as 3600 rpm. A  $1\text{ }\mu\text{m}$  thick polypyrrole electrode is used in this study because a high doping level and a high efficiency have been observed for this thickness (107). All the potentials are referred to the SCE. The resulting anodic (oxidation) and cathodic (reduction) current densities are specified as being positive and negative because of the chosen coordinate system, respectively.

### 1. Experimental Results

Experimental cyclic voltammograms for a  $1\text{ }\mu\text{m}$  thick polypyrrole film in 1M LiClO<sub>4</sub>-PC electrolyte at scan rates of 10 and 20 mV/sec are presented in Fig. 7. Two main considerations can be derived by the analysis of these cyclic voltammograms; well defined doping-undoping behaviors and large capacitance effects.

The current density is well defined as positive and negative for doping and

Table X. Operating conditions used for cyclic voltammograms of polypyrrole.

Operating Temperature ( $T$ )	298.15 K
Negative Potential Limit ( $E_{\text{neg}}$ )	-0.8 V (vs. SCE)
Positive Potential Limit ( $E_{\text{pos}}$ )	+0.8 V (vs. SCE)
Potential Scan Rate ( $v_s$ )	10 & 20 mV/sec
Disk Rotation Velocity ( $\Omega$ )	377 rad/sec
Reference Electrode Potential ( $\Phi_{\text{ref}}$ )	0.0 V (vs. SCE)
Geometric Electrode Surface Area ( $A$ )	1 cm <sup>2</sup>
Thickness of Polypyrrole Film ( $\delta_{\text{pp}}$ )	1 $\mu\text{m}$
Thickness of Electrolyte Diffusion Layer ( $\delta_{\text{dl}}$ )	0.01 cm
Reference Concentration of Li <sup>+</sup> ( $c_{+,\text{ref}}$ )	0.001 mol/cm <sup>3</sup>
Reference Concentration of ClO <sub>4</sub> <sup>-</sup> ( $c_{-,\text{ref}}$ )	0.001 mol/cm <sup>3</sup>

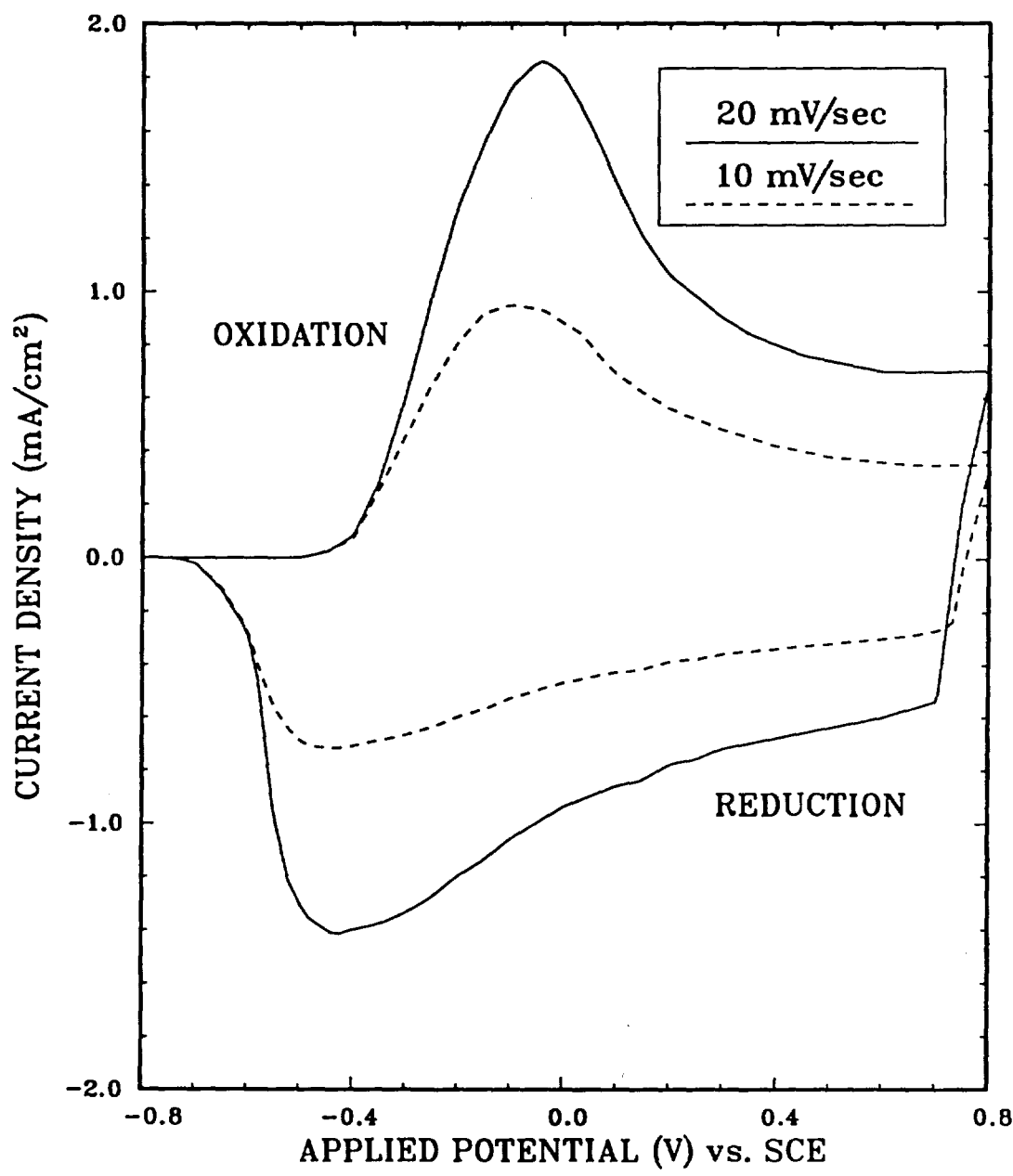


Fig. 7. Experimental cyclic voltammograms for a 1  $\mu\text{m}$  polypyrrole film in 1M LiClO<sub>4</sub>-PC electrolyte at scan rates of 10 and 20 mV/sec.

undoping processes, and immediately changes sign when the scan is reversed. The electrochromic properties of polypyrrole are clearly demonstrated showing that polypyrrole is actually reduced and oxidized; brown-black at doped state and light yellow at undoped state. The cyclic voltammograms are not symmetrical but quasi-reversible. The oxidative and reductive charges in each cycle are the equivalent and are independent of scan rate. The cathodic peaks are significantly broader than the anodic peaks. The peak height is proportional to the scan rate as is expected for a reversible surface process (97). Accordingly, it can be suggested that the electrochemical behavior in cyclic voltammetry can be explained in relation to the diffusion of counterion. The electrochemical characteristics of the  $1\mu\text{m}$  polypyrrole film in the 1M LiClO<sub>4</sub>-PC electrolyte obtained from these experimental cyclic voltammograms are summarized in Table XI.

A large capacitive background current density ( $i_c$ ) in the potential region between +0.2 and +0.8 V vs. SCE (where the film is not oxidized or reduced) observed and is proportional to the scan rate. The related capacitance,  $C_l$ , may be obtained by simple calculation based on the expression (76,109)

$$C_l = \frac{i_c}{v_s} \quad (66)$$

Table XI. Electrochemical characteristics of the  $1\mu\text{m}$  polypyrrole film in the 1M LiClO<sub>4</sub>-PC electrolyte.

Scan Rate ( $v_s$ )	10 mV/sec	20 mV/sec
Anodic Peak Potential ( $E_{pa}$ )	-0.1 V	-0.04 V
Cathodic Peak Potential ( $E_{pc}$ )	-0.43 V	-0.45 V
Anodic Peak Current Density ( $i_{pa}$ )	+0.95 mA	+1.86 mA
Cathodic Peak Current Density ( $i_{pc}$ )	-0.72 mA	-1.42 mA
Anodic Charge Density ( $Q_{ca}$ )	+56.3 mC/cm <sup>2</sup>	+56.3 mC/cm <sup>2</sup>
Cathodic Charge Density ( $Q_{cc}$ )	-53.8 mC/cm <sup>2</sup>	-53.8 mC/cm <sup>2</sup>

The related capacitance of fully oxidized polypyrrole from these experimental cyclic voltammogram has a value of about  $35 \text{ mF/cm}^2$  (compared to the usual  $\mu\text{F/cm}^2$  values for the bare electrodes), which is similar to values obtained by other laboratory (76,109). The origin of such large capacitance in polymer films has been discussed in detail by Tanguy *et al.* (46) and Mermilliod *et al.* (137). The behavior observed is similar to that of a capacitor with very high capacitance and is due to the highly porous structure of polypyrrole films (41).

The polypyrrole film is very stable between  $-0.8 \text{ V}$  and  $+0.8 \text{ V}$  vs. SCE. It is possible to obtain more than 200 cycles without significant loss of the coulombic capacity of the electrode. This indicates that the electroactivity is not destroyed and that counterion insertion and extraction is quite reversible. Extending negative limit had little effect on the cyclic voltammograms characteristics. However, when the upper limit is taken more positive, there is a progressive loss of capacity and film deterioration takes place after a few cycles.

## 2. Simulated Results

The simulated cyclic voltammograms for the polypyrrole film can be obtained by using the model developed above and fixed parameter values given in Tables IV, V, VII, X, and XII as shown in Fig. 8. The estimated values of parameters in Table XII are obtained by comparison between experimental and simulated cyclic voltammograms and are discussed in the later section.

The current density relative to the projected electrode area,  $i$ , are obtained by integrating the local transfer current per unit volume ( $aj_1$ ) over the porous polypyrrole electrode region:

$$i = \int_{y=0}^{y=y_{pp}} aj_1 dy \quad (67)$$

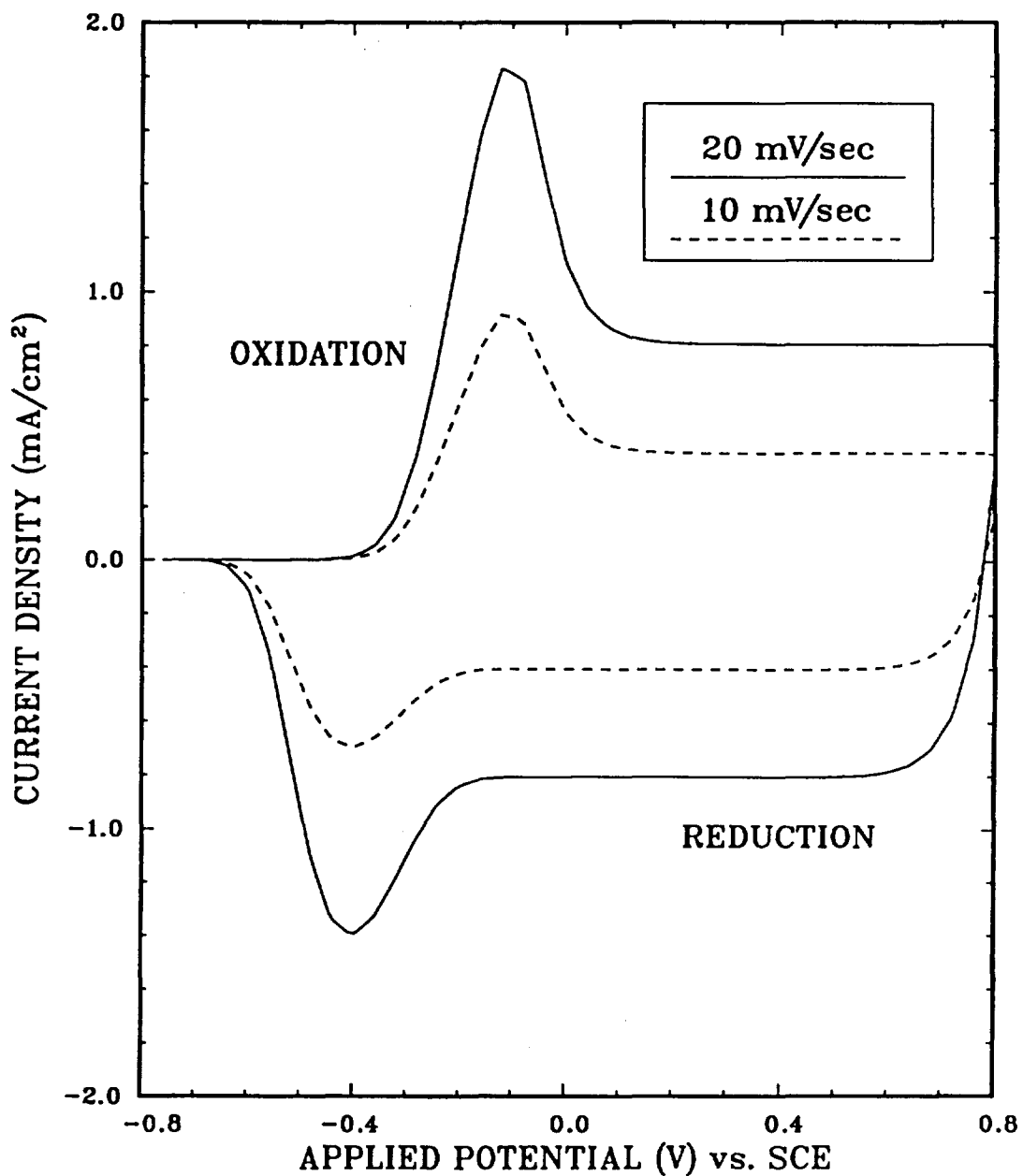


Fig. 8. Simulated cyclic voltammograms for a 1  $\mu\text{m}$  polypyrrole film in 1M LiClO<sub>4</sub>-PC electrolyte at scan rates of 10 and 20 mV/sec.

It is noted that the value of the current density should be equal to the superficial current density in the solid phase ( $i_1$ ) at the current collector/polypyrrole electrode interface ( $y = 0$ )

$$i = i_1 \Big|_{y=0} \quad (68)$$

This is because all of the current leaves the cell *via* the current collector.

As discussed earlier, the current density in the cyclic voltammogram of the polypyrrole film consists of two distinctive components, faradaic current density caused by the electrochemical reaction [1] and capacitive current density caused by the double layer within the porous polypyrrole film,  $i_f$  and  $i_c$ . These are obtained by integrating the local faradaic and capacitive transfer currents per unit volume ( $a j_f$  and  $a j_c$ ) over the porous polypyrrole electrode region as shown in Eq. [67]. Typical cyclic voltammogram and its components of 1  $\mu\text{m}$  polypyrrole film at a scan rate of 20 mV/sec are shown in Fig. 9 as a function of the applied potential.

At potentials negative of -0.4 V, polypyrrole electrode is in its fully neutral state. For anodic sweep of potential (increasing potential), neutral polypyrrole starts to converge to oxidized state at potentials positive of -0.4 V. The electrochemical oxidation yields the consumption of both faradaic and capacitive

Table XII. Fixed parameter values used for polypyrrole.

Faradaic Charge of Neutral Polypyrrole ( $Q_{f,\text{red}}$ )	$1.0 \times 10^{-5} \text{ C/cm}^3$
Faradaic Charge of Oxidized Polypyrrole ( $Q_{f,\text{oxd}}$ )	$120.0 \text{ C/cm}^3^\dagger$
Porosity of Neutral Polypyrrole ( $\epsilon_{\text{red}}$ )	$1.0 \times 10^{-2}$
Porosity of Oxidized Polypyrrole ( $\epsilon_{\text{oxd}}$ )	$1.0 \times 10^{-3}$
Double Layer Constant ( $a^*$ )	$2.8 / \text{V}^\dagger$
Zero Charge Potential ( $\eta_{1,\text{pzc}}$ )	-0.3 V (vs. SCE) <sup>†</sup>
Exponent on Porosity Term (ex)	0.5 <sup>†</sup>

<sup>†</sup> Estimated values

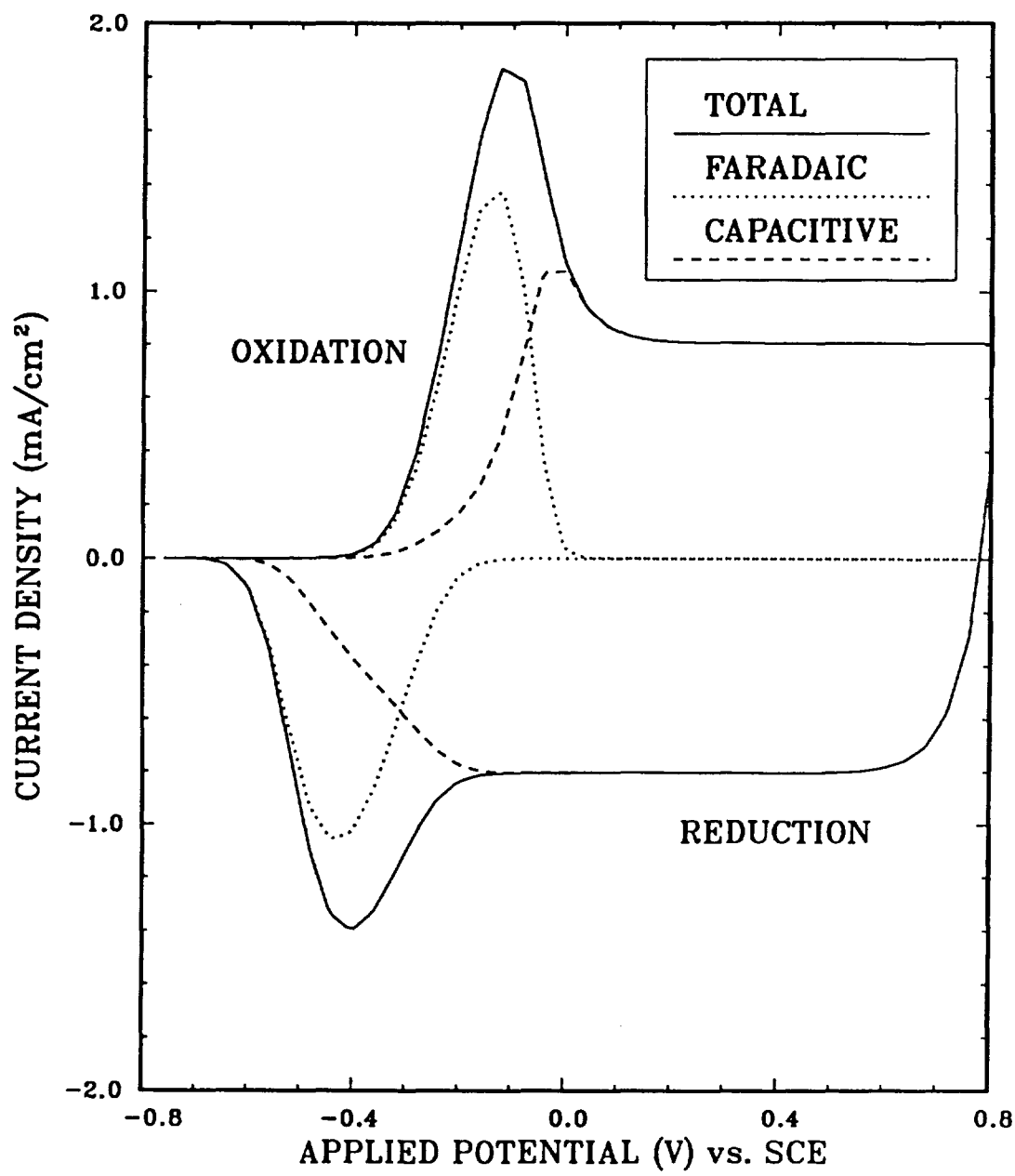


Fig. 9. Decomposition of a cyclic voltammogram into its two components, the faradaic and capacitive current densities, at a scan rate of 20 mV/sec.

charges within polypyrrole film. The faradaic current density ( $i_f$ ) initially increases with time because of the increasing driving force (applied potential), then decreases because of the limited electroactive area (neutral polypyrrole sites) and the concentration of counterion within the polymer film as the polypyrrole electrode is significantly oxidized. However, the capacitive current density ( $i_c$ ) increases continuously with time until the polypyrrole electrode is fully oxidized. At potentials positive of +0.2 V, the oxidation reaction is complete and entire polypyrrole electrode is in its fully oxidized state. That is, the current density is entirely dominated by the double layer effects because no more oxidation of the polypyrrole can occur. The related capacitance ( $C_l$ ) of fully oxidized polypyrrole from these simulated cyclic voltammogram has a value of about  $38 \text{ mF/cm}^2$  and is well matched with that obtained from experiment.

When the scan is reversed to cathodic direction (decreasing potential), the pure capacitive current density immediately changed sign. Oxidized polypyrrole start to converge to neutral state at potentials negative of +0.2 V, and yield decreasing faradaic and capacitive charges. At a potential -0.6 V, entire polypyrrole electrode is again in its fully neutral state.

#### Dependent Variables Profiles

The dynamic profiles of the dependent variables in the porous polypyrrole electrode region at a scan rate of 20 mV/sec are shown in Figs. 10 through 12 as function of applied potential ( $E$ ) and position ( $y$ ). In the position coordinate,  $y = 0$  represents the platinum current collector side and  $y = 1$  represents the electrolyte diffusion layer side as shown in Fig. 6.

The dynamic concentration profiles of the anion ( $\text{ClO}_4^-$ ) within the porous polypyrrole electrode region at a scan rate of 20 mV/sec are shown in Fig. 10.

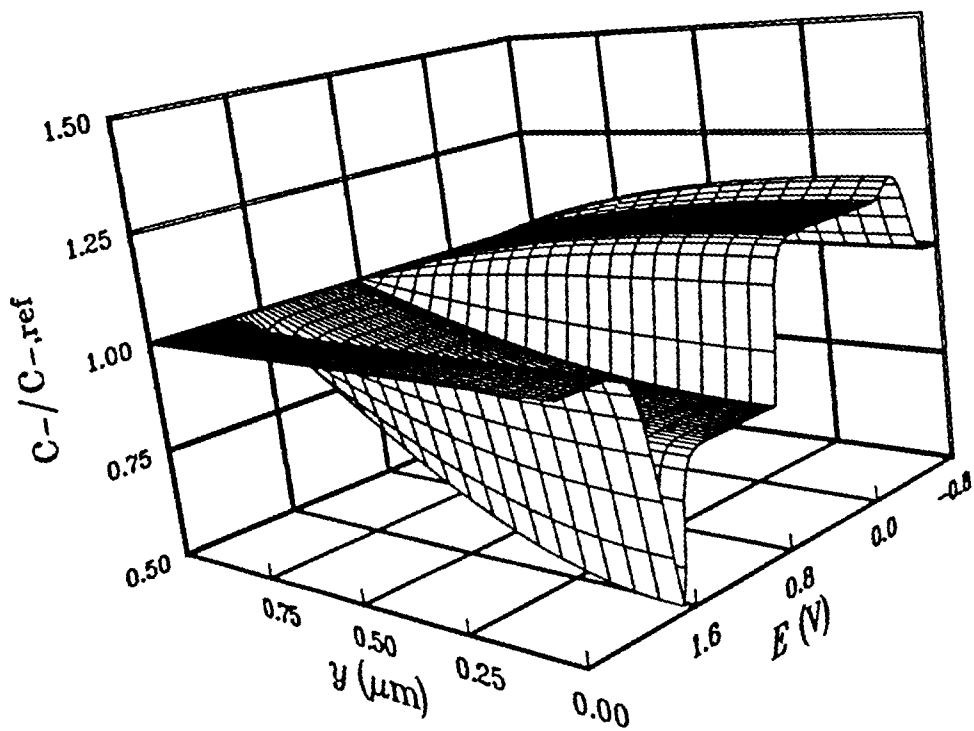


Fig. 10. Dimensionless concentration profiles of the anion ( $\text{ClO}_4^-$ ) within the polypyrrole electrode region at a scan rate of 20 mV/sec.

The concentration is made dimensionless relative to its reference concentrations ( $c_{-,ref}$ ). It is noted that the concentration profiles of the cation ( $\text{Li}^+$ ) have similar distributions because of the electroneutrality.

Initially, the concentration of the anion ( $\text{ClO}_4^-$ ) is uniform throughout the cell at reference concentration ( $c_{-,ref}$ ). For anodic scan, anions are consumed at the porous polypyrrole electrode region because of oxidation of polypyrrole and increase of double layer charge. The reacting species ( $\text{ClO}_4^-$ ) is transported from the bulk to the porous electrode layer where it diffuses and migrates to reactive sites within the porous layer. After polypyrrole has been fully oxidized, the concentration distribution within the porous polypyrrole electrode region bounced back to certain equilibrium state. This is because no more oxidation of polypyrrole occurs and counterions are consumed by double layer charge only.

For cathodic scan, the oxidized polypyrrole sites are reduced and the opposite phenomena are occurred. Anions ( $\text{ClO}_4^-$ ) are produced within the porous polypyrrole electrode region because of reduction of polypyrrole and decrease of double layer charge. The reacting species ( $\text{ClO}_4^-$ ) is transported from the porous electrode region to the bulk. Since the effective diffusivities of  $\text{Li}^+$  and  $\text{ClO}_4^-$  within the porous layer are much smaller than the free stream diffusivity of these species, the concentration gradients within the porous region must be larger to make up for the slower movement of the ions.

Figure 11 shows the profiles of the faradaic charge per unit volume consumed within polypyrrole electrode due to the electrochemical reaction [1] at a sweep rate of 20 mV/sec. The faradaic charge per unit volume is made dimensionless by using the maximum faradaic charge value ( $Q_{f,oxd}$ ) as the reference point.

Initially, polypyrrole electrode is in its fully neutral state ( $Q_f = Q_{f,red}$ ) and

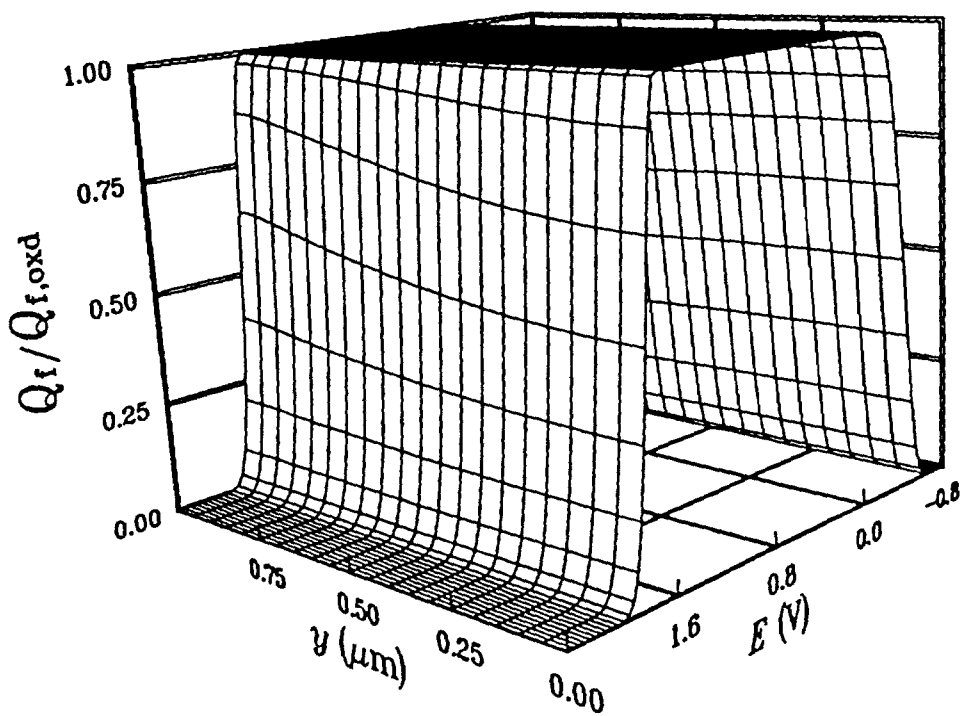


Fig. 11. Dimensionless faradaic charge profiles within the polypyrrole electrode region at a scan rate of 20 mV/sec.

is ready to be oxidized. For anodic scan, the faradaic charge is accumulated throughout the polypyrrole electrode region by the electrochemical reaction [1]. The faradaic charge accumulation in the outer layer of the polypyrrole electrode (electrolyte diffusion layer side) is faster because of the concentration gradient effect within polypyrrole electrode as shown in Fig. 11. After polypyrrole has been fully oxidized, the faradaic charge distribution becomes uniform at  $Q_f = Q_{f,oxd}$ . During reduction, the faradaic charge is withdrawn slower in the inner layer of the polypyrrole electrode (current collector side) because of the diffusion limitation. Note that charge accumulates rapidly throughout the entire electrode.

The electrochemical properties (such as, porosity, conductivity, diffusivity, mobility, etc.) have the similar distribution throughout the polypyrrole electrode region because of the assumption that these properties are proportional to the faradaic charge per unit volume consumed within polypyrrole electrode (See Eqs. [13], [14], [22], [23], and [24]).

Figure 12 shows the distribution of potential difference between solid and solution phases, driving force for the electrochemical reaction [1] and the double layer charge, within the porous polypyrrole electrode region at a sweep rate of 20 mV/sec. For convenience, the potential difference is represented by  $\Phi_1 - \Phi_2 - E$ .

The potential difference increases with time indicating that the electrochemical reaction must proceed at a faster rate to compensate for decreasing available active surface area and reactive species in solution phase. It shows that the potential difference at the inner layer (current collector side) is higher because of diffusion limitation of counterion. The positive and negative values lead cathodic (reduction) and anodic (oxidation) reactions, respectively.

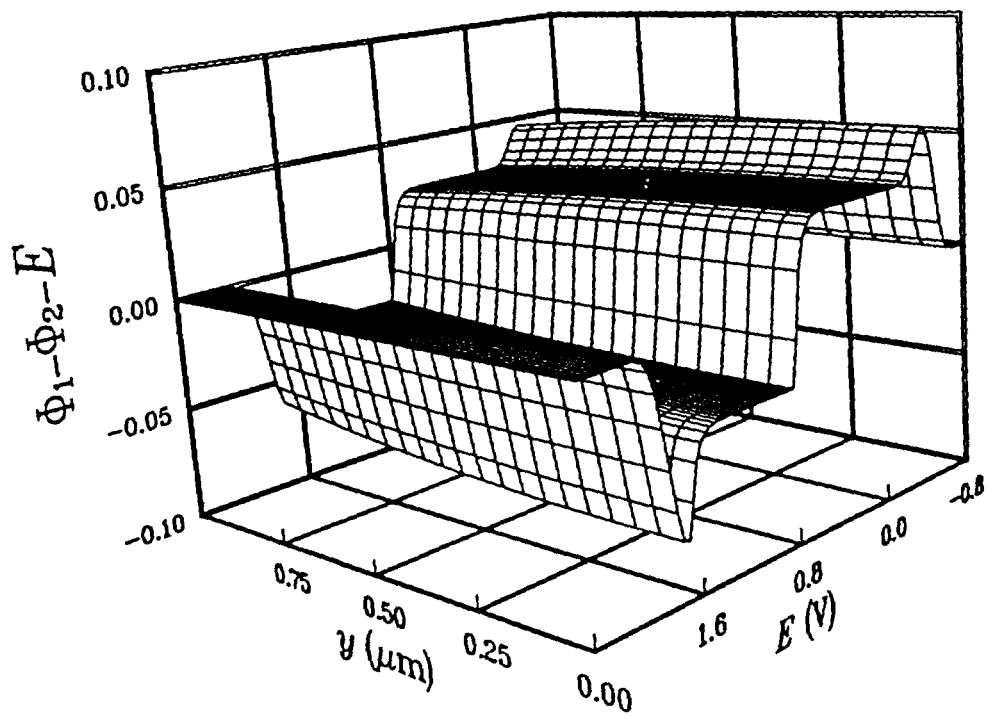


Fig. 12. Potential difference between solid and solution phases within the polypyrrole electrode region at a scan rate of 20 mV/sec.

### 3. Sensitivity Analysis

Since the results predicted by the model depend on the independent parameters describing the physical and electrochemical characteristics of system, it is necessary to examine the sensitivity of the model predictions on these parameters and identify parameters which can be discarded from the further parametric analysis. If the model predictions are relatively insensitive to a parameter, then a fairly wide range of values for that parameter could be used without significantly affecting the predictions of the model. It often the case that the more parameters that are estimated, the more uncertain are the estimates due to interaction between the parameters, poor scaling, and round-off error (138).

The sensitivity coefficient of each parameter of interest,  $S_k$ , can be determined as follows:

$$S_k = \sum_{E=-0.8}^{E=0.8} \frac{\Delta i_a(E)}{m\Delta P_k} \quad (69)$$

where

$$\Delta i_a(E) = |i_a(E) - i_a^*(E)|$$

$$\Delta P_k = |(P_k - P_k^*)/P_k^*|$$

$i_a$  = predicted anodic current density with  $P_k$

$i_a^*$  = predicted anodic current densities with  $P_k^*$

$P_k$  = perturbed value of parameter k

$P_k^*$  = reference value of parameter k

$m$  = number of data points

For convenience, only anodic (oxidation) current density responses are used to analyze the sensitivity of the model predictions in here. Anodic current density responses shown in Fig. 8 and their conditions are used as the reference case. When an interesting parameter is perturbed slightly (i.e., multiplying by 1.05

to the reference value) while holding the values of all other parameters equal to that of the reference case, a new set of data of predicted anodic current density responses ( $i_a$ ) vs. applied potential ( $E$ ) is obtained. Then, the difference in the anodic current density responses between the reference and perturbed cases ( $\Delta i_a$ ) is calculated at each potential interval and summed over the entire potential region used. The results of the sensitivity analysis are shown in Tables XIII and XIV.

Table XIII shows the sensitivity of the anodic current density to the physical parameters, such as the porosity of polypyrrole electrode ( $\epsilon_p$ ), the thickness of polypyrrole electrode ( $\delta_{pp}$ ), and the thickness of diffusion layer ( $\delta_{dl}$ ). The predicted anodic current density responses are found to be more sensitive to the electrode thickness ( $\delta_{pp}$ ) and porosity ( $\epsilon_p$ ) than the thickness of the diffusion layer ( $\delta_{dl}$ ). This is expected because the switching process of polypyrrole electrode is limited by ion transfer rate within porous structure. The effective diffusivities of  $\text{Li}^+$  and  $\text{ClO}_4^-$  within the porous layer are much smaller than the free stream diffusivity of these species. The fact that the current density responses are relatively insensitive to the thickness of the diffusion layer is comforting because it is usually much easier to measure the electrode thickness and porosity with high degree of accuracy than that is possible for the diffusion layer. Note also that the porosity of the electrode has to be measured experimentally. A porosity

Table XIII. Sensitivity analysis on various physical parameters.

Physical Parameters	Sensitivity Coefficient ( $S_k$ )
Thickness of Polypyrrole Film ( $\delta_{pp}$ )	0.68867
Porosity of Polypyrrole Film ( $\epsilon_p$ )	0.20020
Thickness of Diffusion Layer ( $\delta_{dl}$ )	0.06169

value calculated theoretically from the material balance on the solid phase is not applicable because it ignores the existence of closed pores.

Table XIV shows the sensitivity of the anodic current density to the electrochemical parameters describing the electrochemical reaction [1] and the double layer effects on switching process. The most influential parameter is the maximal faradaic charge of polypyrrole ( $Q_{f,oxd}$ ). This is expected because the amount of electroactive material is proportional to this quantity. The double layer constant ( $a^*$ ) and the zero charge potential ( $\eta_{1,pzc}$ ) are next followed by the anodic transfer coefficient ( $\alpha_{a1}$ ) and the exchange current per unit volume ( $ai_{o1,ref}$ ). The electrokinetic parameters describing the doping/undoping of polypyrrole have less influence than those describing the double layer effects. This could be due to the fact that polypyrrole has the large capacitive background current density as shown in Fig. 7.

In a similar manner, a sensitivity analysis could be used to determine the operating conditions where the sensitivity of a parameter is maximal as shown in Table XV. The effects of scan rate ( $v_s$ ) on the performance of cyclic voltammogram are very significant. The oxidation and reduction peak height is proportional to the scan rate as is expected for a reversible surface process. However, the oxidation and reduction charge densities in each cycle are the same

Table XIV. Sensitivity analysis on various electrochemical parameters.

Electrochemical Parameters	Sensitivity Coefficient ( $S_k$ )
Maximal Faradaic Charge ( $Q_{f,oxd}$ )	0.66469
Double Layer Constant ( $a^*$ )	0.52289
Zero Charge Potential ( $\eta_{1,pzc}$ )	0.49472
Anodic Transfer Coefficient ( $\alpha_{a1}$ )	0.12216
Exchange Current Density ( $ai_{o1,ref}$ )	0.08758

and do not depend on the scan rate. The effects of rotating speed ( $\Omega$ ) on the performance of cyclic voltammogram are not significant. Increasing rotating speed cause more convective effects in the electrolyte diffusion layer. However, convective effect by rotating disk electrode is negligible within the porous polypyrrole electrode region.

#### 4. Effects of Parameters

Many factors come into play when calculating the sensitivity coefficients. For example, the exchange current density and transfer coefficient strongly influence the initial slope in the cell current density. On the other hand, the maximum faradaic charge and double layer constant have more influence later when polypyrrole films are significantly oxidized. Thus, it is necessary to understand the detailed effects of each independent parameter, which is identified as relatively sensitive on model prediction. The effects of the maximal faradaic charge ( $Q_{f,oxd}$ ), the double layer constant ( $a^*$ ), the anodic transfer coefficient ( $\alpha_{a1}$ ), and the exchange current density ( $a_{i_{01,ref}}$ ), on the cyclic voltammograms are examined and estimated next in detail.

Figure 13 shows the effects of the maximum faradaic charge ( $Q_{f,oxd}$ ) in the cyclic voltammograms. This parameter affected both faradaic and capacitive current densities. The value does not influence the initial slope of the current density. However, the larger value of maximal faradaic charge yields higher and

Table XV. Sensitivity analysis on various operating conditions.

Operating Conditions	Sensitivity Coefficient ( $S_k$ )
Potential Scan Rate ( $v_s$ )	0.66468
Disk Rotation Velocity ( $\Omega$ )	0.00002

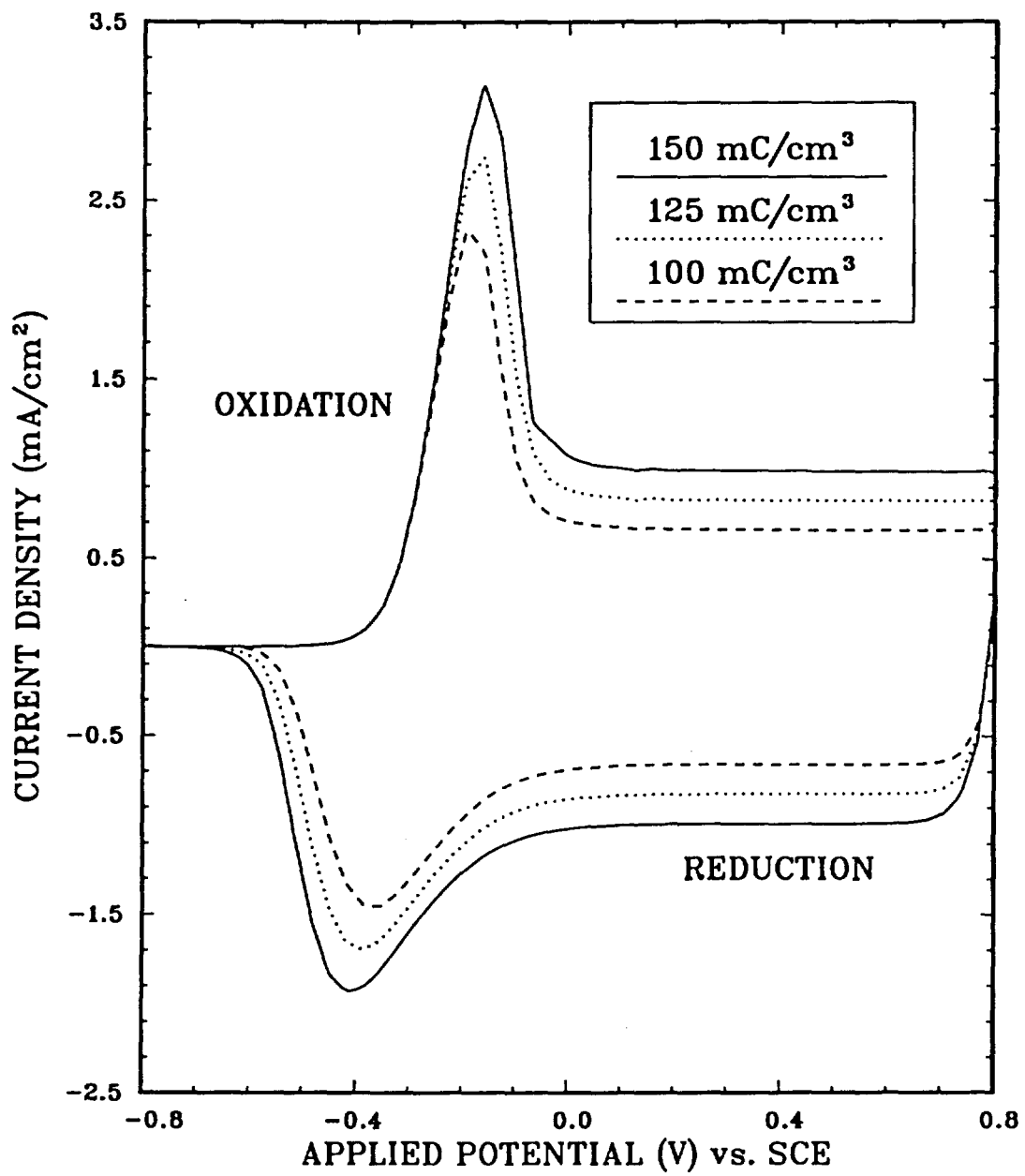


Fig. 13. The effects of maximal faradaic charge ( $Q_{f,oxd}$ ) on the cyclic voltammograms at a scan rate of 20 mV/sec.

broader peak current densities, and higher background capacitive current density. This is because the amount of electroactive material is proportional to this value.

Figure 14 shows the effects of double layer constant ( $a^*$ ) in the cyclic voltammograms. The region, where polypyrrole is significantly reduced, is not affected because this parameter does influence only the double layer charging. Because the local capacitive transfer current per unit volume ( $aj_c$ ) is proportional to this parameter by Eq. [36], larger value of proportional constant ( $a^*$ ) yields higher capacitive current density.

Figures 15 and 16 show the effects of the electrokinetic parameters describing the electrochemical reaction of polypyrrole. These parameters show significant effects in the region where polypyrrole is oxidizing or reducing. No effects are observed in the background capacitive current density. Figure 15 shows the effects of anodic transfer coefficient ( $\alpha_{a1}$ ) in the cyclic voltammograms. This value strongly influences the shape of the peak current density. Increasing anodic transfer coefficient ( $\alpha_{a1}$ ) yields higher and narrower anodic peak current density. The opposite is true for cathodic direction because the sum of anodic and cathodic transfer coefficients ( $\alpha_{a1}$  and  $\alpha_{c1}$ ) is set equal to 1.

Figure 16 shows the effects of exchange current per unit volume ( $ai_{o1,ref}$ ) in the cyclic voltammograms. This parameter shows the most significant influence in the peak current density. Increasing exchange current per unit volume yields increasing both anodic and cathodic peak current densities, and reducing potential difference between anodic and cathodic peak. This is because the electrochemical reaction rate is proportional to this value.

The value of each independent parameter discussed above has been estimated by comparing the peak and background current densities predicted by the model

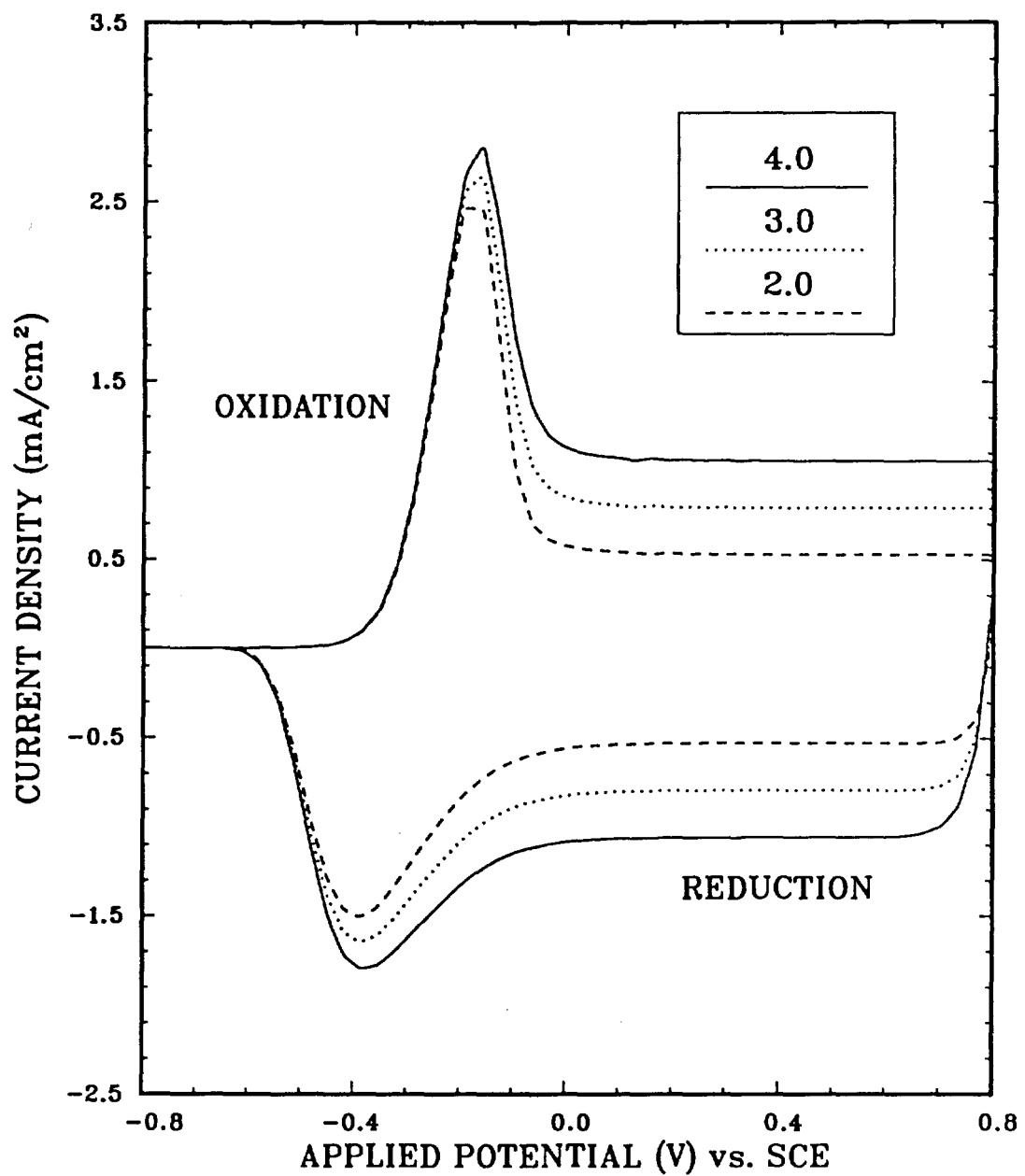


Fig. 14. The effects of double layer constant ( $a^*$ ) on the cyclic voltammograms at a scan rate of 20 mV/sec.

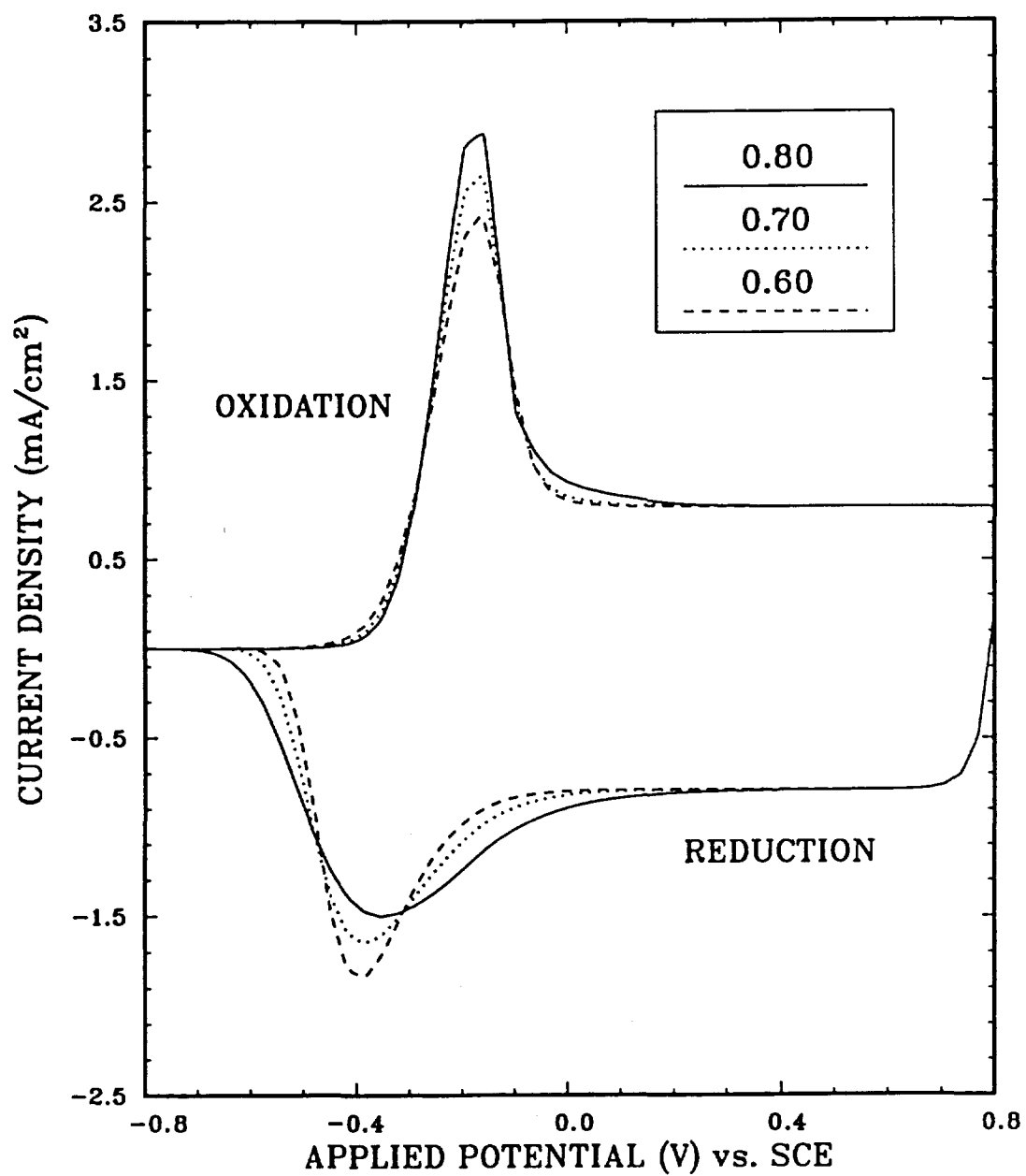


Fig. 15. The effects of anodic transfer coefficient ( $\alpha_{a1}$ ) on the cyclic voltammograms at a scan rate of 20 mV/sec.

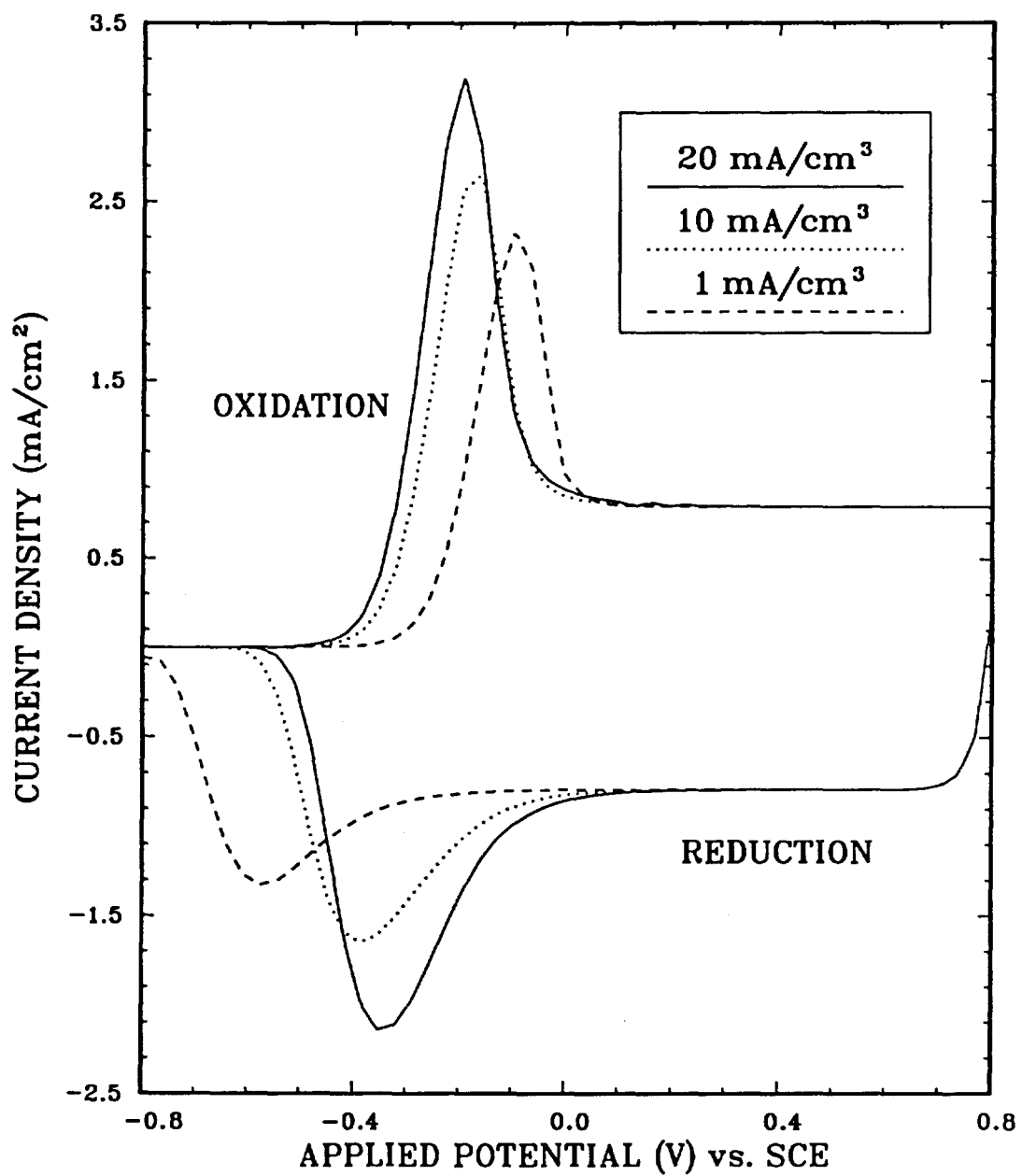


Fig. 16. The effects of exchange current per unit volume ( $a_{i01,\text{ref}}$ ) on the cyclic voltammograms at a scan rate of 20 mV/sec.

with the experimental results. Tables VII and XII summarize these values. The dependent parameters (diffusion coefficients, mobilities, conductivities, etc.) can be calculated from the relationships given in the model development using the values of the independent parameters estimated here. For example, the effective diffusion coefficients of the counterion ( $\text{ClO}_4^-$ ) within the doped and undoped states of the polypyrrole film are  $4.0 \times 10^{-11} \text{ cm}^2/\text{sec}$  and  $1.0 \times 10^{-9} \text{ cm}^2/\text{sec}$ , respectively. These values are smaller than those obtained from experimental measurements. This may be due to the large capacitive and uncompensated resistance effects in polypyrrole films which are not addressed properly in experiments.

#### D. Conclusions and Recommendations

The electronically conducting polypyrrole film has been synthesized electrochemically and used in cyclic voltammetry to study the electrochemical characteristics. The experimental results show that:

- a. The simple one-step electrochemical oxidation of pyrrole monomer yields a flexible, metallic, and organic polymer film.
- b. The polypyrrole film has a quasi-reversible switching behavior with large capacitive background effects.
- c. The switching process of the polypyrrole film is accompanied by distinctive color changes, brown-black at doped state and light yellow at undoped state.
- d. The polypyrrole film can be cycled more than 200 times without significant loss of the coulombic capacity of the electrode.

These observations make polypyrrole a prospective candidate in the area of energy

storage devices.

The mathematical model based on the porous electrode, dilute solution, and double layer theories, coupled to the Butler-Volmer type rate expression has been developed to predict the cyclic voltammograms of a polypyrrole film under identical conditions of the experiments. The simulated results show that:

- a. Despite the fact that the present model involves a number of simplifications such as the presumption that the electronic conductivity varies linearly with the doping level, a comparison of the simulated and experimental cyclic voltammograms shows quantitative agreement.
- b. The modified Butler-Volmer type rate expression can be applied for the quasi-reversible switching behavior of polypyrrole. This assumes that the appearance of the quasi-reversible peak in the cyclic voltammograms for conducting polymers is not necessary evidence for the presence of an additional redox process.
- c. The profiles of the dependent variables show that the switching process is governed by the availability of the counterion to the polypyrrole electrode and the amount of electroactive sites. Thus, the performance of the polypyrrole based devices could be improved by physical modifications that increase electroactive surface area and optimize the rate of ionic charge transport.
- d. Sensitivity analysis shows that the parameters describing the double layer effects have more influence than those describing the electrokinetic process. This observation suggests that more emphasis should be placed on evaluating the capacitive effects affiliated with the doping state of polypyrrole.

Better agreement between the simulated and experimental data will be obtained if different charge transport mechanisms are considered for the doping and undoping processes. In addition, the factors which determine the electrochemical characteristics of polypyrrole are the doping level and its functional relationship to the microscopic structure, conductivity, and capacitance. In the absence of any experimental or theoretical data, the preassumptions used are adequate for these preliminary analysis. With pertinent experimental or theoretical data to quantify these factors, the model can be used, together with parameter estimation techniques, to determine the electrochemical characteristics of polypyrrole.

The model developed here can be modified to study cyclic voltammetric behavior of other conducting polymers, such as polythiophene, polyaniline, polycarbazole, etc., by simply adjusting the input parameters and their relationships. Also, the model can be extended to predict other electroanalytical techniques, such as AC impedance, chronocoulometry, and chronoabsorptometry. AC impedance can be useful to obtain more detail of double layer effects.

## V. SECONDARY BATTERY

The electronically conductive polypyrrole has received tremendous interest as energy storage materials in recent years. Among the potential applications, the most promising is the lithium/polypyrrole secondary battery system (105-110). Combining polypyrrole with lithium in a secondary battery provides an inexpensive and noncorrodible battery with a high cell potential and unusual design flexibility.

Conducting polymers in general possess several technologically important features in the battery technology. The polymeric electrodes differ from conventional electrodes in that the polymer does not dissolve and is not redeposited during charge-discharge cycles, although some swelling of the polymer does occur during oxidation or reduction. This absence of dissolution and redeposition is expected to promote longer life for polymer electrodes owing to the absence of mechanical changes in electrode dimensions and so on, such as those observed with many conventional electrodes. Also, in most batteries complete deep discharge leads to rapid deterioration. Hence only partial utilization of the energy density of a battery can be achieved if it is only partly discharged in order to prolong its effective operating life. The energy density of a polymer electrode can, however, be completely utilized in repeated deep discharges at good discharge rates without adverse effects. The flexibility of polymeric films may be significant in their use in certain types of thin batteries. It would appear that the use of organic substances as electrode-active materials in batteries for certain specific types of uses is still in its infancy.

A disadvantage of all polymer electrode is that they will be expected to

exhibit smaller volumetric energy densities than conventional electrodes, since organic materials are usually less dense than metals and inorganic substances. To what extent this is a serious disadvantage will depend on the use to which the cell in which they are incorporated might be put.

Although the conductive polymers have already attracted considerable attention in battery technology, a secondary battery system based on these polymers is still in the experimental stage and its charge/discharge behavior is not fully understood. To gain a better understanding of the dynamic behavior and to provide guidance toward designs of new secondary batteries utilizing electrochemically conductive polymers, a one-dimensional mathematical model is presented here for the charge/discharge behavior of the lithium/polypyrrole system.

The model is used to predict the dynamic behavior of the cell during charge and discharge at constant applied current density. The spatial and time dependence of concentration, electrochemical potential, and electrode capacity profiles within the cell are presented. Also, the effects of various design parameters, such as the thickness of the polypyrrole electrode, the reservoir, and the separator, are discussed.

#### A. System Descriptions

A typical monopolar Li/LiClO<sub>4</sub>-PC/PPy secondary battery cell is presented schematically in Fig. 17. One unit cell is considered here, consisting of a polypyrrole positive electrode which has been electrochemically coated on a platinum current collector, a electrolyte reservoir containing 1M LiClO<sub>4</sub> in propylene carbonate, a separator consisting of a porous inert material, and a lithium metal negative electrode. The lithium electrode is treated as own current

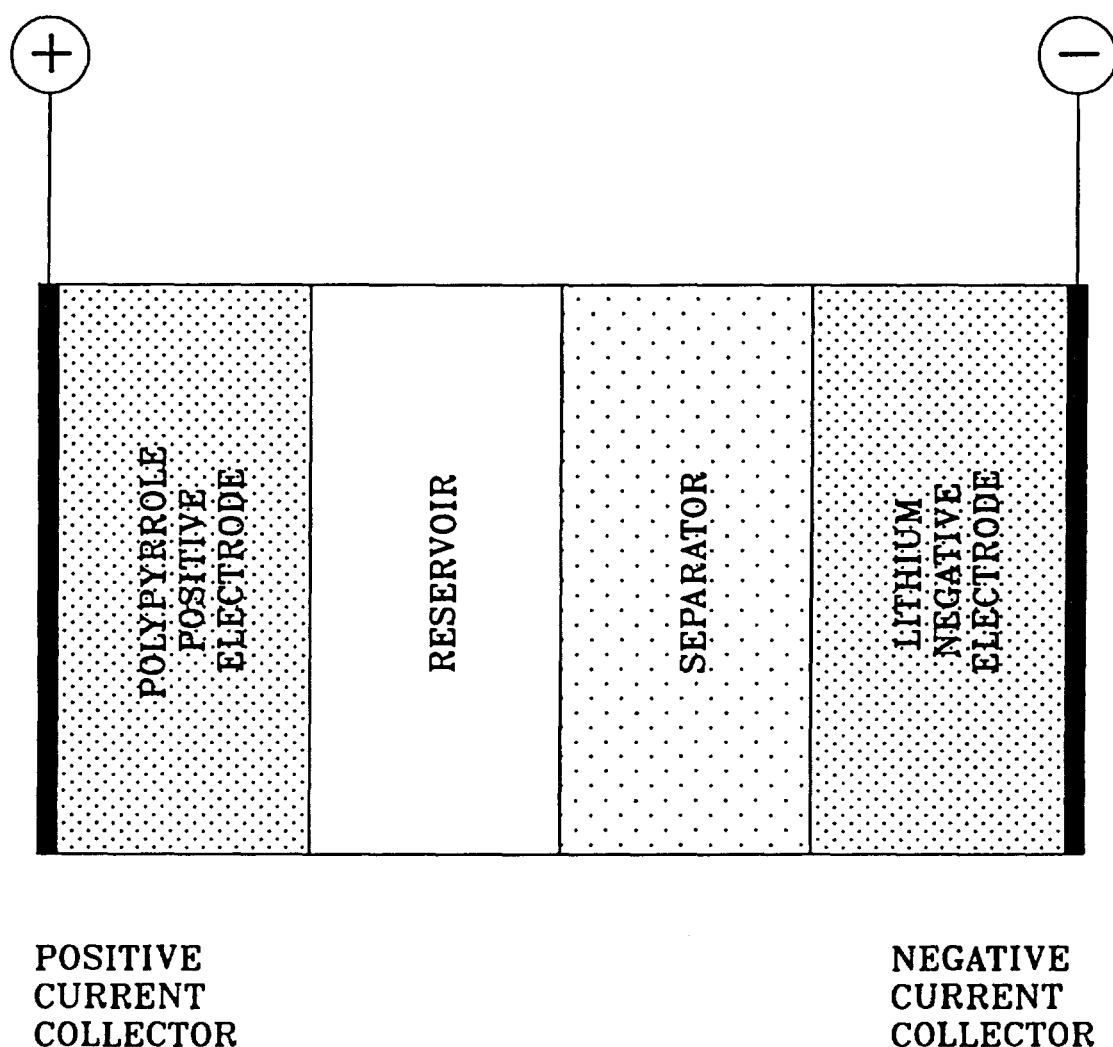


Fig. 17. A schematic diagram of a typical monopolar  $\text{Li}/\text{LiClO}_4\text{-PC/PPy}$  secondary battery cell.

collector. These four elements of the cell are repeated alternately to form a monopolar stack of cells called a battery (139).

## B. Model Descriptions

The model presented here is for predicting the charge/discharge behavior of the lithium/polypyrrole secondary battery cell at a constant current density. The modeling regions of the cell, which are relevant to the development of the model equations, are schematically presented in Fig. 18. The regions include three main regions, two boundaries, and two inter-regional interfaces, and must be modeled simultaneously. These are the boundary interface between the platinum current collector and the polypyrrole positive electrode ( $y = 0$ ); the porous polypyrrole positive electrode region of width  $\delta_{\text{ppe}}$  (region 1); the inter-regional interface between the polypyrrole positive electrode and the electrolyte reservoir ( $y = y_{\text{ppe}}$ ); the electrolyte reservoir region of width  $\delta_{\text{res}}$  (region 2); the inter-regional interface between the reservoir and the separator ( $y = y_{\text{res}}$ ); the separator region of width  $\delta_{\text{sep}}$  (region 3); the boundary interface between the separator and the lithium negative electrode ( $y = y_{\text{sep}}$ ).

The cell is operated at the constant applied current density of  $i_{\text{cell}}$  by a galvanostat. For discharge, the current flows from the lithium negative electrode to the polypyrrole positive electrode through the separator and reservoir. For charge, the opposite is true. The reaction mechanisms at the polypyrrole positive electrode, the lithium negative electrode, and the overall system are discussed in Chapter III (See Eqs. [1], [2], and [3]).

In all of the regions, the unknowns are the concentration of  $\text{Li}^+$  ( $c_+$ ), the concentration of  $\text{ClO}_4^-$  ( $c_-$ ), the local faradaic charge per unit volume ( $Q_f$ ),

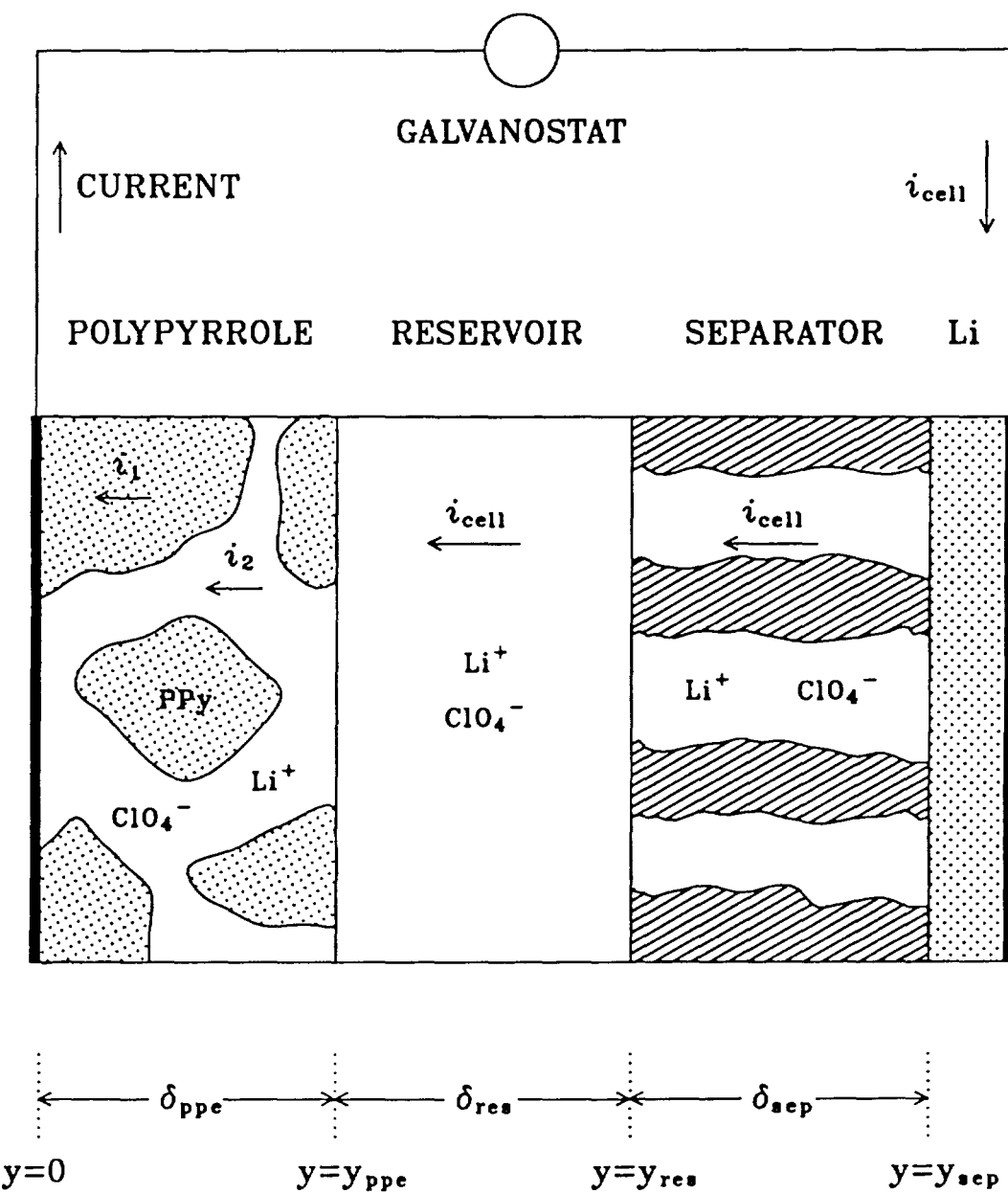


Fig. 18. A schematic diagram of modeling regions in  $\text{Li}/\text{LiClO}_4\text{-PC}/\text{PPy}$  secondary battery cell.

the potential of the solid phase ( $\Phi_1$ ), and the potential of the solution phase ( $\Phi_2$ ). Because the cell is charged and discharged at a constant current density, values for the unknowns depend on the perpendicular distance from the platinum current collector of the polypyrrole positive electrode ( $y$ ) and time ( $t$ ), and they are obtained by solving the system of governing equations and assumptions for each region of the cell described next.

### 1. Governing Equations – Polypyrrole Positive Electrode

Polypyrrole positive electrode region consists of a solid phase of polypyrrole and a solution phase of an organic electrolyte that penetrates the void spaces in the porous structure as shown in Fig. 18. Since the system operated at a constant current density by galvanostat in charge and discharge processes (instead of operating at a potential scan by potentiostat in the cyclic voltammetry), the governing equations in this region are similar to that in the porous polypyrrole electrode region in chapter IV except Current Balance used instead of Transfer Current Balance.

#### Material Balance for Dissolved Species

A one dimensional material balance equation for species  $i$  in the porous polypyrrole positive electrode is given by (See Eq. [29])

$$\frac{\partial(\epsilon_p c_i)}{\partial t} = z_i F \frac{\partial}{\partial y} \left( u_{i,p} c_i \frac{\partial \Phi_2}{\partial y} \right) + \frac{\partial}{\partial y} \left( D_{i,p} \frac{\partial c_i}{\partial y} \right) - \frac{s_{1,i} a j_1}{n_1 F} \quad (70)$$

#### Charge Balance

The state of the local faradaic charge within the polypyrrole film per unit volume ( $Q_f$ ) can be obtained by integrating the local faradaic transfer current

per unit volume ( $aj_f$ ) as follows (See Eq. [32]):

$$\frac{\partial Q_f}{\partial t} = a i_{o1, \text{ref}} \left\{ \left( 1 - \theta \right) \left( \frac{c_-}{c_{-, \text{ref}}} \right) \exp \left( \frac{\alpha_{a1} F}{RT} \eta_1 \right) - \theta \exp \left( \frac{-\alpha_{c1} F}{RT} \eta_1 \right) \right\} \quad (71)$$

### Current Balance

The current density flowing through the porous polypyrrole positive electrode ( $i_{\text{cell}}$ ) consists of the superficial current densities in the solid and solution phases ( $i_1$  and  $i_2$ ) as shown in Fig. 18

$$i_{\text{cell}} = i_1 + i_2 \quad (72)$$

Since the superficial current densities in the solid and solution phases ( $i_1$  and  $i_2$ ) are given by (See Eqs. [39] and [41])

$$i_1 = -\sigma_p \frac{\partial \Phi_1}{\partial y} \quad (73)$$

$$i_2 = -\kappa_p \frac{\partial \Phi_2}{\partial y} - F \sum_i z_i D_{i,p} \frac{\partial c_i}{\partial y} \quad (74)$$

the current balance in this region can be expressed as

$$-\sigma_p \frac{\partial \Phi_1}{\partial y} - \kappa_p \frac{\partial \Phi_2}{\partial y} - F \sum_i z_i D_{i,p} \frac{\partial c_i}{\partial y} = i_{\text{cell}} \quad (75)$$

### Electroneutrality

It is assumed here that the thickness of double layer within the pore is very thin to compare with pore size, and the solution inside the pores obeys the electroneutrality relationship, which describes as follows:

$$\sum_i z_i c_i = 0 \quad (76)$$

## 2. Governing Equations – Reservoir

The reservoir is the region between the polypyrrole positive electrode and the separator, and is initially filled with the electrolyte of 1M LiClO<sub>4</sub>-PC as shown in Fig. 18. The reservoir serves to supply electrolyte to the positive and negative electrodes as it is consumed via electrochemical reactions and double layer charging.

Mass transfer in the reservoir is governed by the following material balance equation for species i (129):

$$\frac{\partial c_i}{\partial t} = -\nabla \cdot \mathbf{N}_i \quad (77)$$

The flux of species i in the reservoir,  $\mathbf{N}_i$ , is due to migration in the electric field and diffusion in the concentration gradient

$$\mathbf{N}_i = -z_i u_i F c_i \nabla \Phi_2 - D_i \nabla c_i \quad (78)$$

Only the axial component of the flux is considered here. Substituting the normal component of Eq. [78] into Eq. [77] gives the one dimensional material balance for a dissolved species i within the reservoir:

$$\frac{\partial c_i}{\partial t} = \frac{z_i D_i F}{RT} \frac{\partial}{\partial y} \left( c_i \frac{\partial \Phi_2}{\partial y} \right) + \frac{\partial^2 c_i}{\partial y^2} \quad (79)$$

The solid electroactive material does not exist in this region, therefore the local faradaic charge ( $Q_f$ ) and the solid potential ( $\Phi_1$ ) are treated as dummy variables and their values are set arbitrarily equal to zero

$$Q_f = 0 \quad (80)$$

$$\Phi_1 = 0 \quad (81)$$

Since all the current flowing through the reservoir is carried by the electrolyte, the superficial current density in the solution phase ( $i_2$ ) can be set equal to the applied current density ( $i_{\text{cell}}$ ), and can be expressed similar to that used in the positive electrode region except that the free stream conductivity ( $\kappa$ ) and diffusivity ( $D_i$ ) applies (See Eq. [74])

$$i_2 = -\kappa \frac{\partial \Phi_2}{\partial y} - F \sum_i z_i D_i \frac{\partial c_i}{\partial y} = i_{\text{cell}} \quad (82)$$

### 3. Governing Equations – Separator

The separator consists of a porous inert material which is mainly used to prevent physical contact between the polypyrrole positive electrode and the lithium negative electrode, and a solution phase which fills the void spaces of the porous structure. Since the solid material is inert, the porosity of separator ( $\epsilon_s$ ) does not change with time and is set arbitrarily equal to a constant. An effective diffusivity ( $D_{i,s}$ ) and mobility ( $u_{i,s}$ ) of species  $i$ , and ionic conductivity of electrolyte ( $\kappa_s$ ) within the separator are obtained in the similar manner as those for the porous polypyrrole electrode region in Chapter IV (See Eqs. [22], [23], and [24]):

$$D_{i,s} = D_i \epsilon_s^{1+\text{ex}} \quad (83)$$

$$u_{i,s} = u_i \epsilon_s^{1+\text{ex}} \quad (84)$$

$$\kappa_s = \kappa \epsilon_s^{1+\text{ex}} \quad (85)$$

The differential material balance equation in the solution phase is formulated for a dissolved species  $i$  in terms of average quantities as follows (129):

$$\frac{\partial(\epsilon_s c_i)}{\partial t} = -\nabla \cdot \mathbf{N}_{i,s} \quad (86)$$

where  $\epsilon_s c_i$  represents the average concentration per total unit volume in separator including the solid inert phase and the electrolyte that occupies the void space within the matrix, and  $N_{i,s}$  represents the flux of species  $i$  within the porous separator region.

The flux of species  $i$  within the separator ( $N_{i,s}$ ) is given by an equation that is similar to that for the reservoir except that the effective diffusivity ( $D_{i,s}$ ) and mobility ( $u_{i,s}$ ) applies (See Eq. [78]):

$$N_{i,s} = -z_i u_{i,s} F c_i \nabla \Phi_2 - D_{i,s} \nabla c_i \quad (87)$$

A one dimensional differential material balance equation for species  $i$  in this region can be obtained by substituting the normal component of Eq. [87] into Eq. [86] as follows:

$$\epsilon_s \frac{\partial c_i}{\partial t} = z_i u_{i,s} F \frac{\partial}{\partial y} \left( c_i \frac{\partial \Phi_2}{\partial y} \right) + D_{i,s} \left( \frac{\partial^2 c_i}{\partial y^2} \right) \quad (88)$$

Since the solid material is inert, the local faradaic charge ( $Q_f$ ) and the solid potential ( $\Phi_1$ ) are treated as dummy variables and their values are set arbitrarily equal to zero as shown in Eqs. [80] and [81].

All of the current flowing through the separator is carried by the electrolyte, the superficial current density in the solution phase ( $i_2$ ) can be set equal to the applied current density ( $i_{cell}$ ), and can be expressed as

$$i_2 = -\kappa_s \frac{\partial \Phi_2}{\partial y} - F \sum_i z_i D_{i,s} \frac{\partial c_i}{\partial y} = i_{cell} \quad (89)$$

#### 4. Boundary and Interface Conditions

To complete the system of equations for the model, the boundary conditions at each end of the cell and inter-regional interfaces must be specified for the

dependent variables:  $c_+$ ,  $c_-$ ,  $Q_f$ ,  $\Phi_1$ , and  $\Phi_2$ . Boundary and interface conditions for these dependent variables are specified in the order of the polypyrrole positive electrode to the lithium negative electrode.

The porous polypyrrole positive electrode is bounded by a platinum current collector on one face ( $y = 0$ ) and by the reservoir on the other ( $y = y_{\text{PPE}}$ ). At the current collector/polypyrrole positive electrode interface ( $y = 0$ ), the rate of consumption (charge) or production (discharge) of each species  $i$  by the electrochemical reaction [1] and the double layer charge ( $R'_{1,i}$ ) is equal to the net normal component of the flux of  $\text{ClO}_4^-$  towards or away from the electrode. Thus

$$-z_i u_{i,p} F c_i \frac{\partial \Phi_2}{\partial y} - D_{i,p} \frac{\partial c_i}{\partial y} = -\frac{s_{1,i} a j_1}{n_1 F} \quad (90)$$

The rate of accumulation of the local faradaic charge per unit volume within the polypyrrole positive electrode ( $Q_f$ ) is obtained from the local faradaic transfer current per unit volume ( $a j_f$ ) as shown in Eq. [71]. At this point, all of the current leaves the cell via the current collector which can be represented with constant  $i_{\text{cell}}$ . Thus, the superficial current density in the solid and solution phases ( $i_1$  and  $i_2$ ) can be set to  $i_{\text{cell}}$  and zero, so that

$$i_1 = -\sigma_p \frac{\partial \Phi_1}{\partial y} = i_{\text{cell}} \quad (91)$$

$$i_2 = -\kappa_p \frac{\partial \Phi_2}{\partial y} - F \sum_i z_i D_{i,p} \frac{\partial c_i}{\partial y} = 0 \quad (92)$$

At the polypyrrole positive electrode/reservoir interface ( $y = y_{\text{PPE}}$ ), the flux of each species  $i$  across the two regions must be continuous, which can be written as follows:

$$-z_i u_{i,p} F c_i \frac{\partial \Phi_2}{\partial y} - D_{i,p} \frac{\partial c_i}{\partial y} = -z_i u_i F c_i \frac{\partial \Phi_2}{\partial y} - D_i \frac{\partial c_i}{\partial y} \quad (93)$$

Because the solid electrode phase ends at this point and all of the current is in the solution phase, the gradient of the local faradaic charge ( $Q_f$ ) and the solid potential ( $\Phi_1$ ) are set equal to zero

$$\frac{\partial Q_f}{\partial y} \Big|_{y_{ppc}} = 0 \quad (94)$$

$$\frac{\partial \Phi_1}{\partial y} \Big|_{y_{ppc}} = 0 \quad (95)$$

Also, the superficial current density in the solution phase ( $i_2$ ) is set equal to the applied current density,  $i_{cell}$ , as follows:

$$i_2 = -\kappa_p \frac{\partial \Phi_2}{\partial y} - F \sum_i z_i D_{i,p} \frac{\partial c_i}{\partial y} = i_{cell} \quad (96)$$

At the reservoir/separator interface ( $y = y_{res}$ ), the boundary conditions are derived in the same manner as those for the positive electrode/reservoir interface. The flux of each species  $i$  across the two regions must be continuous

$$-z_i u_i F c_i \frac{\partial \Phi_2}{\partial y} - D_i \frac{\partial c_i}{\partial y} = -z_i u_{i,s} F c_i \frac{\partial \Phi_2}{\partial y} - D_{i,s} \frac{\partial c_i}{\partial y} \quad (97)$$

and the superficial current density ( $i_2$ ) in the solution phase is set equal to constant  $i_{cell}$

$$i_2 = -\kappa \frac{\partial \Phi_2}{\partial y} - F \sum_i z_i D_i \frac{\partial c_i}{\partial y} = i_{cell} \quad (98)$$

The local faradaic charge ( $Q_f$ ) and the solid potential ( $\Phi_1$ ) are treated as dummy variables and are arbitrarily set equal to zero as shown in Eqs. [80] and [81].

At the separator/lithium negative electrode interface ( $y = y_{sep}$ ), the rate of consumption (charge) or production (discharge) of a  $\text{Li}^+$  by the electrochemical reaction [2] is equal to the net normal component of the flux of  $\text{Li}^+$  towards or away from the electrode

$$-z_+ u_{+,s} F c_+ \frac{\partial \Phi_2}{\partial y} - D_{+,s} \frac{\partial c_+}{\partial y} = \frac{s_2 + j_2}{n_2 F} \quad (99)$$

where  $j_2$  represents local transfer current density for the electrochemical reaction [2] and is discussed in Chapter III. Combining Eqs. [18] and [99] yields

$$\begin{aligned} -z_+ u_{+,s} F c_+ \frac{\partial \Phi_2}{\partial y} - D_{+,s} \frac{\partial c_+}{\partial y} = \\ \frac{s_{2,+}}{n_2 F} i_{o2,\text{ref}} \left\{ \exp\left(\frac{\alpha_{a2} F}{RT} \eta_2\right) - \exp\left(\frac{-\alpha_{c2} F}{RT} \eta_2\right) \right\} \end{aligned} \quad (100)$$

The normal component of the flux of  $\text{ClO}_4^-$  is assumed to be equal to zero

$$-z_- u_{-,s} F c_- \frac{\partial \Phi_2}{\partial y} - D_{-,s} \frac{\partial c_-}{\partial y} = 0 \quad (101)$$

The local faradaic charge ( $Q_f$ ) is treated as a dummy variable and is arbitrarily set equal to zero (See Eq. [80]). The potential in the solid lithium ( $\Phi_1$ ) at this point is set arbitrarily equal to zero volt:

$$\Phi_1 = 0 \quad (102)$$

This is done to provide a reference point and consequently a particular solution for the model. Of course, the solid potential ( $\Phi_1$ ) could be alternatively set to zero at the other end of the cell (i.e., at the current collector/polypyrrole positive electrode interface). At this point ( $y = y_{\text{sep}}$ ), all the current in the cell leaves the electrolyte and enters the lithium negative electrode by the electrochemical reaction [2]

$$i_{\text{cell}} = -j_2 \quad (103)$$

It is noted that the electroactive area is same as the projected electrode area at this point. Substituting Eq. [18] into Eq. [103] yields

$$-i_{o2,\text{ref}} \left\{ \exp\left(\frac{\alpha_{a2} F}{RT} \eta_2\right) - \exp\left(\frac{-\alpha_{c2} F}{RT} \eta_2\right) \right\} = i_{\text{cell}} \quad (104)$$

As mentioned earlier, the lithium electrode is treated in here as own current collector.

## 5. Initial Conditions

Initial conditions are necessary for the variables which depend explicitly on time. For convenience, it is assumed that the cell is in its fully discharged state and ready to be charged. Consequently, the local faradaic charge per unit volume is initially set equal to  $Q_{f,\text{red}}$ , a minimal charge state, throughout the porous polypyrrole positive electrode. Therefore, porosity ( $\epsilon_p$ ) and conductivity ( $\sigma_p$ ) of the polypyrrole positive electrode are initially set equal to  $\epsilon_{\text{red}}$  and  $\sigma_{\text{red}}$ , values at this reduced state, throughout the porous polypyrrole positive electrode. In the other regions, these variables are treated as a dummy variable and are arbitrarily set equal to zero.

The concentration of each species  $i$  throughout the cell is set equal to its reference concentration:

$$c_i = c_{i,\text{ref}} \quad (105)$$

The conductivity of the electrolyte ( $\kappa$ ) can be obtained by combining Eqs. [24] and [105]. Other dependent variables ( $\Phi_1$ , and  $\Phi_2$ ) do not require initial conditions and are arbitrarily set equal to zero at  $t = 0$  for all  $y$ .

## 6. Solution Method

The governing equations, boundary conditions, and interface conditions for the determination of the quantities  $c_+$ ,  $c_-$ ,  $Q_f$ ,  $\Phi_1$ , and  $\Phi_2$ , have been summarized in Table XVI. The system of equations is solved in the similar manner as discussed in chapter IV.

The whole cell is divided into  $NJ$  mesh points with  $J = 1$  designated to be the interface of the platinum current collector and polypyrrole positive electrode,  $J = NJ1$  designated to be the inter-regional interface of the polypyrrole positive

electrode and electrolyte reservoir,  $J = NJ2$  designated to be the inter-regional interface of the electrolyte reservoir and separator, and  $J = NJ$  to be the interface of the separator and negative lithium electrode. Mesh point spacing may vary in each region because of the difference in the thickness of each region and the number of nodal points used.

Once the values of unknowns ( $c_+$ ,  $c_-$ ,  $Q_f$ ,  $\Phi_1$ , and  $\Phi_2$ ) are obtained, values of  $i_1$  and  $i_2$  for each region, and  $Q_c$  can be obtained from those dependent variables using Eqs. [39], [41], and [33]. The applied current density ( $i_{cell}$ ) flowing through the cell is constant and is equal to the sum of the current density flowing in the solid phase ( $i_1$ ) and the solution phase ( $i_2$ ).

Table XVI. System of equations for charge/discharge behavior  
of lithium/polypyrrole secondary battery cell.

#### A. Governing equations.

Variables	Region 1	Region 2	Region 3
$c_+$	70	79	88
$c_-$	70	79	88
$Q_f$	71	80	80
$\Phi_1$	75	81	81
$\Phi_2$	76	82	89

#### B. Boundary and interface conditions.

Variables	$y = 0$	$y = y_{ppe}$	$y = y_{res}$	$y = y_{sep}$
$c_+$	90	93	97	100
$c_-$	90	93	97	101
$Q_f$	32	94	80	80
$\Phi_1$	91	95	81	102
$\Phi_2$	92	96	98	104

### C. Results and Discussion

The model is used to simulate the dynamic charge/discharge behavior of a typical Li/LiClO<sub>4</sub>-PC/PPy secondary battery cell under various operating conditions. The effects of various design parameters, such as the thickness of the electrode, the reservoir, and separator, etc., on the cell discharge performance are also examined.

The values used for the operating conditions in charging and discharging processes are given in Table XVII. It is assumed that charge/discharge process occurs under the constant current density of 0.2 mA/cm<sup>2</sup> at room temperature. The charge and discharge current densities are specified as being positive and negative because of the chosen coordinate system, respectively. A 1  $\mu\text{m}$  thick polypyrrole film is used in this study because a high doping level and a high efficiency have been observed for this thickness (107). To minimize ohmic loss in a cell, the separator is chosen to have an overall porosity of 0.5 to permit better diffusion of electrolyte and migration of ions between electrodes. The thickness of the reservoir and the separator are chosen arbitrarily to contain 30% of electrolyte for a fully charged cell. All the potentials are referred to the Li/Li<sup>+</sup> electrode.

Table XVII. Operating conditions used for charge/discharge behavior of lithium/polypyrrole secondary battery cell.

Operating Temperature ( $T$ )	298.15 K
Applied Cell Current Density ( $i_{\text{cell}}$ )	0.2 mA/cm <sup>2</sup>
Geometric Electrode Surface Area ( $A$ )	1.0 cm <sup>2</sup>
Thickness of Polypyrrole Positive Electrode ( $\delta_{\text{ppe}}$ )	1.0 $\mu\text{m}$
Thickness of Reservoir ( $\delta_{\text{res}}$ )	3.0 $\mu\text{m}$
Thickness of Separator ( $\delta_{\text{sep}}$ )	2.0 $\mu\text{m}$
Porosity of Separator ( $\epsilon_s$ )	0.5
Reference Potential ( $\Phi_{\text{ref}}$ )	0.0 (vs. Li)

### 1. Charge and Discharge Behavior

The simulated charge/discharge curve of the lithium/polypyrrole secondary battery cell at the applied current density of  $0.2 \text{ mA/cm}^2$  are obtained by using the model developed above and fixed parameter values given in Tables IV, V, VII, VIII, XII, and XVII as shown in Fig. 19. The cell potential,  $\Phi_{\text{cell}}$ , represents the difference between the potential of the solid phase at the current collector of the polypyrrole positive electrode at  $y = 0$  and that of the lithium negative electrode at  $y = y_{\text{sep}}$ . For convenience, the charge and discharge processes are terminated when the faradaic charge state of the cell ( $Q_f/Q_{f,\text{oxd}}$ ) reaches 99.9% and 0.1%, respectively.

The values of predicted cell potential are 3.444 V for 99.9% charged state and 2.853 V for 0.01% charged state, respectively. At the end of the discharge, the sharp potential drop indicates that the polymer becomes insulator. The average discharge potential ( $\Phi_{\text{ave}}$ ) of the typical cell is estimated as 3.160 V from the discharge curve in Fig. 19.

Important properties of a battery are the energy and power densities. The energy density of the cell is defined here as the amount of energy extracted per unit mass of polypyrrole in the cell and is calculated by using the following equation (105):

$$\text{Energy Density} = \frac{I_{\text{cell}} \Phi_{\text{ave}} t_d}{M} \quad (106)$$

where,  $I_{\text{cell}}$  represents the total cell current,  $t_d$  represents the discharge time of the cell, and  $M$  represents the mass of the polypyrrole electrode. The total cell current ( $I_{\text{cell}}$ ) can be obtained by multiplying by the cell current density ( $i_{\text{cell}}$ ) by the cross-sectional area of the electrode ( $A$ ). The theoretical energy density obtained from the discharge curve in Fig. 19 is about 191.9 Wh/kg of polypyrrole

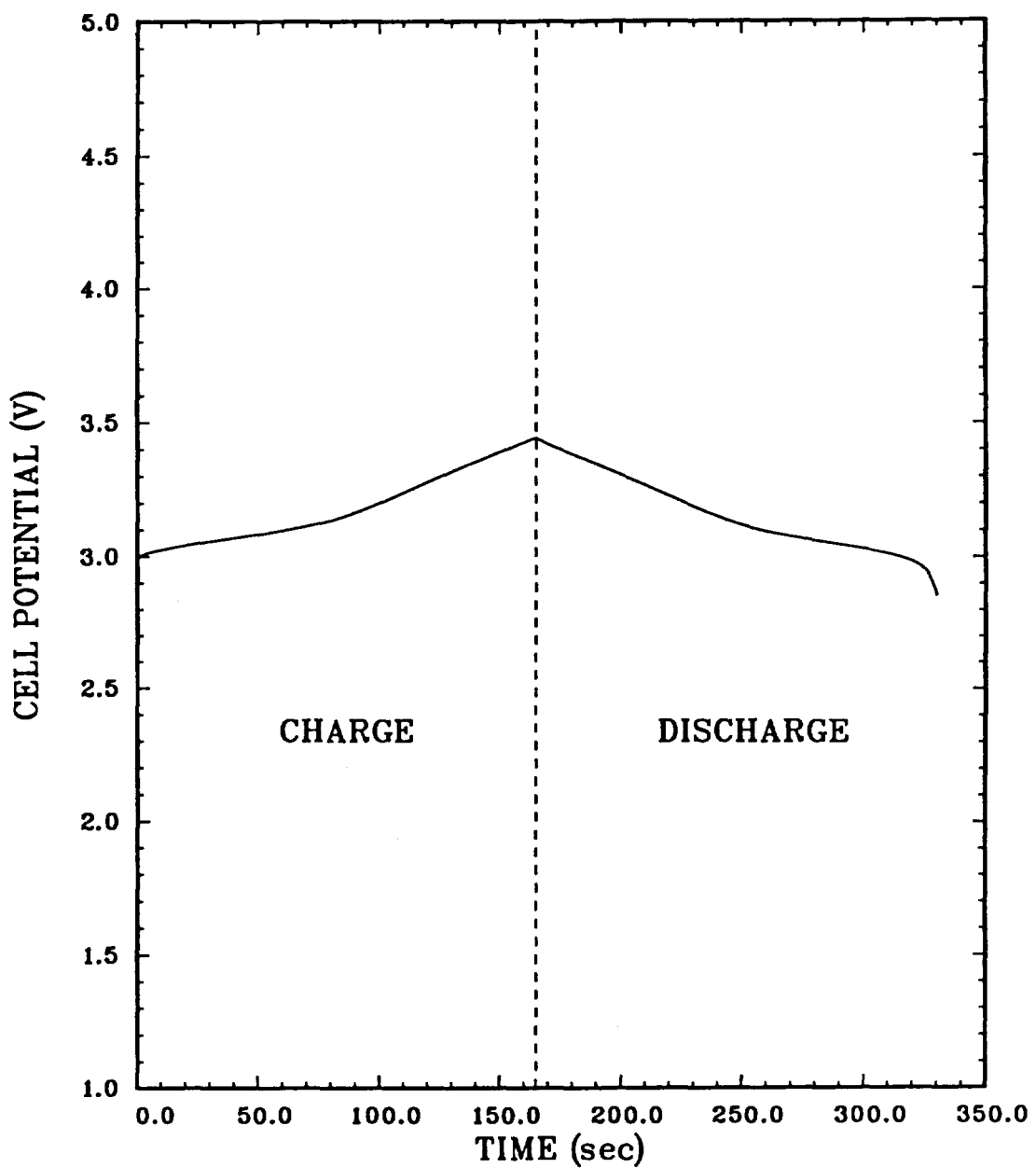


Fig. 19. Simulated charge and discharge behaviors of a typical Li/LiClO<sub>4</sub>-PC/Ppy secondary battery cell at  $i_{cell} = 0.2 \text{ mA/cm}^2$ .

positive electrode.

The power density of the cell is defined as the rate of delivering energy per unit mass of polypyrrole in the cell and is calculated as follows (105):

$$\text{Power Density} = \frac{I_{\text{cell}} \Phi_{\text{ave}}}{M} \quad (107)$$

The theoretical power density obtained from the discharge curve in Fig. 19 is about 4185 W/kg of polypyrrole positive electrode. The characteristics of the cell estimated from this study are summarized in Table XVIII. Direct comparison of the theoretical prediction to those of the experimental data available in the literature is not attempted, although the predictions of charge/discharge behavior seems reasonable.

The cell potential versus time curve shown in Fig. 19 increases with a certain initial slope which changes to a different slope midway through both charge and discharge. This is because the charging and discharging processes are affected by two distinctive factors, faradaic and capacitive current densities ( $i_f$  and  $i_c$ ) as shown in Fig. 20 as a function of time. They are obtained by integrating the local faradaic and capacitive transfer current ( $a j_f$  and  $a j_c$ ) over the porous polypyrrole positive electrode region as discussed in Eq. [66].

Table XVIII. Electrochemical characteristic of one square centimeter lithium/polypyrrole secondary battery cell during discharge.

Mass of Polypyrrole Positive Electrode ( $M$ )	$1.51 \times 10^{-4}$ g
Applied Cell Current ( $I_{\text{cell}}$ )	0.2 mA
Average Cell Potential ( $\Phi_{\text{ave}}$ )	3.160 V
Discharge Time ( $t_d$ )	165.0 sec
Energy Density	191.9 Wh/Kg <sup>†</sup>
Power Density	4185 W/Kg <sup>†</sup>

<sup>†</sup> Based on the mass of the polypyrrole positive electrode.

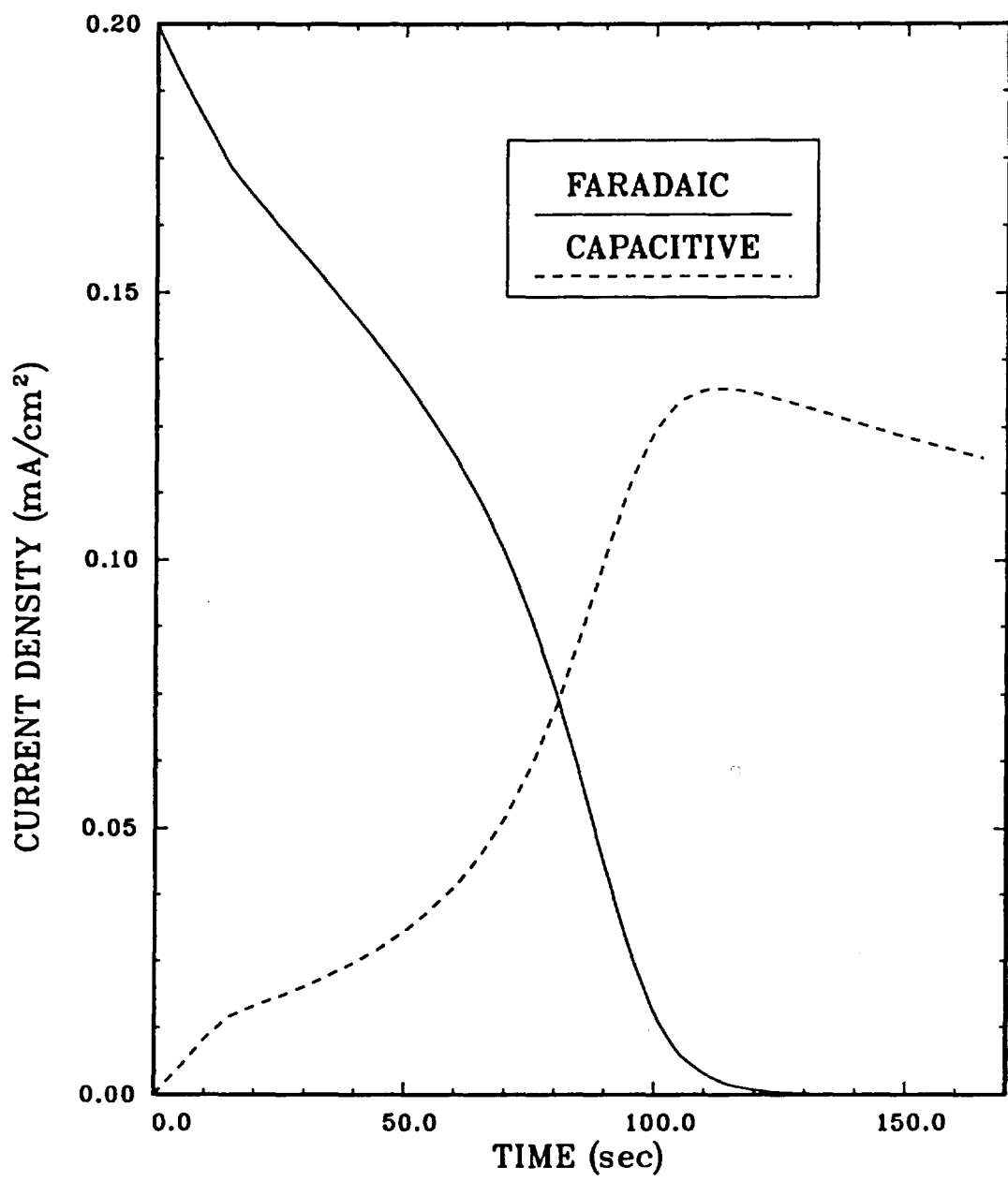


Fig. 20. Faradaic and capacitive current components within the polypyrrole positive electrode during charge at  $i_{\text{cell}} = 0.2 \text{ mA/cm}^2$ .

During charge, the first slope in Fig. 20 is dominated by the faradaic effect, while the second slope is dominated by the capacitive effect. The faradaic current density ( $i_f$ ) decreases with time because the electroactive area (reduced polypyrrole sites) and the concentration of the counterion decrease as the cell is charging. However, the capacitive current density ( $i_c$ ) increases with time because oxidized polypyrrole sites increase continuously with time until the polypyrrole electrode is fully oxidized at about 100 seconds. When the polypyrrole positive electrode is fully oxidized, faradaic current density becomes flat (no further oxidation of polypyrrole occurs), while capacitive current density still exists because of the double layer on the polypyrrole which is fully oxidized and the total current density is dominated by capacitive effect only. For discharge, the opposite phenomena are true.

## 2. Dependent Variables Profiles

The dynamic profiles of the dependent variables across a typical cell during charge and discharge at a constant current density of  $0.2 \text{ mA/cm}^2$  are shown in Figs. 21 through 23 as functions of time ( $t$ ) and position ( $y$ ). In the position coordinate,  $y = 0$  represents the interface between platinum current collector/polypyrrole positive electrode and  $y = 6$  represents the interface between the separator/lithium negative electrode as shown in Fig. 18. In the time coordinate, the cell is in its fully discharged state and ready to be charged at  $t = 0$ .

The dynamic concentration profiles of the anion ( $\text{ClO}_4^-$ ) are shown in Fig. 21. The concentration is made dimensionless relative to its reference concentrations ( $c_{-,ref}$ ). It is noted that the concentration profiles of the cation ( $\text{Li}^+$ ) have similar distributions because of the electroneutrality.

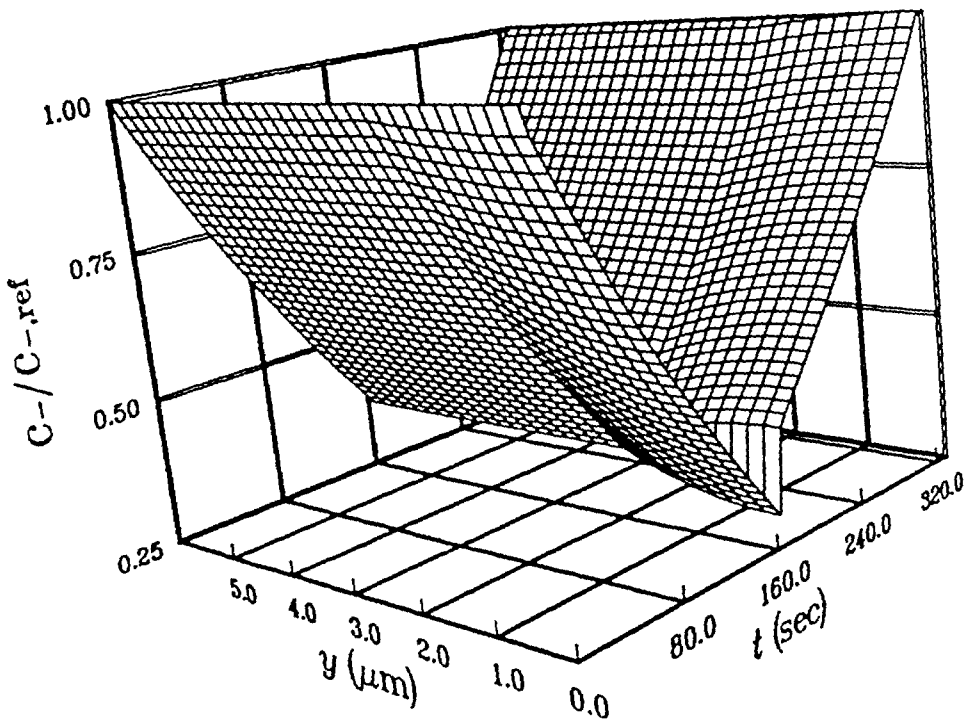


Fig. 21. Dimensionless concentration profiles of the anion ( $\text{ClO}_4^-$ ) across a typical cell during charge and discharge at  $i_{\text{cell}} = 0.2 \text{ mA/cm}^2$ .

Initially, the concentration of the anion is uniform throughout the cell at reference concentration ( $c_{-,ref}$ ). Applying a constant current density of 0.2 mA/cm<sup>2</sup> causes the anions to be consumed at the polypyrrole positive electrode by the oxidation of polypyrrole (electrochemical reaction [1]) and double layer charging. Also, cations are consumed at the lithium negative electrode by the reduction of lithium (electrochemical reaction [2]). The reacting species (ClO<sub>4</sub><sup>-</sup> for the polypyrrole electrode and Li<sup>+</sup> for the lithium electrode) are transported from the reservoir to the electrodes.

For discharge, the opposite phenomena are true. Anions are produced at the polypyrrole positive electrode by the reduction of polypyrrole and decrease of double layer charge. Also, cations are produced at the lithium negative electrode by the oxidation of lithium (electrochemical reaction [2]). The reacting species (ClO<sub>4</sub><sup>-</sup> for the polypyrrole electrode and Li<sup>+</sup> for the lithium electrode) are transported from the electrodes to the reservoir. Since the effective diffusivity of Li<sup>+</sup> and ClO<sub>4</sub><sup>-</sup> within the porous regions (polypyrrole positive electrode and separator) are smaller than the free stream diffusivity of those species, the concentration gradients within the porous regions must be larger to make up for the slower movement of the ions.

Figure 22 shows the faradaic charge profiles. The faradaic charge per unit volume is made dimensionless by using the maximum faradaic charge value ( $Q_{f,oxd}$ ) as the reference point. It is noted that the faradaic charges in the reservoir and separator regions are treated as dummy variables and their value are set arbitrarily equal to zero.

Initially, the polypyrrole positive electrode is in its fully neutral state at  $Q_f = Q_{f,red}$  and is ready to be oxidized. By applying a constant current density

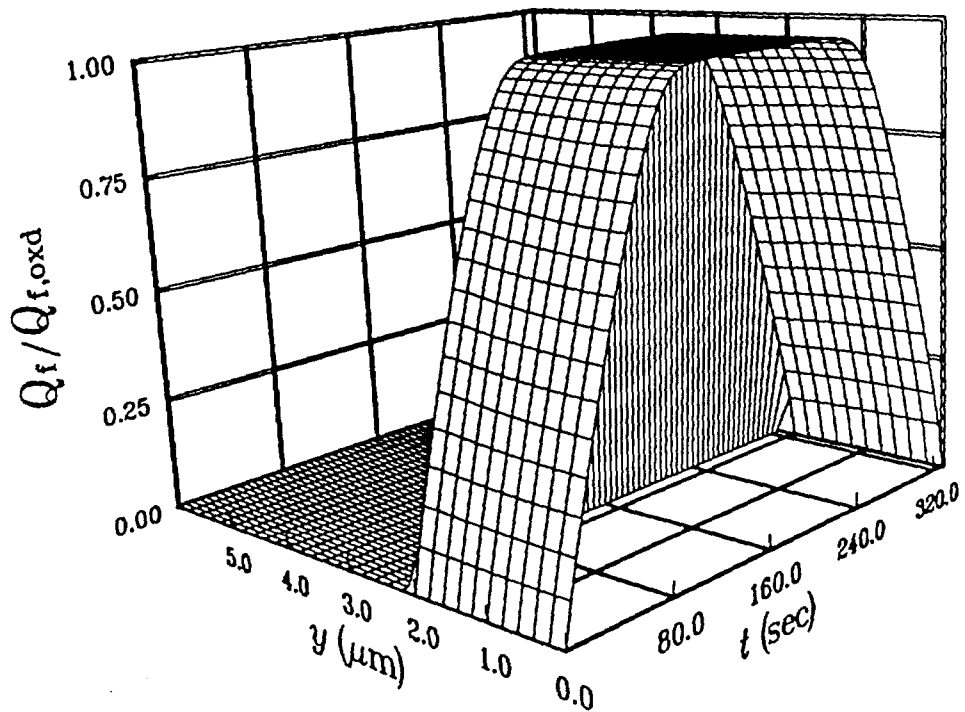


Fig. 22. Dimensionless faradaic charge profiles across a typical cell during charge and discharge at  $i_{\text{cell}} = 0.2 \text{ mA/cm}^2$ .

of  $0.2 \text{ mA/cm}^2$ , the faradaic charge is accumulated throughout the polypyrrole electrode by the electrochemical reaction [1]. The faradaic charge accumulation in the outer layer of the polypyrrole electrode (reservoir side) is faster because of the concentration gradient effect within polypyrrole electrode as shown in Fig. 21. After the polypyrrole electrode has been fully oxidized, the charge distribution becomes uniform again at  $Q_f = Q_{f,\text{oxd}}$ . During discharge, the opposite phenomena are true. The faradaic charge is withdrawn slower in the inner layer of the polypyrrole electrode (current collector side) because of the diffusion limitation.

The electrochemical properties of polypyrrole positive electrode (such as, porosity, conductivity, diffusivity, mobility, etc.) have the similar distributions throughout the polypyrrole positive electrode because of the assumption that these properties are proportional to the faradaic charge consumed within the polypyrrole electrode.

Figure 23 shows the potential profiles of the solution phase. The solution potential decreases during charge and increases during discharge. These are due to the compensation for changing available electroactive area in the solid phase and reactive species in the solution phase. During charge, the solution potential decreases with two different slope because of two distinctive factors, faradaic and capacitive effects, as discussed in Fig. 20. For discharge, opposite phenomena are true. At the end of discharge, the sharp potential increase indicates that the cell is fully discharged.

### 3. Effects of Operating Conditions

The effects of various operating conditions on the charge/discharge cell performance can be examined by the model developed here. For example, the

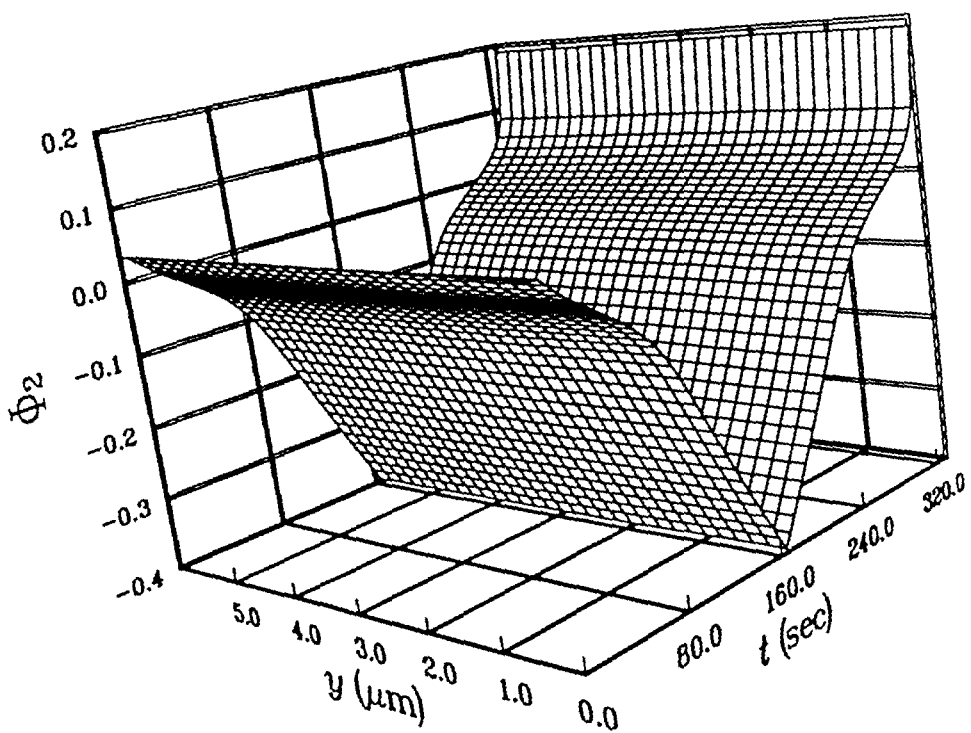


Fig. 23. Solution potential profiles across a typical cell during charge and discharge at  $i_{\text{cell}} = 0.2 \text{ mA/cm}^2$ .

effects of discharge rate on the predicted behavior of the cell discharge are examined in Fig. 24. By increasing discharge rates 0.2, 0.3, and 0.4 mV/sec, the energy densities of the cell decrease 191.9, 191.0, and 172.4 Wh/kg of polypyrrole positive electrode. This clearly illustrates that the cell is better utilized at lower discharge rate. At discharge rate higher than 0.5 mV/sec, the cell is dead before the cell is completely utilized because of the effect of pore-plugging, which prevents the counterion in the reservoir from diffusing into the pores and supporting the electrode reaction [1] and the double layer charging.

#### 4. Effects of Design Parameters

The effects of various cell physical parameters on the predicted behavior of the cell and their implications can be examined by the model developed here. Since the capacity of the cell is determined by the amount of electrode active material and the amount of electrolyte available in the system, the effects of the thickness of the polypyrrole positive electrode, reservoir, and separator on the discharge cell performance at a constant current density of  $0.2 \text{ mA/cm}^2$  are examined in Figs. 25 through 27.

Figure 25 shows the effect of the thickness of the polypyrrole positive electrode (equivalent to changing the amount of polypyrrole electroactive material). Increasing the thickness of the polypyrrole electrode yields more electroactive sites so that a slightly larger cell discharge potential and a longer discharge time are obtained.

Figure 26 shows the effect of the thickness of the reservoir (equivalent to changing the amount of electroactive counterion). Increasing the thickness of the reservoir yields a slightly smaller cell discharge potential and a shorter discharge time. This is because the thicker reservoir tends to increase ohmic drop, although

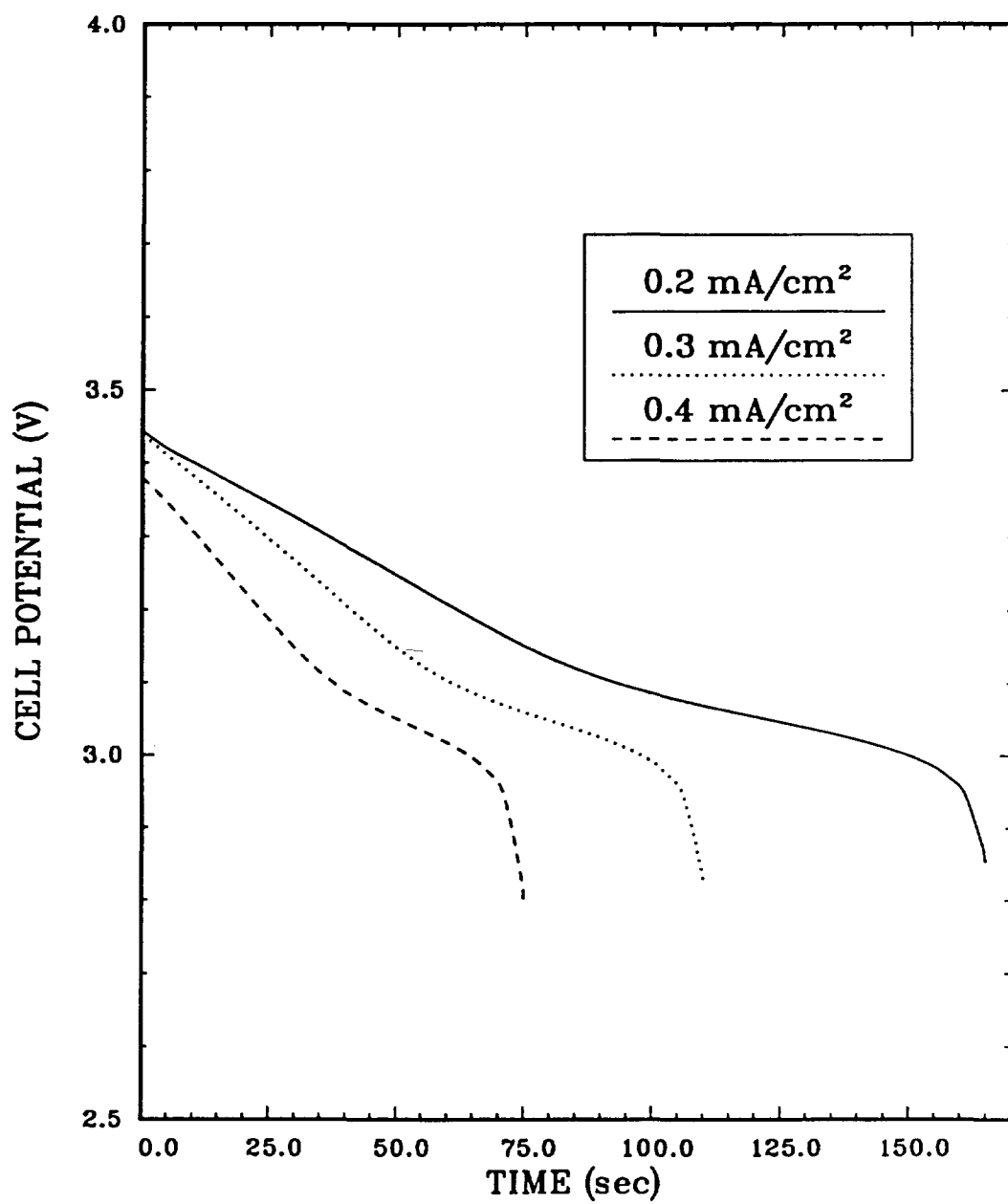


Fig. 24. The effect of the discharge rate on the cell discharge performance.

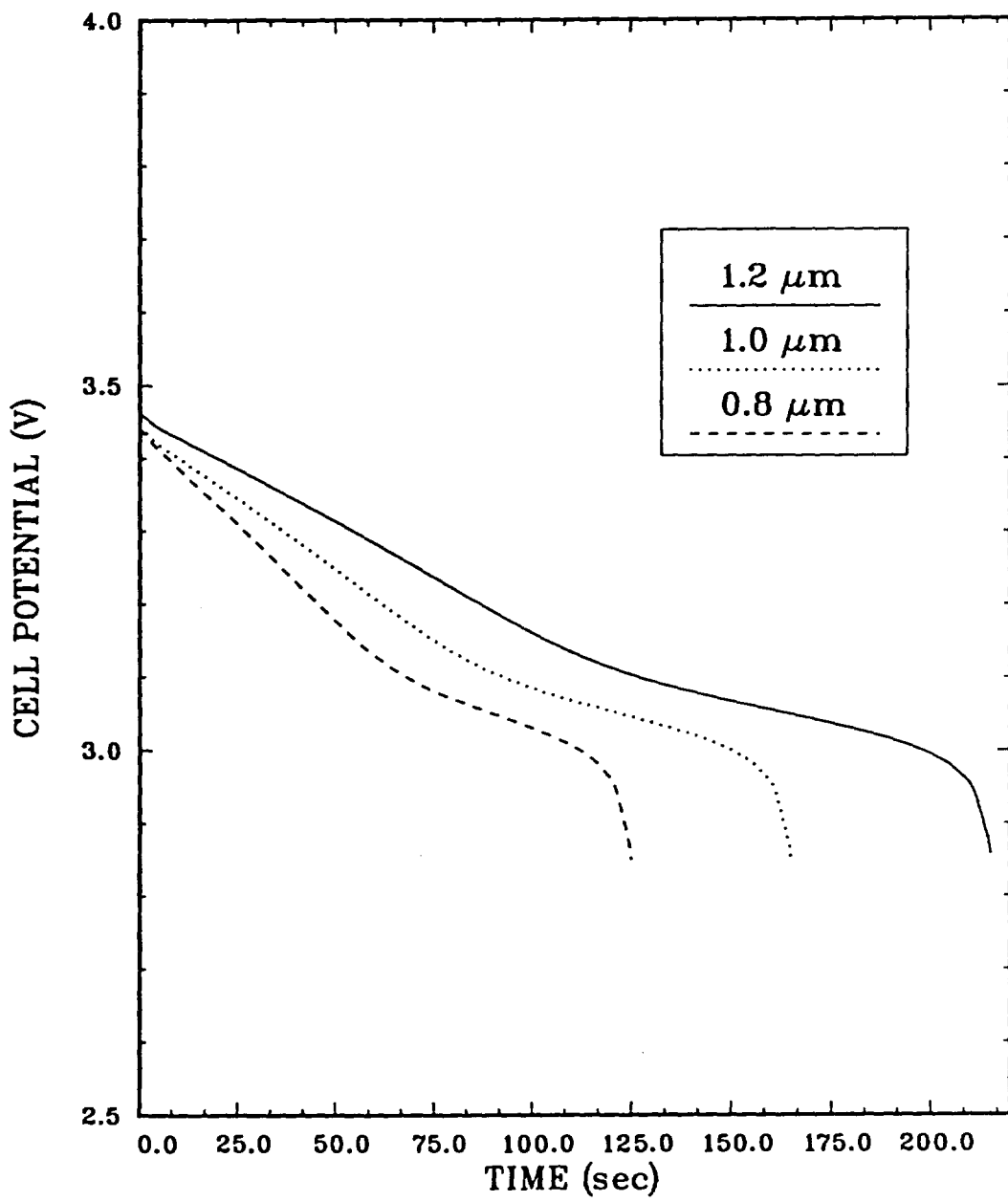


Fig. 25. The effect of the thickness of the polypyrrole positive electrode on the cell discharge performance at  $i_{\text{cell}} = 0.2 \text{ mA/cm}^2$ .

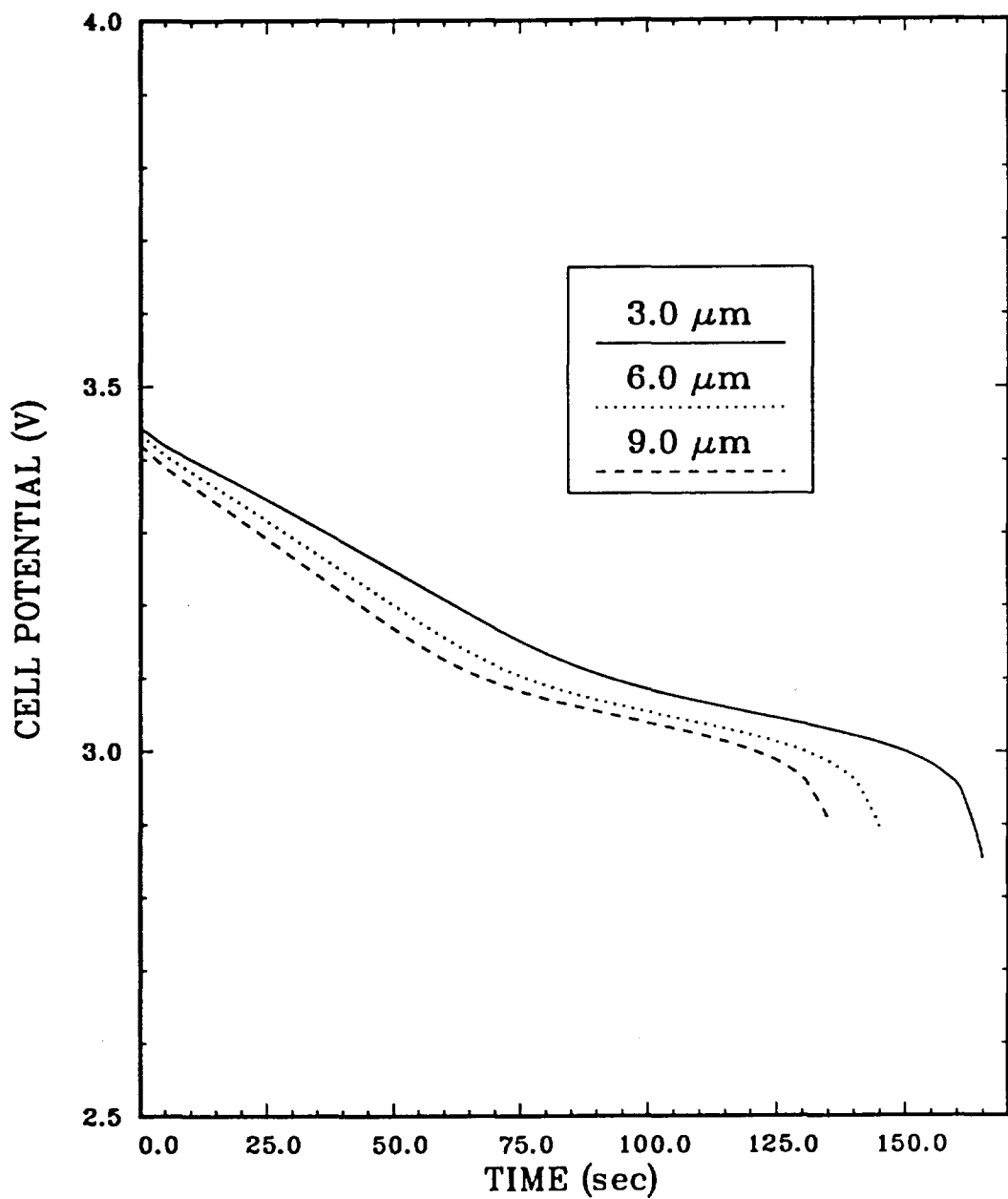


Fig. 26. The effect of the thickness of the reservoir on the cell discharge performance at  $i_{\text{cell}} = 0.2 \text{ mA/cm}^2$ .

more reactive species.

Figure 27 shows the effect of the thickness of the separator. Also, increasing the thickness of the separator yields a slightly smaller cell discharge potential and a shorter discharge time. This is because the thicker separator tends to increase ohmic drop.

Consequently, the optimal values of design parameters discussed above have to be determined in conjunction with other design parameters and operating conditions.

#### D. Conclusions and Recommendations

A one dimensional mathematical model for a lithium/polypyrrole secondary battery system is developed and used to predict dynamic behaviors of charging and discharging processes. A set of independent design criteria is specified and the model is used to show the effects of changes in these criteria on the cell performance. The results of this work show that:

- a. A comparison of the predicted results from this model to those of the experimental data available in the literature shows a qualitative agreement. Based on the theoretical calculations, lithium/polypyrrole secondary battery system can offer higher energy density, power density, and cell potential than any existing battery system.
- b. Discharging process at room temperature is governed by the amount of the electroactive sites within polypyrrole positive electrode and the availability of the counterion to those sites. Thus, the cell performance could be improved by modifying the microscopic structure of polypyrrole positive electrode which yields more electroactive sites and easier

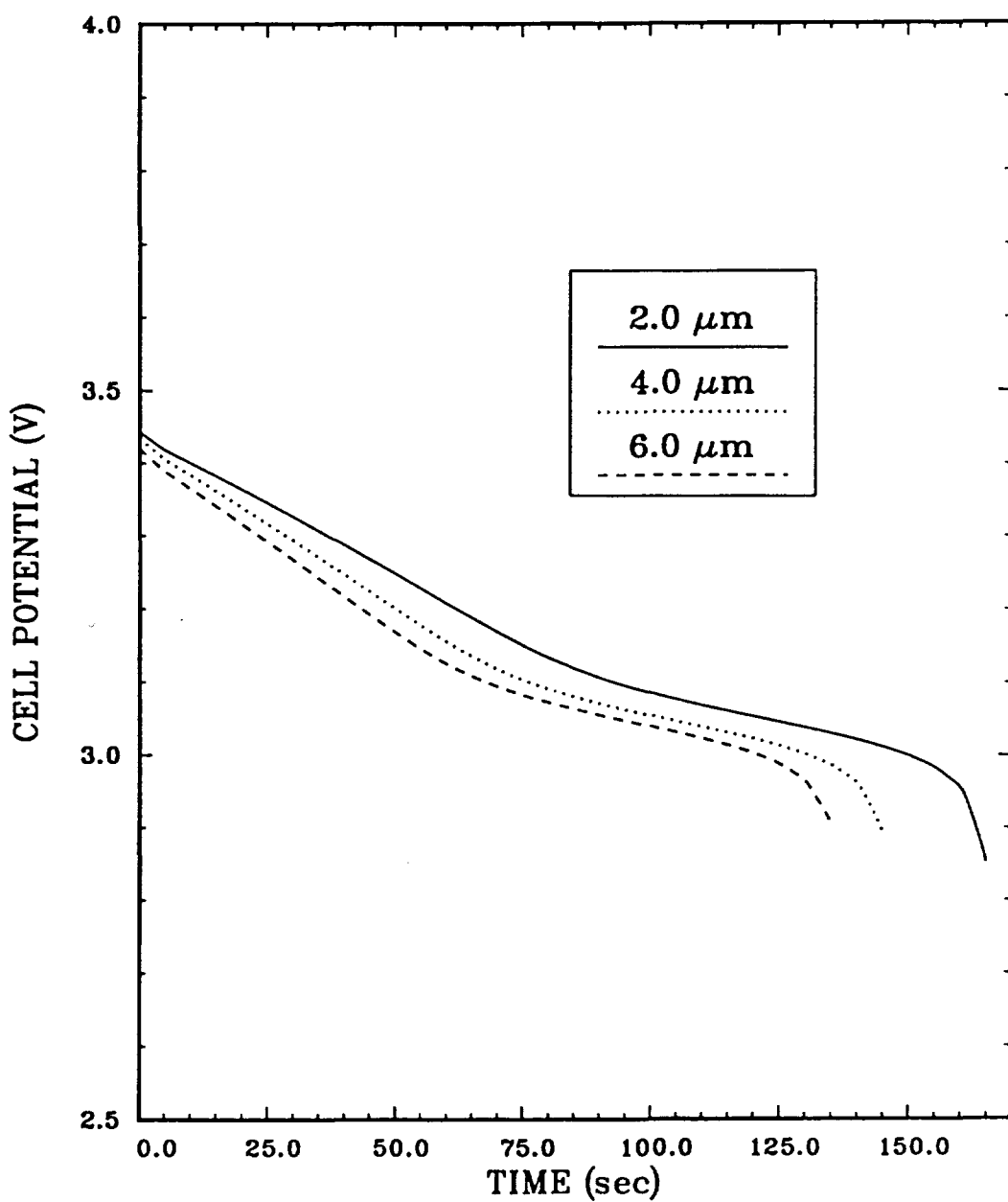


Fig. 27. The effect of the thickness of the separator on the cell discharge performance at  $i_{\text{cell}} = 0.2 \text{ mA/cm}^2$ .

counterion diffusion.

A large number of cases could be studied using the model to help better understand the physical phenomena occurring at charge/discharge process and thus determine optimal and safe designs for various cell specifications and discharge rates. It may be possible to use this model together with experimental data and parameter estimation techniques to determine the characteristic of charge/discharge behavior of the lithium/polypyrrole secondary battery cell. The lithium/polypyrrole model developed here could be modified to study other polymeric battery systems. Improvements of the model could be yield by accounting the capacity loss in the cycling and the self discharge reaction mechanisms.

## LIST OF SYMBOLS

<u>Symbol</u>	<u>Definition</u>
$A$	Geometric electrode surface area, $\text{cm}^2$
$a$	Specific surface area of polypyrrole film, $/\text{cm}$
$a'$	Rotating disk electrode constant, 0.51023
$a^*$	Double layer constant, $/\text{V}$
$C_k(J)$	$k^{\text{th}}$ unknown at node $J$
$C_l$	Related capacitance of polypyrrole film
$c_i$	Concentration of species $i$ , $\text{mol}/\text{cm}^3$
$c_{i,\text{ref}}$	Reference concentration of species $i$ , $\text{mol}/\text{cm}^3$
$D_i$	Diffusion coefficient of species $i$ , $\text{cm}^2/\text{sec}$
$D_{i,p}$	Effective diffusion coefficient of species $i$ within the polypyrrole film, $\text{cm}^2/\text{sec}$
$D_{i,s}$	Effective diffusion coefficient of species $i$ within the separator, $\text{cm}^2/\text{sec}$
$E$	Applied potential (potential difference between the current collector and reference electrode), $\text{V}$
$E_{\text{neg}}$	Negative potential limit, $\text{V}$
$E_{\text{pa}}$	Anodic peak potential, $\text{V}$
$E_{\text{pc}}$	Cathodic peak potential, $\text{V}$
$E_{\text{pos}}$	Positive potential limit, $\text{V}$
$e$	Quantity of charge on the electron, $1.60219 \times 10^{-19} \text{ C}$
$\text{ex}$	Exponent on the porosity term, 0.5
$F$	Faraday's constant, $96487 \text{ C/mol}$
$\Delta G$	Gibbs free energy change in a chemical process, $\text{kJ}$
$I_{\text{cell}}$	Total cell current, $\text{A}$
$i$	Current density based on projected electrode area, $\text{A}/\text{cm}^2$
$i_a$	Anodic current density with perturbed value of parameter $k$ , $\text{A}/\text{cm}^2$
$i_a^*$	Anodic current density with reference value of parameter $k$ , $\text{A}/\text{cm}^2$
$i_c$	Capacitive current density based on projected electrode area, $\text{A}/\text{cm}^2$
$i_{\text{cell}}$	Applied cell current density based on projected electrode area, $\text{A}/\text{cm}^2$
$i_f$	Faradaic current density based on projected electrode area, $\text{A}/\text{cm}^2$
$i_{o,j,\text{ref}}$	Exchange current density based on projected electrode area at reference concentrations for reaction $j$ , $\text{A}/\text{cm}^2$
$i_{\text{pa}}$	Anodic peak current density based on projected electrode area, $\text{A}/\text{cm}^2$
$i_{\text{pc}}$	Cathodic peak current density based on projected electrode area, $\text{A}/\text{cm}^2$
$i_1$	Superficial current density in the solid phase based on projected

$i_2$	electrode area, A/cm <sup>2</sup>
$\Delta i_a$	Superficial current density in the solution phase based on projected electrode area, A/cm <sup>2</sup>
$\Delta i_a$	Difference of anodic current densities between reference and perturbed values of parameter k, A/cm <sup>2</sup>
$j_c$	Local capacitive transfer current density within the polypyrrole positive electrode based on electroactive area, A/cm <sup>2</sup>
$j_f$	Local faradaic transfer current density within the polypyrrole positive electrode based on electroactive area, A/cm <sup>2</sup>
$j_1$	Local transfer current density within the polypyrrole positive electrode based on electroactive area, A/cm <sup>2</sup>
$j_2$	Local transfer current density at the lithium negative electrode based on electroactive area, A/cm <sup>2</sup>
$M_i$	Chemical formula of species i
$m$	Number of data points for sensitivity analysis
$N(E_f)$	Density of electronic states at the Fermi level
$\mathbf{N}_i$	Flux vector of species i, mol/cm <sup>2</sup> -sec
$\mathbf{N}_{i,p}$	Flux vector of species i within the polypyrrole film, mol/cm <sup>2</sup> -sec
$\mathbf{N}_{i,s}$	Flux vector of species i within the separator, mol/cm <sup>2</sup> -sec
$n_j$	Number of electrons transferred for reaction j
$P_k$	Perturbed value of parameter k
$P_k^*$	Reference value of parameter k
$\Delta P_k$	Dimensionless difference between perturbed and reference values of parameter k
$Q$	Local charge of the polypyrrole film per unit volume, C/cm <sup>3</sup>
$Q_c$	Local capacitive charge of the polypyrrole film per unit volume, C/cm <sup>3</sup>
$Q_{ca}$	Anodic charge density of the polypyrrole film based on projected electrode area C/cm <sup>2</sup>
$Q_{cc}$	Cathodic charge density of the polypyrrole film based on projected electrode area, C/cm <sup>2</sup>
$Q_f$	Local faradaic charge of the polypyrrole film per unit volume, C/cm <sup>3</sup>
$Q_{f,oxd}$	Faradaic charge of the fully oxidized polypyrrole film per unit volume, C/cm <sup>3</sup>
$Q_{f,red}$	Faradaic charge of the fully neutral polypyrrole film per unit volume, C/cm <sup>3</sup>
$R$	Universal gas constant, 8.3143 J/mol-K
$R'_{j,i}$	Pseudohomogenous reaction rate of species i for reaction j, mol/cm <sup>3</sup> -sec
$S_k$	Sensitivity coefficient of parameter k
$s_{j,i}$	Stoichiometric coefficient of species i for reaction j

$T$	Absolute temperature, K
$t$	Time, sec
$t_d$	Discharge time of the lithium/polypyrrole secondary battery cell, sec
$t_i$	Transference number of species i
$\Delta t$	Time step, sec
$U_j$	Theoretical open circuit potential at the surface concentration for reaction j, V
$U_{j,ref}$	Theoretical open circuit potential at reference concentration for reaction j, V
$u_i$	Mobility of species i, mol-cm <sup>2</sup> /J-sec
$u_{i,p}$	Effective mobility of species i within polypyrrole electrode, mol-cm <sup>2</sup> /J-sec
$u_{i,s}$	Effective mobility of species i within separator, mol-cm <sup>2</sup> /J-sec
$V$	Volume of polypyrrole film, cm <sup>3</sup>
$\mathbf{v}$	Electrolyte velocity vector, cm/sec
$v_s$	Scan rate, V/sec
$v_y$	Electrolyte velocity in the normal direction, cm/sec
$y$	Perpendicular distance from the current collector/polypyrrole electrode interface, cm
$y_{dl}$	Position of the bulk solution in y coordinate, cm
$y_{pp}$	Position of the polypyrrole electrode/diffusion layer interface in y coordinate, cm
$y_{ppe}$	Position of the positive electrode/reservoir interface in y coordinate, cm
$y_{res}$	Position of the reservoir/separator interface in y coordinate, cm
$y_{sep}$	Position of the separator/negative electrode interface in y coordinate, cm
$\Delta y$	Distance between node points, cm
$z_i$	Charge number of species i

### Greek

$\alpha_{aj}$	Anodic transfer coefficient for reaction j
$\alpha_{cj}$	Cathodic transfer coefficient for reaction j
$\delta_{dl}$	Thickness of the electrolyte diffusion layer, cm
$\delta_{pp}$	Thickness of the polypyrrole film, cm
$\delta_{ppe}$	Thickness of the polypyrrole positive electrode, cm
$\delta_{res}$	Thickness of the reservoir, cm
$\delta_{sep}$	Thickness of the separator, cm
$\epsilon_p$	Porosity of the polypyrrole film
$\epsilon_{oxd}$	Porosity of the fully oxidized polypyrrole film
$\epsilon_{red}$	Porosity of the fully neutral polypyrrole film

$\epsilon_s$	Porosity of the separator
$\eta_j$	Overpotential for reaction j, V
$\eta_{j,pzc}$	Overpotential at the point of zero charge for reaction j, V
$\kappa$	Free-stream solution conductivity, / $\Omega$ -cm
$\kappa_p$	Effective solution conductivity within the polypyrrole film, / $\Omega$ -cm
$\kappa_s$	Effective solution conductivity within the separator, / $\Omega$ -cm
$\Lambda$	Equivalent conductance of binary electrolyte, $\text{cm}^2/\Omega\text{-cm}$
$\lambda$	Doping level of polypyrrole film
$\lambda_i$	Ionic conductance, $\text{cm}^2/\Omega\text{-cm}$
$\lambda_{max}$	Maximum doping level of polypyrrole film, 0.30
$\theta$	Fractional doping level of polypyrrole film,
$\mu$	Viscosity, g/cm-sec
$\nu$	Kinematic viscosity, $\text{cm}^2/\text{sec}$
$\rho$	Density of polypyrrole film, g/cm <sup>3</sup>
$\rho_s$	Density of 1M LiClO <sub>4</sub> -PC solution, g/cm <sup>3</sup>
$\sigma_{oxd}$	Electronic conductivity of the fully oxidized polypyrrole film, / $\Omega$ -cm
$\sigma_p$	Electronic conductivity of the polypyrrole film, / $\Omega$ -cm
$\sigma_{red}$	Electronic conductivity of the fully neutral polypyrrole film, / $\Omega$ -cm
$\tau$	Tortuosity of the polypyrrole film
$\Phi_{cell}$	Cell potential, V
$\Phi_{ave}$	Average cell potential during discharge, V
$\Phi_{ref}$	Reference electrode potential, V
$\Phi_1$	Potential at the solid phase, V
$\Phi_2$	Potential at the solution phase, V
$\Omega$	Disk rotation velocity, rad/sec

#### Subscript

+	Cation, Li <sup>+</sup>
-	Anion, ClO <sub>4</sub> <sup>-</sup>

## REFERENCES

1. A. F. Diaz and J. Bargon, "Handbook of Conducting Polymers, Volume 1," T. A. Skotheim, Ed., p. 81, Marcel Dekker, Inc., New York, NY (1986).
2. G. B. Street, "Handbook of Conducting Polymers, Volume 1," T. A. Skotheim, Ed., p. 265, Marcel Dekker, Inc., New York, NY (1986).
3. J. Bargon, S. Mohmand, and R. J. Waltman, *IBM J. Res. Dev.*, **27**, 330 (1983).
4. A. Angeli, *Gazz. Chim. Ital.*, **46**, II, 279 (1916).
5. A. Angeli and L. Alessandri, *Gazz. Chim. Ital.*, **46**, II, 283 (1916).
6. A. Dall'Olio, G. Dascola, V. Varacca, and V. Bocchi, *Compt. Rend. Sci. Scr.*, **C**, **267**, 433 (1968).
7. V. V. Walatka, Jr., M. M. Labes, and J. H. Perlstein, *Phys. Rev. Lett.*, **31**, 1139 (1973).
8. R. L. Greene, G. B. Street, and L. J. Suter, *Phys. Rev. Lett.*, **34**, 577 (1975).
9. H. Shirakawa, E. J. Louis, A. G. MacDiarmid, C. K. Chiang, and A. J. Heeger, *J. Chem. Soc., Chem. Commun.*, 578 (1977).
10. C. K. Chiang, C. R. Fincher, Jr., Y. W. Park, A. J. Heeger, H. Shirakawa, E. J. Louis, S. C. Gau, and A. G. MacDiarmid, *Phys. Rev. Lett.*, **39**, 1098 (1977).
11. C. K. Chiang, M. A. Druy, S. C. Gau, A. J. Heeger, E. J. Louis, A. G. MacDiarmid, Y. W. Park, and H. Shirakawa, *J. Am. Chem. Soc.*, **100**, 1013 (1978).
12. P. J. Nigrey, A. G. MacDiarmid, and A. J. Heeger, *J. Chem. Soc., Chem. Commun.*, 594 (1979).

13. P. J. Nigrey, D. MacInnes, Jr., D. P. Nairns, A. G. MacDiarmid, and A. J. Heeger, *J. Electrochem. Soc.*, **128**, 1651 (1981).
14. P. J. Nigrey, A. G. MacDiarmid, and A. J. Heeger, *Mol. Cryst. Liq. Cryst.*, **83**, 309 (1982).
15. J. R. Ellis, "Handbook of Conducting Polymers, Volume 1," T. A. Skotheim, Ed., p. 489, Marcel Dekker, Inc., New York, NY (1986).
16. A. F. Diaz, K. K. Kanazawa, and G. P. Gardini, *J. Chem. Soc., Chem. Commun.*, 635 (1979).
17. K. K. Kanazawa, A. F. Diaz, R. H. Geiss, W. D. Gill, J. F. Kwak, J. A. Logan, J. F. Rabolt, and G. B. Street, *J. Chem. Soc., Chem. Commun.*, 854 (1979).
18. L. W. Shacklette, R. R. Chance, D. M. Ivory, G. G. Miller, and R. H. Baughman, *Synth. Met.*, **1**, 307 (1979/1980).
19. K. K. Kanazawa, A. F. Diaz, M. T. Krounbi, and G. B. Street, *Synth. Met.*, **4**, 119 (1981).
20. T. Yamamoto, K. Sanechika, and A. Yamamoto, *J. Polym. Sci. Polym. Lett. Ed.*, **18**, 9 (1980).
21. G. Tourillon and F. Garnier, *J. Electroanal. Chem.*, **135**, 173 (1982).
22. R. J. Waltman, J. Bargon, and A. F. Diaz, *J. Electrochem. Soc.*, **131**, 1452 (1984).
23. R. J. Waltman, J. Bargon, and A. F. Diaz, *J. Phys. Chem.*, **87**, 1459 (1983).
24. G. Tourillon and F. Garnier, *J. Electroanal. Chem.*, **161**, 51 (1984).
25. R. McNeill, R. Siudak, J. H. Wardlaw, and D. E. Weiss, *Austr. J. Chem.*, **16**, 1056 (1963).
26. G. P. Gardini, *Adv. Heterocycl. Chem.*, **15**, 67 (1973).

27. M. Salmon, K. K. Kanazawa, A. F. Diaz, and M. Krounbi, *J. Polym. Sci., Polym. Lett. Ed.*, **20**, 187 (1982).
28. G. F. Smith, *Adv. Heterocycl. Chem.*, **2**, 287 (1963).
29. G. B. Street, T. C Clarke, M. Krounbi, K. K. Kanazawa, V. Lee, P. Pfluger, J. C. Scott, and G. Weiser, *Mol. Cryst. Liq. Cryst.*, **83**, 253 (1982).
30. S. Asavapiriyant, G. K. Chandler, G. A. Gunawardena, and D. Pletcher, *J. Electroanal. Chem.*, **177**, 229 (1984).
31. T. F. Otero and E. De Larreta, *Synth. Met.*, **26**, 79 (1988).
32. G. Zotti, C. Callarin, and N. Comisso, *J. Electroanal. Chem.*, **235**, 259 (1987).
33. M. Salmon, A. F. Diaz, A. J. Logan, M. Krounbi, and J. Bargon, *Mol. Cryst. Liq. Cryst.*, **83**, 265 (1982).
34. G. B. Street, *J. Phys. Paris*, **C3**, 44, 599 (1983).
35. R. J. Waltman and J. Bargon, *Can. J. Chem.*, **64**, 76 (1986).
36. E. M. Genies, G. Bidan, and A. F. Diaz, *J. Electroanal. Chem.*, **149**, 101 (1983).
37. G. B. Street, T. C Clarke, R. H. Geiss, V. Y. Lee, A. Nazzal, P. Pfluger, J. C. Scott, *J. Phys. Paris Colloq.*, **599**, C3 (1983).
38. J. Roncali, F. Garnier, M. Lemaire, and R. Garreau, *Synth. Met.*, **15**, 323 (1986).
39. G. B. Street, R. H. Geiss, S. E. Lindsey, A. Nazzal, and P. Pfluger, "Preceedings of the conference on electronic Excitation and Interaction Process in Organic Molecular Aggregates," P. Reineker, H. Haken, and H. C. Wolf, Ed., p. 265, Springer, New York, NY (1983).
40. A. F. Diaz, J. I. Castillo, J. A. Logan, and W. Lee, *J. Electroanal. Chem.*,

- 129, 115 (1981).
41. R. A. Bull, F. F. Fan, and A. J. Bard, *J. Electrochem. Soc.*, **129**, 1009 (1982).
  42. P. Burgmayer and R. W. Murray, "Handbook of Conducting Polymers, Volume 1," T. J. Skotheim, Ed., p. 507, Marcel Dekker, Inc., New York, NY (1986).
  43. M. Gazard, "Handbook of Conducting Polymers, Volume 1," T. J. Skotheim, Ed., p. 673, Marcel Dekker, Inc., New York, NY (1986).
  44. P. Burgmayer and R. W. Murray, *J. Am. Chem. Soc.*, **104**, 6139 (1982).
  45. P. Burgmayer and R. W. Murray, *J. Phys. Chem.*, **88**, 2515 (1984).
  46. J. Tanguy, N. Mermilliod, and M. Hoclet, *J. Electrochem. Soc.*, **134**, 795 (1987).
  47. J. Tanguy, N. Mermilliod, and M. Hoclet, *Synth. Met.*, **18**, 7 (1987).
  48. R. M. Penner and C. R. Martin, *J. Phys. Chem.*, **93**, 984 (1989).
  49. A. K. Hauser and J. Newman, *J. Electrochem. Soc.*, **136**, 2820 (1989).
  50. A. F. Diaz and K. K. Kanazawa, *Chem. Scr.*, **17**, 145 (1981).
  51. K. K. Kanazawa, A. F. Diaz, W. D. Gill, P. M. Grant, G. B. Street, G. P. Gardini, and J. F. Kwak, *Synth. Met.*, **1**, 329 (1979/80).
  52. K. J. Wynne and G. B. Street, *Macromolecules*, **18**, 2361 (1985).
  53. P. Pfluger, G. Weiser, J. C. Scott, and G. B. Street, "Handbook of Conducting Polymers, Volume 2," T. J. Skotheim, Ed., p. 1373, Marcel Dekker, Inc., New York, NY (1986).
  54. R. Erlandsson, O. Inganäs, I. Lundström, and W. R. Salaneck, *Synth. Met.*, **10**, 303 (1985).
  55. B. F. Cvetko, M. P. Brungs, R. P. Burford, and M. Skyllas-Kazacos, *J. Appl.*

- Electrochem.*, **17**, 1198 (1987).
56. O. Inganäs, R. Erlandsson, C. Nylander, and I. Lundström, *J. Phys. Chem. Solids*, **45**, 427 (1984).
  57. J. L. Bredas, R. R. Chance, and R. Silberg, *Mol. Cryst. Liq. Cryst.*, **77**, 319 (1981).
  58. J. L. Bredas, B. Themans, J. M. Andre, R. R. Chance, D. S. Boudreault, and R. Silberg, *J. Phys. Coll.*, **44**, C3-373 (1983).
  59. P. M. Grant and I. P. Batra, *Syn. Met.*, **1**, 193 (1979/1980).
  60. W. P. See, J. R. Schrieffer, and A. J. Heeger, *Phys. Rev. Lett.*, **42**, 1698 (1979).
  61. N. F. Mott and E. A. Davis, "Electronic Processes in Non-crystalline Materials," Clarendon Press, Oxford (1969).
  62. R. R. Chance, J. L. Bredas, and R. Silbey, *Phys. Rev. B.*, **29**, 4491 (1984).
  63. S. Kivelson, *Phys. Rev. B.*, **25**, 3798 (1982).
  64. N. F. Mott, *J. Phys. C., Solid State Phys.*, **13**, 5433 (1980).
  65. Y. Shen, K. Carneiro, C. Jacobsen, R. Qian, and J. Qiu, *Synth. Met.*, **18**, 77 (1987).
  66. R. R. Chance, D. S. Boudreauz, J. L. Bredas, and R. Silbey, "Handbook of Conducting Polymers, Volume 2," T. J. Skotheim, Ed., p. 915, Marcel Dekker, Inc., New York, NY (1986).
  67. W. P. Su, Jr., Schrieffer, and A. J. Heeger, *Phys. Rev. B*, **22**, 2099 (1980).
  68. K. L. Ngai and R. W. Rendell, "Handbook of Conducting Polymers, Volume 2," T. J. Skotheim, Ed., p. 967, Marcel Dekker, Inc., New York, NY (1986).
  69. A. F. Diaz, V. Vasquez, and A. M. Duran, *IBM J. Res. Dev.*, **25**, 42 (1981).
  70. R. Noufi, A. J. Frank, and A. J. Nozik, *J. Electrochem. Soc.*, **128**, 2596

- (1981).
71. R. Noufi, A. J. Frank, and A. J. Nozik, *J. Am. Chem. Soc.*, **103**, 1849 (1981).
  72. T. Skotheim, L. G. Petterson, O. Inganäs, and I. Lundström, *J. Electrochem. Soc.*, **129**, 1737 (1982).
  73. E. M. Genies and J. M. Pernaut, *Synth. Met.*, **10**, 117 (1984/85).
  74. R. M. Penner, L. S. Van Dyke, and C. R. Martin, *J. Phys. Chem.*, **92**, 5274 (1988).
  75. K. Naoi and T. Osaka, *J. Electrochem. Soc.*, **134**, 2479 (1987).
  76. S. Panero, P. Prosperi, S. Passerini, B. Scrosati, and D. D. Perlmutter, *J. Electrochem. Soc.*, **136**, 3729 (1989).
  77. J. H. Kaufman, K. K. Kanazawa, and G. B. Street, *Phys. Rev. Lett.*, **53**, N. 26, 2461 (1984).
  78. F. Chao, J. L. Baudoin, M. Costa, and P. Lang, *Makromol. Chem. Makromol. Symp.*, **8**, 173 (1987).
  79. S. W. Feldberg, *J. Am. Chem. Soc.*, **106**, 4671 (1984).
  80. P. G. Pickup and R. A. Osteryoung, *J. Electroanal. Chem.*, **195**, 271 (1985).
  81. J. Prejza, I. Lundström, and T. Skotheion, *J. Electrochem. Soc.*, **129**, 1685 (1982).
  82. R. Noufi, D. Tench, and L. F. Warren, *J. Electrochem. Soc.*, **127**, 2310 (1980).
  83. A. J. Frank and K. Honda, paper presented at the 182nd American Chemical Society Meeting, Las Vegas, NV, April 1981
  84. R. A. Bull, F. R. Fan, and A. J. Bard, *J. Electrochem. Soc.*, **130**, 1636 (1983).

85. A. J. Frank, *Mol. Cryst. Liq. Cryst.*, **83**, 341 (1982).
86. S. J. Hahn, W. J. Gajda, P. O. Vogelhut, and M. V. Zeller, *Synth. Met.*, **14**, 89 (1986).
87. D. S. Maddison and J. Unsworth, *Synth. Met.*, **30**, 47 (1989).
88. M. Satoh, K. Kaneto, and K. Yoshino, *Synth. Met.*, **14**, 289 (1986).
89. Y. Yatsuda, H. Sakai, and T. Osaka, *J. Chem. Soc., Jpn.*, **7**, 1331 (1985).
90. K. Okabayashi, F. Goto, K. Abe, T. Yoshida, and M. Morimoto, in "Proceedings of 25th Battery Symposium," In Japan, p. 260 (1984).
91. M. Ogasawara, K. Funahashi, and K. Iwata, *Mol. Cryst. Liq. Cryst.*, **118**, 159 (1985).
92. R. M. Penner and C. R. Martin, *J. Electrochem. Soc.*, **113**, 2206 (1986).
93. K. Naoi, A. Ishijima, and T. Osaka, *J. Electroanal. Chem.*, **217**, 203 (1987).
94. M. A. De Paoli, R. J. Waltman, A. F. Diaz, and J. Bargon, *J. Chem. Soc., Chem. Commun.*, 1016 (1984).
95. M. A. De Paoli, R. J. Waltman, A. F. Diaz, and J. Bargon, *J. Polym. Sci., Polym. Chem. Ed.*, **23**, 1687 (1985).
96. S. E. Lindsey and G. B. Street, *Synth. Met.*, **10**, 67 (1985).
97. F. Fan and A. J. Bard, *J. Electrochem. Soc.*, **133**, 301 (1986).
98. R. M. Penner and C. R. Martin, *J. Electrochem. Soc.*, **133**, 310 (1986).
99. P. Novák, O. Inganäs, and R. Bjorklund, *J. Electrochem. Soc.*, **134**, 1341 (1987).
100. P. Novák and O. Inganäs, *J. Electrochem. Soc.*, **135**, 2485 (1988).
101. A. Nazzal and G. B. Street, *J. Chem. Soc., Chem. Commun.*, 375 (1985).
102. N. Kumar, B. D. Malhotra, and S. Chandra, *J. Polym. Sci. Polym. Lett. Ed.*, **23**, 57 (1985).

103. O. Inganäs, B. Liedberg, and W. Chang-Ru, *Synth. Met.*, **11**, 239 (1985).
104. S. Kuwabata, S. Ito, and H. Yoneyama, *J. Electrochem. Soc.*, **135**, 1691 (1988).
105. T. Osaka, K. Naoi, H. Sakai, and S. Ogano, *J. Electrochem. Soc.*, **134**, 285 (1987).
106. T. Osaka, K. Naoi, S. Ogano, and S. Nakamura, *J. Electrochem. Soc.*, **134**, 2096 (1987).
107. S. Panero, P. Prosperi, and B. Scrosati, *Electrochim. Acta*, **32**, 1465 (1987).
108. A. Mohammadi, O. Inganäs, and I. Lundström, *J. Electrochem. Soc.*, **133**, 947 (1986).
109. F. Trinidad, J. Alonso-Lopez, and M. Nebot, *J. App. Electrochem.*, **17**, 215 (1987).
110. H. Münstedt, G. Köhler, H. Möhwald, D. Naegele, R. Bitthin, G. Ely, and E. Meissner, *Synth. Met.*, **18**, 259 (1987).
111. R. Noufi, D. Tench, and L. F. Warren, *J. Electrochem. Soc.*, **127**, 1625 (1980).
112. F. F. Fan, B. Wheeler, A. J. Bard, and R. Noufi, *J. Electrochem. Soc.*, **128**, 2042 (1981).
113. T. Skotheim, O. Inganäs, J. Prejza, and I. Lundström, *Mol. Cryst. Liq. Cryst.*, **83**, 329 (1982).
114. T. Skotheim, I. Lundström, and J. Prejza, *J. Electrochem. Soc.*, **128**, 1625 (1981).
115. A. J. Frank and R. J. Honda, *J. Phys. Chem.*, **86**, 1933 (1982).
116. G. Cooper, R. Noufi, A. J. Frank, and A. J. Nozik, *Nature*, **295**, 578 (1982).
117. A. F. Diaz, M. Salmon, and J. Addy, *Proceedings of the First European*

*Display Research Conference*, Munich, p. 111, VDE-Verlag GmbH, Berlin (1981)

118. O. Inganäs and I. Lundström, *J. Electrochem. Soc.*, **131**, 1129 (1984).
119. K. Murao and K. Suzuki, *J. Chem. Soc., Chem. Commun.*, 238 (1984).
120. K. Kaneto, S. Takeda, and K. Yoshino, *Jpn. J. Appl. Phys.*, **24**, L553 (1985).
121. H. S. White, G. P. Kittlesen, and M. S. Wrighton, *J. Am. Chem. Soc.*, **106**, 5375 (1984).
122. J. S. Newman, "Electrochemical Systems," Prentice-Hall, Englewood Cliffs, NJ (1973).
123. R. Keller, J. N. Foster, D. C. Hanson, J. F. Hon, and J. S. Muirhead, "Properties of nonaqueous Electrolyte," NAS 3-8521, NASA CR-1425 (1969).
124. F. Breivogel and M. Eisenberg, *Electrochem. Acta.*, **14**, 459 (1969).
125. M. Salmon, *J. Phys. Chem.*, **73**, 3299 (1969).
126. R. Jasinski, in "Advanced in Electrochemistry and Electrochemical Engineering, vol. 8" C. W. Tobias, Ed., pp 253-335, John Wiley & Sons, Inc., New York, NY (1971).
127. W. G. Cochran, *Proc. Cambridge Phil. Soc.*, **30**, 365 (1934).
128. M. H. Rogers and G. N. Lance, *J. Fluid Mechan.*, **7**, 617 (1960).
129. J. Newman and W. Tiedemann, *AIChE*, **21**, 25 (1975).
130. J. S. Dunning, Ph. D. Dissertation, University of California, Los Angeles, CA (1971).
131. J. A. Trainham, Jr., Ph. D. Dissertation, University of California, Los Angeles, CA (1979).
132. S. Whitaker, "A Simple Geometrical Derivation of the Spatial Averaging

- Theorem," *Chemical Engineering Education*, 18 (Winter 1985).
133. T. V. Nguyen, Ph. D. Dissertation, Texas A&M University, College Station, TX (1988).
  134. W. E. Ryan, R. E. White, and S. L. Kelly, *J. Electrochem. Soc.*, **134**, 2154 (1987).
  135. J. Van Zee, G. Kleine, R. E. White, and J. Newman, in "Electrochemical Cell Design," R. E. White, Ed., pp 377-389, Plenum Press, New York, NY (1984).
  136. B. Carnahan, H. A. Luther, and J. O. Wilkes, "Applied Numerical Methods," John Wiley & Sons, New York, NY (1969).
  137. N. Mermilliod, J. Tanguy, and F. Petiot, *J. Electrochem. Soc.*, **133**, 1073 (1986).
  138. P. E. Gill, W. Murray, and M. H. Wright, "Practical Optimization," Academic Press, New York, NY (1984).
  139. M. Barak, Editor, "Electrochemical Power Sources: Primary and Secondary Batteries," The Institution of Electrical Engineers, New York (1980).

## APPENDIX A

## ELECTROCHEMICAL POLYMERIZATION OF POLYPYRROLE FILMS

Electronically conducting polypyrrole film is deposited electrochemically on the polished surface of platinum rotating disk electrode in the system shown in Fig. 5. Supporting electrolyte is propylene carbonate solution containing 0.1M LiClO<sub>4</sub> and 0.1M pyrrole monomer.

Electrochemical synthesis is carried out using an EG&G Princeton Applied Research (PAR) Model 173 potentiostat/galvanostat equipped with a PAR Model 179 digital coulometer. Applying a constant current density of 1 mA/cm<sup>2</sup> for 240 seconds yields 1 μm thick polypyrrole film with little difficulty. The film thickness is controlled by monitoring the amount of total charge consumed during polymerization. That is, the film thickness is proportional to the total passed charge, and 0.24 C/cm<sup>2</sup> of passed charge yields 1 μm thick polypyrrole film (29,30). The surface of platinum disk electrode is cleaned and polished to a mirror finish with 1 μm, 0.3 μm, then 0.05 μm alumina powder (Banner Scientific) on a Metron polishing cloth before polymerization. After the electrochemical synthesis, the cell is thoroughly rinsed with propylene carbonate and then filled with 1M LiClO<sub>4</sub>-PC electrolyte solution to perform the cyclic voltammetry.

All chemicals used are reagent grade (Aldrich Chemicals). Pyrrole is distilled twice in a vacuum and then stored under nitrogen. LiClO<sub>4</sub> is used without further purification. The propylene carbonate used as a solvent is further purified by fractional distillation and percolation through activated alumina. The water in the propylene carbonate is removed by adding molecular sieves for a few days.

## VITA

Taewhan Yeu was born on [REDACTED] to Dalyoung Yeu and Hwoaja Koak in [REDACTED] which is second largest city in South Korea. He finished basic education, in Pusan. In 1975, he moved to Seoul and attended Chung-Ang University. He majored in Chemical Engineering at this University until August 1976 when he went to army for 3 years duty. He began graduate studies in Chemical Engineering at University of Detroit in August 1982. In August 1985, he transferred to Texas A&M University to continue Ph.D. in Chemical Engineering. He married Kyung Mi on June 25, 1988. They are the proud parents of one son, Christopher Edward, born on January 20, 1990.

The Author's permanent mailing address is:

Taewhan Yeu

293-5 Manduck-Dong, Buck-Gu

Pusan, Korea 601-81

End Date Aug 7, 1991